NOTE TO USERS

This reproduction is the best copy available

UMI

DISSERTATION

THE IMPACT OF DELIBERATE SODIUM INCORPORATION ON $CuInSe_2$-BASED SOLAR CELLS

Submitted by

Jennifer Elaine Granata

Department of Physics

In partial fulfillment of the requirements

for the Degree of Doctor of Philosophy

Colorado State University

Fort Collins, Colorado

Spring 1999

COLORADO STATE UNIVERSITY

DECEMBER 2, 1998

WE HEREBY RECOMMEND THAT THE DISSERTATION PREPARED UNDER OUR SUPERVISION BY JENNIFER E. GRANATA ENTITLED THE IMPACT OF DELIBERATE SODIUM INCORPORATION ON $CuInSe_2$-BASED SOLAR CELLS BE ACCEPTED AS FULFILLING IN PART REQUIREMENTS FOR THE DEGREE OF DOCTOR OF PHILOSOPHY.

Committee on Graduate Work

Adviser

Department Head

ABSTRACT OF DISSERTATION

THE IMPACT OF DELIBERATE SODIUM INCORPORATION ON $CuInSe_2$-BASED SOLAR CELLS

The beneficial effect of sodium incorporation in $CuInSe_2$-based solar cells is systematically and quantitatively explored in this thesis. For the first time, a range of sodium concentrations that yield optimal device performance is presented. The primary cause of solar-cell performance improvement is shown to be grain-boundary passivation, but a secondary cause in some cases comes about through an alteration of the growth process. A model is presented based on these observations. The parameters most affected by the sodium concentration are open-circuit voltage, fill factor, and dopant density.

$CuInSe_2$ thin films and photovoltaic devices are analyzed to determine how much sodium is needed to improve device performance, and to uncover the effect of sodium at grain boundary surfaces and in the bulk material. A broad range of sodium concentrations in $CuInSe_2$ from 0.001 to 0.15 at% Na is found to result in optimal device performance, which includes high efficiency, high fill factor, high dopant density, low series resistance, and good diode quality. Efficiencies improve by as much as 4% when sodium is added. Beyond this range, both device and material properties degrade. It is

assumed that this range supplies sufficient sodium for well-passivated grain boundaries, but not so much as to produce secondary phases, which tend to reduce solar cell performance. Diode junction quality improves with the addition of sodium, as observed by improvements in fill factor and diode quality factor.

Analysis of the trends observed in the change in diode parameters with increasing sodium concentration reveals that sodium affects both grain boundary and bulk properties. Secondary ion mass spectroscopy and scanning electron microscope data suggest that the sodium most likely resides at grain boundary surfaces. This analysis leads to a model that explains nearly all the changes that occur in the presence of sodium. A grain-boundary passivation model, including (a) the direct effects of sodium and (b) sodium as a catalyst to oxygen, explains the increase in open-circuit voltage, dopant density, and capacitance. It is likely that when sodium is co-evaporated, it (c) affects the bulk layer by layer by altering the growth process, without remaining in the bulk. Adding sodium during $CuInSe_2$ growth can add flexibility in choosing substrate materials and can reduce constraints on $CuInSe_2$ fabrication control, both important points for manufacturers of $CuInSe_2$-based solar cells.

Jennifer Elaine Granata
Department of Physics
Colorado State University
Fort Collins, CO 80523
Spring 1999

ACKNOWLEDGMENTS

This thesis is the culmination of many years of work in the classroom, in the laboratory, and in the field of life. It would not have been possible without the help of numerous people. I would like to take this opportunity to thank them.

Special thanks goes to my advisor, Jim Sites, for his prodding, his insights, his patience and his sense of humor. I also thank you, Jim, for the opportunities and the professional exposure you have given me. Thanks also to my committee: Marty Gelfand, Sandy Kern and Carmen Menoni, for reviewing this manuscript and for various help and insights along the way.

I thank my colleagues at CSU, past and present: Ingrid Eisgruber, Rick Sasala, Xiaoxiang Liu, Gunther Stollwerck, Jon Sharp, Karl Schmidt, Brendon Murphy, Harry Sax and Jason Hiltner, for fruitful scientific discussions as well as providing a comfortable and fun working atmosphere. Special thanks to Ingrid for kindnesses too numerous to count, and to Jason for always being ready for a food break.

I wish to thank Siemens Solar Industries, Solarex, Inc., and the National Renewable Energy Laboratory (NREL) for supplying glass and Mo samples.

This work could not have been completed without the people and the resources at NREL. I thank John Tuttle for his initial tutelage and for sparking my interest in this subject. Thanks to Troy Berens for helpful conversations and invaluable help in learning

to run the deposition system, but most of all, Troy, thanks for your friendship. I thank Kannan Ramanathan for help with everything; most of all for helping me keep my sanity and a sense of humor. Thanks to Falah Hasoon for being a "partner in crime," and for all the SEM work. And to the rest of the CIS team: Holm Wiesner, Jeff Alleman, Jim Dolan, James Keane, Miguel Contreras, Rommel Nouti and Raghu Bhattacharya, I say thank you for your support, both technical and moral. As for technical support with the materials, I have many people to thank on the Characterization team. Sally Asher, Matt Young, Alice Mason, John Webb, David Niles, Jay Riker, Brain Keyes, Amy Schwarzlander, Rick Matson - thank you for taking the time to not only do the analysis for me, but to understand the problem and to try, each in your own way, to help me solve it. I owe much of my education to all of you.

There are many other people at NREL who helped along the way with their laughter and encouragement, and with good discussion. Thanks especially to Carole Allman; my cubicle mates Jeanne McGraw and Chris Carlson; and Alex Zunger.

So many friends have stood by me during these difficult years. Thank you Doug, Dave, Eric and Ned for the many nights of Pinochle and dancing that helped me maintain my humanity. Thanks also to Beth, Ted and Cheryl-Ann, for putting up with all my moods and supporting me along this roller coaster ride. From across the miles, I thank Chris, Shannon, Nik, Karl and numerous others for the smiles that helped keep me going.

A special thank-you to Dr. Beal for pushing me into this endeavor and watching closely along the way. Thank you for ever being a mentor and friend.

There are not enough words to express my appreciation to my family. Without your love and support, I would not be here today. Thank you for always encouraging me to do my best and for accepting me, warts and all.

"In the beginning, when God created the universe, . . . everything was engulfed in total darkness, and the power of God was moving over the water. Then God commanded, 'Let there be light' - and light appeared."
Genesis 1:1-3

"You are like light for the whole world. A city built on a hill cannot be hid. No one lights a lamp and puts it under a bowl; instead he puts it on the lampstand, where it gives light for everyone in the house. In the same way your light must shine before people, so that they will see the good things you do and praise your Creator in heaven."
Matthew 5:14-16

"'I am the light of the world,' Jesus said. 'Whoever follows me will have the light of life and will never walk in darkness.'"
John 8:12

"There shall be no more night, and they will not need lamps or sunlight, because the Lord God will be their light..."
Revelation 22:5

TABLE OF CONTENTS

LIST OF TABLES

LIST OF FIGURES

CHAPTER 1

INTRODUCTION

Solar energy offers a clean, viable energy source for the future, and has the potential to become one of the world's primary energy producers. To achieve this goal, solar cells, based on photovoltaic materials, must be efficient and cost-effective. Thin-film solar cells, including amorphous silicon, $CuIn(Ga)Se_2$ and CdTe, have emerged in the last 30 years as a balance to the crystalline technologies including silicon and GaAs. Although the thin-film materials are likely to achieve lower maximum efficiencies than their crystalline counterparts, they are less expensive and easier to produce. In a field ruled by economic trade-offs, a reduction in the amount of raw materials used can mean the difference between success and failure. It is shown in this work that the presence of sodium in $CuInSe_2$-based solar-cell devices in particular can increase the efficiency of these devices and reduce constraints on manufacturing them.

The group in the photovoltaics laboratory in the Colorado State University Department of Physics has chosen to concentrate its efforts on thin-film solar cell technologies; specifically $CuIn(Ga)Se_2$ and CdTe. Work with $CuIn(Ga)Se_2$ (CIS or CIGS) has made great strides in the last five years, achieving a single cell, laboratory device efficiency of 17.7% [1]. This efficiency is just under three-quarters of the

theoretical maximum of 24%. Many laboratory devices average 12-15% in efficiency. CdTe devices have reached an efficiency of near 16% in the laboratory [2,3]; this is just under two-thirds of the maximum efficiency of 25.5%. CdTe test device efficiencies consistently average 10 - 13%.

Historically, the highest efficiency laboratory-size $CuIn(Ga)Se_2$ devices have been fabricated on soda-lime glass [1,4]. The original explanation why these substrates work so well pointed to a compatibility of the thermal expansion coefficients of the substrate and the photovoltaic material [5]. This explanation is somewhat suspect, however, since there are layers of other materials between the glass and the $CuIn(Ga)Se_2$ which do not have compatible thermal expansion coefficients.

In recent years, interest has returned to understanding why soda-lime glass works so well as a substrate for $CuInSe_2$ devices in particular. It has been discovered that component atoms, such as sodium, potassium and calcium, diffuse out of the glass and into the $CuIn(Ga)Se_2$ absorber film during growth. Experiments have shown that the presence of sodium in particular has a positive effect on device performance, mainly by increasing open-circuit voltage, fill factor and effective dopant density. Some researchers have also found that sodium increases grain size and grain texture. A literature review of this subject is in the following chapter. Although much has been done in this area, many questions remain unanswered. The following questions are the focus of this dissertation. How much sodium is needed to affect these characteristics? Does the sodium mainly affect grain boundary surfaces, or is the bulk affected as well? How does the sodium affect the junction quality? What mechanisms are involved?

Deliberate incorporation of sodium in $CuInSe_2$ onto both sodium-containing and non-sodium-containing substrates demonstrates a range of sodium concentrations that yield optimal device performance. $CuInSe_2$-based solar cell device performance is optimal with sodium concentrations in the range of 0.001 to 0.15 at% Na. It is assumed that this range supplies sufficient sodium for well-passivated grain boundaries, but not so much as to produce secondary phases, which may diminish device performance. The main improvements are in open-circuit voltage and hole concentration, with secondary improvements in fill factor. Diode junction quality also improves. Beyond this range, both device parameters and material properties show significant degradation.

Analysis of the affected parameters demonstrates that sodium has the greatest effect on grain boundary properties, with a secondary effect on bulk-related properties. These observations lead to a model of the mechanisms involved when sodium is present in $CuInSe_2$ based on grain-boundary passivation and growth-alteration.

From a technological perspective, deliberately adding sodium enhances device performance and reduces constraints on key areas of $CuInSe_2$ solar-cell fabrication. Extrinsically incorporating sodium during $CuInSe_2$ deposition may allow researchers and manufacturers greater flexibility in choosing substrate materials.

This work brings the world one step closer to finding clean energy solutions to the problem of providing energy for everyone.

CHAPTER 2

BACKGROUND

This chapter lays the groundwork and motivation for the work presented in this thesis. Included are the physics of solar cells, the details of the chalcopyrite materials used, an introduction to device characterization, and the background and previous work that has been done on the sodium issue. A review of the semiconductor physics pertinent to this field is presented first to lay the groundwork for understanding the workings of solar cell devices. An overview is given, and the reader is directed to noted references for more in-depth coverage. The term "CIS" will be used at times in this thesis to denote thin-film $CuInSe_2$ and its cation-vacancy counterparts, as well as the $CuInSe_2$ thin-film technology in general.

2.1 $CuInSe_2$ Solar Cells

The basis of the solar cell is the p-n semiconductor junction. See references 6 and 7 for an overview of semiconductors and p-n junction theory. The property which makes a semiconductor useful as a photovoltaic material is a bandgap fairly well matched to the solar spectrum (the radiation spectrum the sun produces). The ideal single-junction photovoltaic semiconductor bandgap for the terrestrial solar spectrum is about 1.4 eV.

Semiconductors in common photovoltaic use range in bandgap from 1.0 eV ($CuInSe_2$) to 1.7 eV (amorphous silicon).

One commonly speaks of only one of the materials in a p-n junction as the primary absorber material, even when heterojunctions are used. In the case of $CuInSe_2$, the p-n junction is theoretically formed at the interface of a p-type $CuInSe_2$ layer and an n-type layer of, most commonly, CdS. The $CuInSe_2$ layer is referred to as the absorber because, ideally, all the electron-hole generation takes place in that layer. It is assumed that the n-type semiconductors used are heavily doped compared to the $CuInSe_2$, so the majority of the space-charge region is in the p-type $CuInSe_2$. Hence, all or nearly all the current collection stems from this layer.

$CuInSe_2$ is fabricated in the substrate configuration; meaning light enters the layers in the opposite order to their fabrication (see Figure 2.1). Soda-lime glass is commonly used as the substrate. A metal back-electrode, or back contact, is the first layer. 1-2 μm of molybdenum (Mo) is most often used, and RF-sputtering is the most common deposition process. 2-4 μm of $CuInSe_2$ is deposited on top of the Mo. Many processes can be used for this layer, which is commonly fabricated to be intrinsically doped p-type. An n-type window layer is deposited on top of the $CuInSe_2$. 50-100 nm of CdS is common and is either sputtered or put down by a chemical bath deposition process. 1-2 μm of a heavily-doped n-type transparent conducting oxide such as ZnO is sputtered on top of the window layer. A metal grid is evaporated on top to enhance current collection. A low-index antireflection coating such as MgF commonly completes the structure.

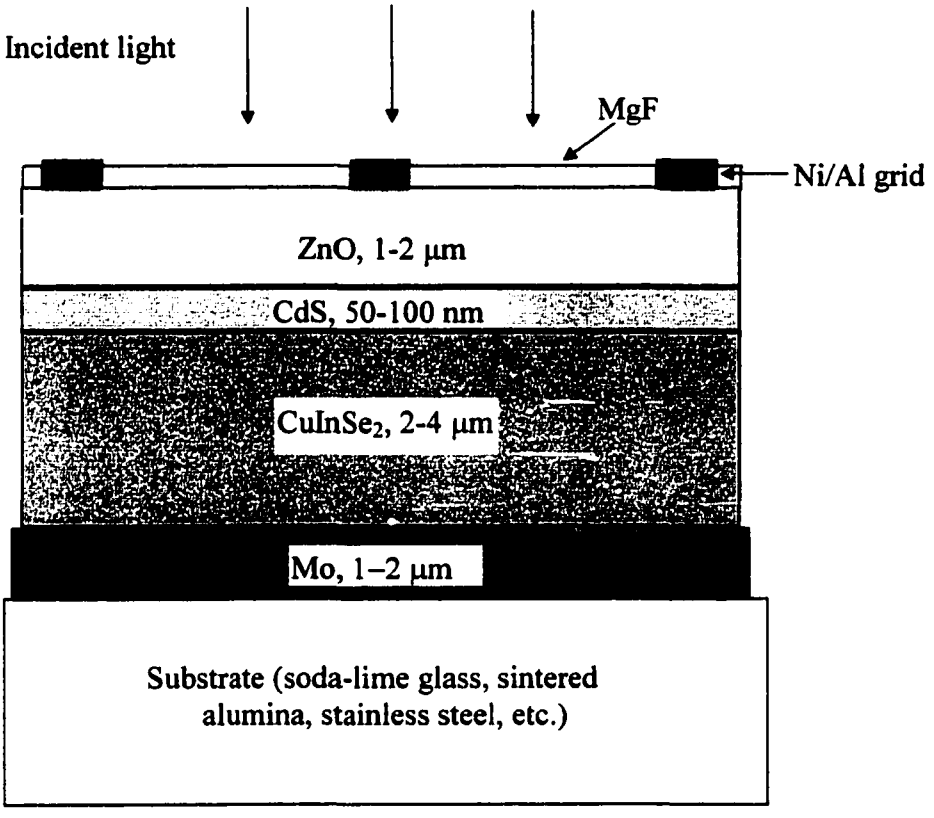

Figure 2.1. Typical substrate configuration used in fabricating $CuInSe_2$ thin film solar cells. Substrate thickness not to scale.

2.2 Thin-Film Chalcopyrite Materials

It is necessary to understand the basic material properties of thin-film $CuInSe_2$ before investigating the changes that occur in the presence of sodium. Much work has already been done on the material properties of thin-film $CuInSe_2$. Two excellent sources are the Ph.D. thesis of Tuttle [8] and the Ph.D. thesis of Gabor [9], and the references therein. The points most essential for understanding this thesis are covered.

2.2.1 Stoichiometry and Native Defects

$CuInSe_2$ is a member of the I-III-IV_2 group of semiconductors that form in the chalcopyrite structure, an approximate supercell of the zincblende structure [10]. This group of semiconductors is a subset of the adamantine family of compounds. The I-III-VI_2 compounds are the ternary analogs of the II-VI binary compounds, which in turn are based on the tetrahedral group IV semiconductors.

Chalcopyrites commonly exhibit a high tolerance to off-molecularity, off-stoichiometry, and native defects, which separates them from their other family members. They can also form defect-chalcopyrite structures, in which a large percentage (as much as 25%) of the cation sites are vacant in a random or ordered way. It is the control of these aspects that has allowed $CuInSe_2$ to become competitive in the field of photovoltaics.

Off-molecularity and valence off-stoichiometry are defined as follows:

$$\Delta x = \frac{[Cu]}{[In]} - 1 \tag{1}$$

$$\Delta z = \frac{2[Se]}{[Cu] + 3[In]} - 1 \tag{2}$$

where square brackets denote the total concentrations of Cu, In and Se. Positive off-molecularity, $\Delta x > 0$, denotes more Cu atoms than In in the film and is referred to as "Cu-rich." $\Delta x < 0$ is referred to as "Cu-poor" or "In-rich." Off-stoichiometry, Δz, refers to the situation in which there is an excess ($\Delta z > 0$) or deficiency ($\Delta z < 0$) of selenium atoms relative to the cations, affecting the number of electrons in the molecular structure. This work is mainly concerned with the case $\Delta x < 0$ and $\Delta z = 0$. Although $CuInSe_2$ can be

fabricated with a large range of combinations of Δx and Δz, empirically there is a small window of these values and combinations that result in good solar-cell quality material.

There are structural differences that accompany the molecular and stoichiometric differences. The structural differences are commonly referred to as different phases. Phase diagrams have been constructed for the Cu_2Se-In_2Se_3 pseudobinary system using bulk crystal information and differential thermal analysis techniques. Two such diagrams that have received much attention are those by Fearheiley [11] and Boehnke [12]. Boehnke's diagram and terminology, reproduced in Figure 2.2, will be used in this work. Typically, the α-phase is considered to be pure chalcopyrite $CuInSe_2$. Boehnke's diagram indicates that for slightly Cu-poor films, the α-phase window is quite small. That is,

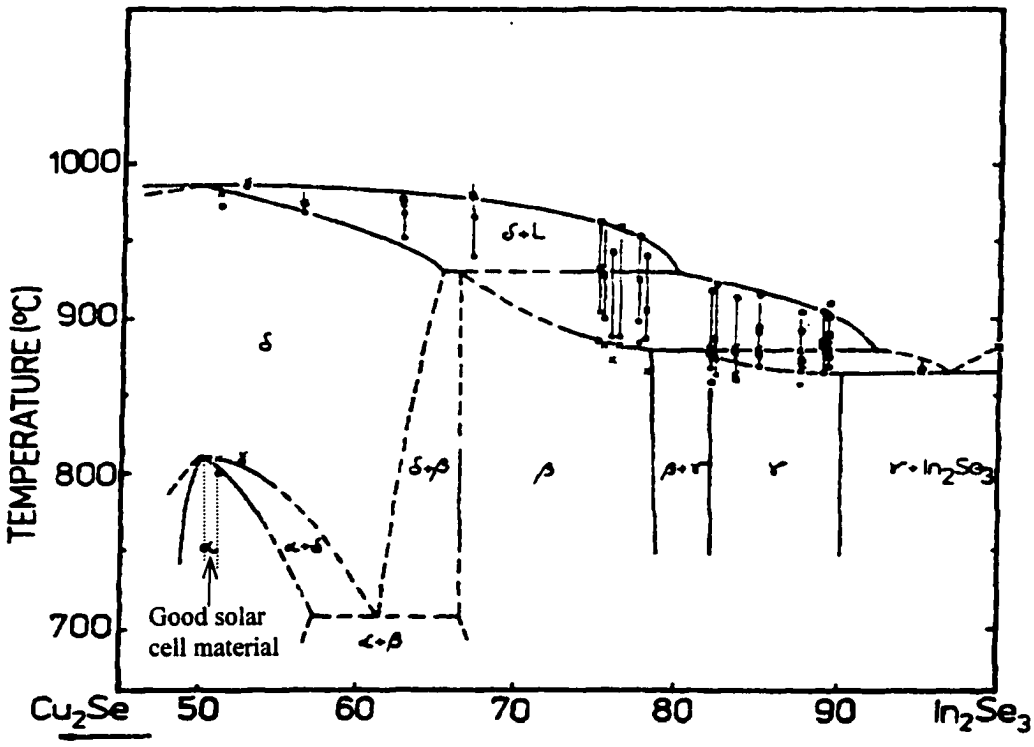

Figure 2.2. Cu_2Se-In_2Se_3 pseudobinary phase diagram after Boehnke. The axes are temperature in degrees C versus mole% In_2Se_3.

high-quality, single-phase $CuInSe_2$ can only exist for a small range of Δx and Δz values. In practice, it is not uncommon for secondary phases to form during thin-film $CuInSe_2$ growth. If sodium could increase the α-phase window, it could result in better films for a wider range of compositions, thereby relaxing fabrication constraints.

Off-molecularity empirically necessary for high-quality thin-film $CuInSe_2$ leads to chemical differences as well as structural differences from the perfect single-crystal case. The chemical changes stem from native defect formation. If cation/anion exchange in the crystal is excluded for now, there are eight native defects in three categories in $CuInSe_2$: vacancies, interstitials, and cation antisites. Vacancies occur when the expected atom is missing from the lattice. Interstitials occur when any atom is placed somewhere in the lattice other than in a lattice site. Antisites occur when an atom sits in an incorrect lattice site. The following lists these defects:

$$\text{Vacancy defects: } V_{Cu},\ V_{In},\ V_{Se}$$

$$\text{Interstitial defects: } Cu_i,\ In_i,\ Se_i$$

$$\text{Antisite defects: } Cu_{In},\ In_{Cu} \qquad (3).$$

Previous work on the theory of the defect physics of $CuInSe_2$, based on Neumann's calculations, assumed the formation energies of the defects did not vary with Fermi level position or chemical potential [13]. Under these assumptions, the order of the formation energies obtained, regardless of values of Δx and Δz, are as follows:

$$In_{Cu} < Cu_{In} < V_{Se} < V_{Cu} < V_{In} < Cu_i < In_i < Se_i \qquad (4).$$

The indium and selenium interstitial defects have calculated formation energies greater than 9 eV, making these defects highly unlikely to form. Therefore, these defects are disregarded in the remaining defect analysis. It was assumed that the defect abundance

followed this order as well. Recently, Zunger, et al., [14] have reported a more complete theory of the defect physics of $CuInSe_2$. Two main findings by Zunger's group pertinent to this thesis are (i) "defect formation energies vary considerably both with the Fermi energy, and with the chemical potential of the atomic species," and (ii) "defect pairs such as ($2V_{Cu}^{-} + In_{Cu}^{2+}$) and ($2Cu_{In}^{2-} + In_{Cu}^{2+}$) have particularly low formation energies..." These findings further explain the existence of the observed ordered (vacancy) compounds such as $CuIn_3Se_5$ (believed to be included in the β-phase), the very efficient p-type self-doping, and the electrically benign character of a large fraction of the defect population. With regard to (i), Zunger's work takes into account the changes in Fermi level and chemical potentials due to changes in molecularity and stoichiometry. The resulting calculated order of formation energies for the Cu-poor, In-rich, p-type $CuInSe_2$, which is the case of interest in this thesis, is as follows, with the previous "rank" shown in the second line (the selenium vacancies were excluded in this work):

$$V_{Cu} < In_{Cu} < V_{In} < Cu_{In} < Cu_i \qquad (5).$$

4 1 5 2 6

The dependence of V_{In}^{0}, In_{Cu}^{2+}, V_{Cu}^{0}, Cu_{In}^{0}, and Cu_i^{+} defect formation energies on the chemical potentials of Cu and In for a given Fermi energy is shown in Figure 2.3, taken from Zunger's work [14]. Points A, B, and C refer to the Δx and Δz extremes. Point A refers to the extreme Cu-rich, In-rich case, with $\mu_{Cu} = \mu_{In} = 0$; point B refers to the extreme Cu-poor, In-rich case, with $\mu_{Cu} = -2.0$ eV, $\mu_{In} = 0$; and point C refers to the extreme Cu-rich, In-poor case, with $\mu_{Cu} = 0$, $\mu_{In} = -2.0$ eV. Pure $CuInSe_2$ exists in a small region centered about the point $\mu_{Cu} - \mu_{In} \cong 0.7$ eV.

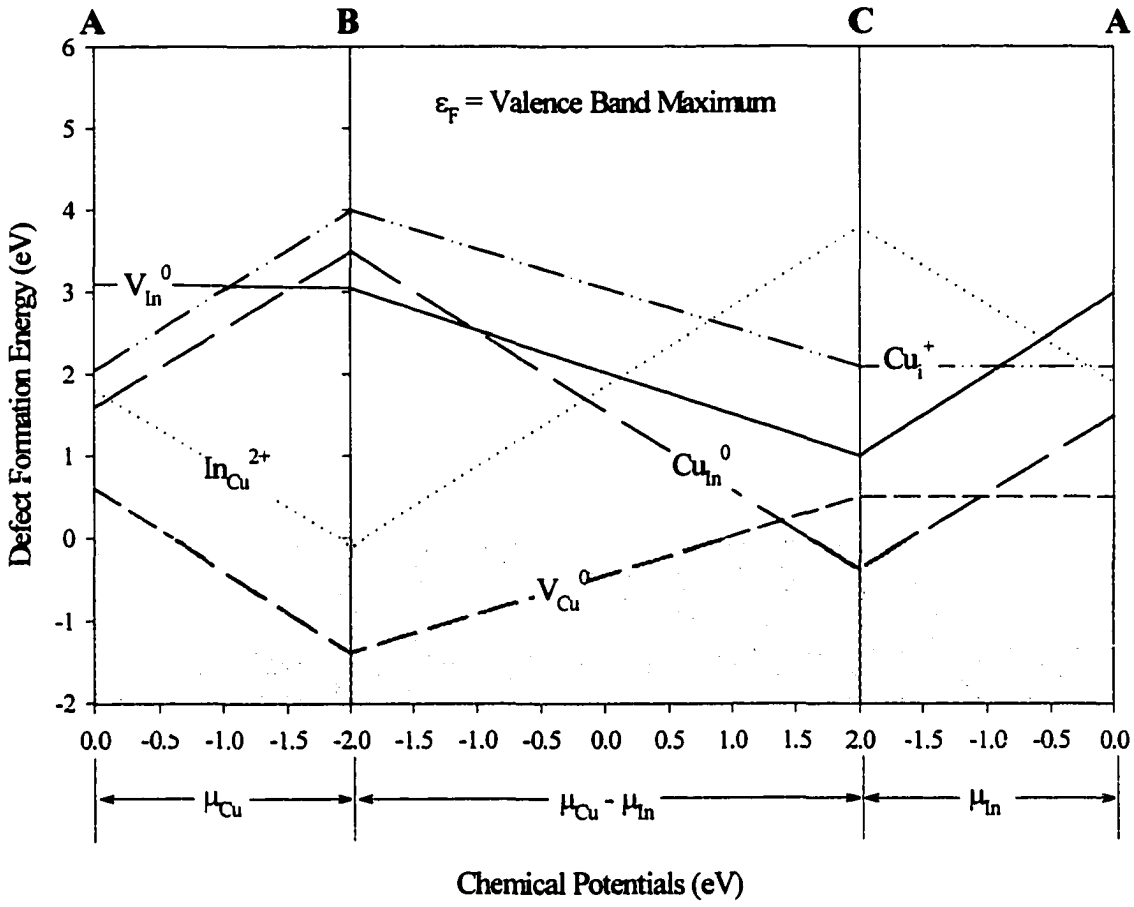

Figure 2.3. Dependence of the defect formation energies on the chemical potentials for a given Fermi energy. After Zunger, et al.

Another important point commonly neglected is that the pairing of defects significantly alters the electric activity. For example, "an isolated V_{Cu} is a shallow acceptor, while an isolated In_{Cu} is a deep donor, but a defect pair based on $2V_{Cu}$ and In_{Cu} is electrically inactive." [14] It is possible that the formation of defects, and/or the formation of defect pairs, is affected by the presence of sodium.

2.2.2 Crystalline Structure

In a perfect $CuInSe_2$ crystal, growth is mainly along the (112) direction. Figure 2.4 shows X-ray diffraction peaks for single-crystal $CuInSe_2$ using Cu-K_α radiation, taken from the JCPDS database. The strongest diffraction lines are for the (112), (220), (204), and (312) planes. The common growth pattern of thin-film $CuInSe_2$ is a columnar crystallite structure. Therefore, thin-film $CuInSe_2$ X-ray diffraction data can be compared to the single crystal case to determine lattice d-spacing (distance between atomic planes), lattice parameters, crystallite size, secondary phase identification, and general structure and orientation. A highly structured film will commonly have a high (112)/[(220),(204)]

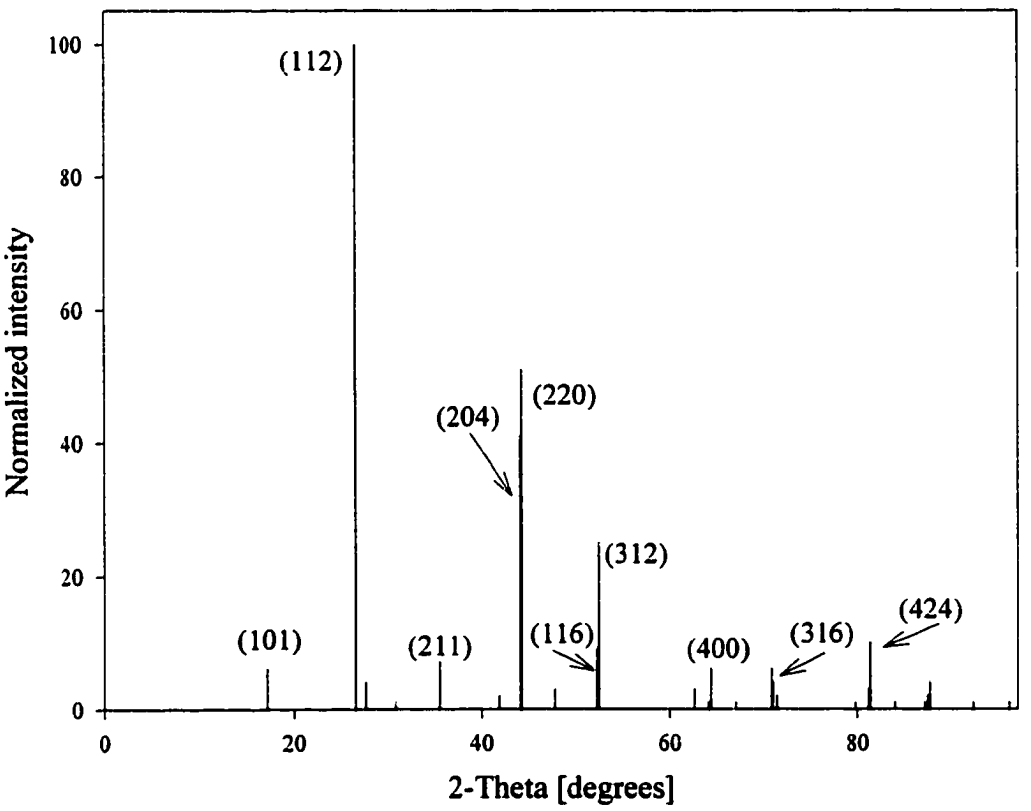

Figure 2.4. Normalized typical X-ray diffraction peaks for single-crystal $CuInSe_2$, taken from the JCPDS database.

peak height ratio, whereas a lower ratio designates a more randomly-oriented film. Figure 2.5 gives examples of two $CuInSe_2$ thin films, both on Mo/soda-lime glass substrates, with quite different structures. The data in the top graph demonstrates a highly structured film with a (112)/[(220),(204)] ratio of 22, whereas the data in the bottom graph shows a more randomly oriented film with a (112)/[(220),(204)] ratio of 4. The difference in structure is also evident in the other main $CuInSe_2$ peak heights. A

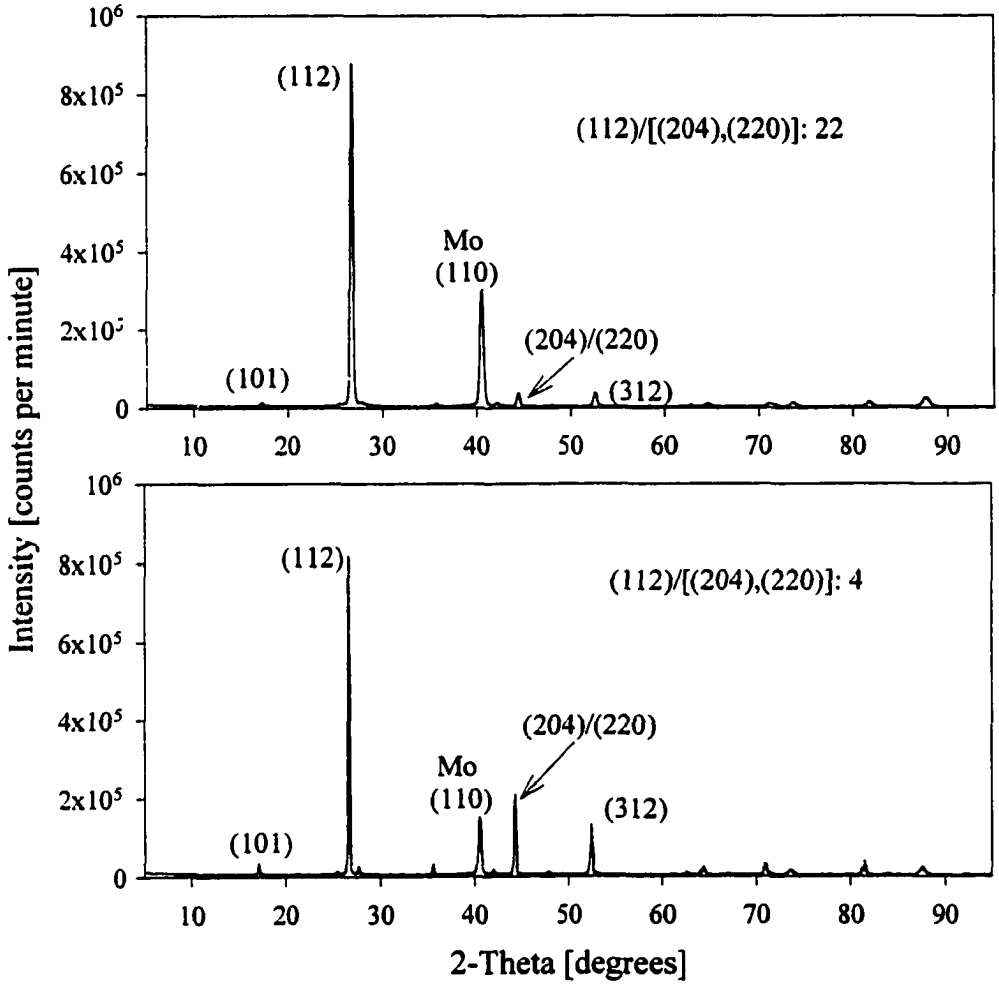

Figure 2.5. Example of X-ray diffraction data for two $CuInSe_2$ thin films.

highly structured film may be indicative of much of the film being in the α-phase. This technique will be useful in determining whether sodium has an effect on the structural properties of $CuInSe_2$. That is, if sodium does increase the α-phase window or suppress the formation of secondary phases, X-ray diffraction can be used to detect differences.

2.2.3 Growth Process

A comparison of Figures 2.4 and 2.5 shows differences between single crystal and thin-film $CuInSe_2$. For some thin films, secondary phases can be detected. Often the β-phase peak appears between 21.5 and 22.5° 2θ. When growing thin-film $CuInSe_2$, the goal is to avoid secondary phase formation and to approach the single crystal structure. This requires in-depth understanding of the growth processes involved. The details of the chemistry and growth of the $CuInSe_2$ ternary system depend very strongly upon the growth technique. The focus here will be on co-evaporation, or physical vapor deposition (PVD), since all the thin films used in this work were grown by the author using this technique.

The PVD process starts with solid materials (Cu, In, Se) which are evaporated in vacuum (~ 10^{-6} Torr). The evaporation rate of the metals is given by the Hertz-Knudsen equation [8]:

$$\frac{dN_e}{A_e dt} = \frac{(p^* - p)}{(2\alpha_v mkT)^2} \; atoms/cm^2 \bullet \sec \qquad (6)$$

where dN_e/dt is the rate at which atoms leave the evaporant surface, p^* is the vapor pressure and p is the hydrostatic pressure, T is the absolute temperature, m is the molecular weight, A_e is the source area, and α_v is the evaporation coefficient. Spatially, the emission follows the cosine emission law [8]. Using these two equations, the number

of atoms per unit area of each species incident upon the substrate can be estimated for a given source temperature.

To determine the concentration of $CuInSe_2$ molecules formed, additional parameters must be considered, including the thermal accommodation and sticking coefficients (which determine how quickly an atom will adsorb to the substrate), the substrate temperature, and the formation processes. For $CuInSe_2$, the process of formation, which is dependent upon the substrate temperature, is most important. The formation process of $CuInSe_2$ from Cu, In, and Se involves the formation of binaries such as Cu_2Se and In_2Se_3. The binaries then react to form $CuInSe_2$.

Understanding these reactions and the temperatures at which they occur is important to avoid secondary phase formation and unreacted binaries, as indicated in the phase diagram in Figure 2.2. Research in this area has lead to "recipes" which are typically used to grow high solar-cell quality $CuInSe_2$.

2.3 Device Characterization

An understanding of material properties is necessary to make the best solar-cell devices. Methods to characterize the materials themselves must be accompanied by methods to characterize and understand the workings of the final product. Although it is important to understand how sodium changes the absorber material, it is also necessary to electrically characterize and model the finished solar cell, and determine the effects of sodium from this perspective.

Since p-n junctions are the basis of diode theory, a solar cell can be modeled as a single diode with a resistor in series, R_{series}, and a leakage path in parallel, r_{shunt}. See Figure 2.6. By measuring a diode curve in the dark, the two resistive terms can generally

be extracted, as well as the ideality factor, or diode quality factor. See reference 15 for details of the extraction.

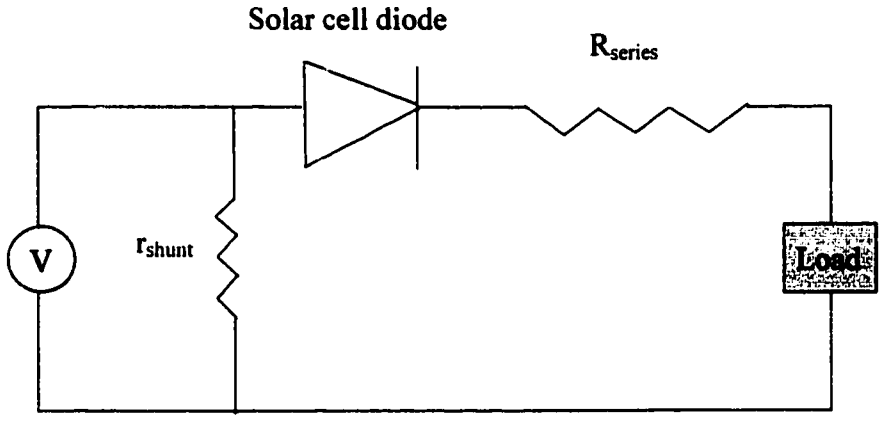

Figure 2.6. Single-diode circuit model of a solar cell.

A diode curve can also be measured in the light and the same analysis performed. In the ideal case, the calculated parameters are unchanged. Incident photons of sufficient energy can excite carriers across the gap, inducing a current. Ideally, this light diode curve, or current-voltage (JV) curve, is simply the dark current-voltage curve shifted by the light-induced current. There are three main parameters taken from the light JV curve that are used to describe how well the device works as a solar cell. These are the open-circuit voltage V_{OC} (voltage at zero current), the short-circuit current density J_{SC} (current/total area at zero voltage), and the fill factor FF (ratio of the maximum power to the $J_{SC}V_{OC}$ product). Together these values are used to determine the solar cell efficiency for a specified solar spectrum:

$$\eta = (FF \times J_{SC} \times V_{OC})/\text{input power} \qquad (7).$$

Figure 2.7 shows a light diode curve for a high-efficiency $CuInSe_2$ device.

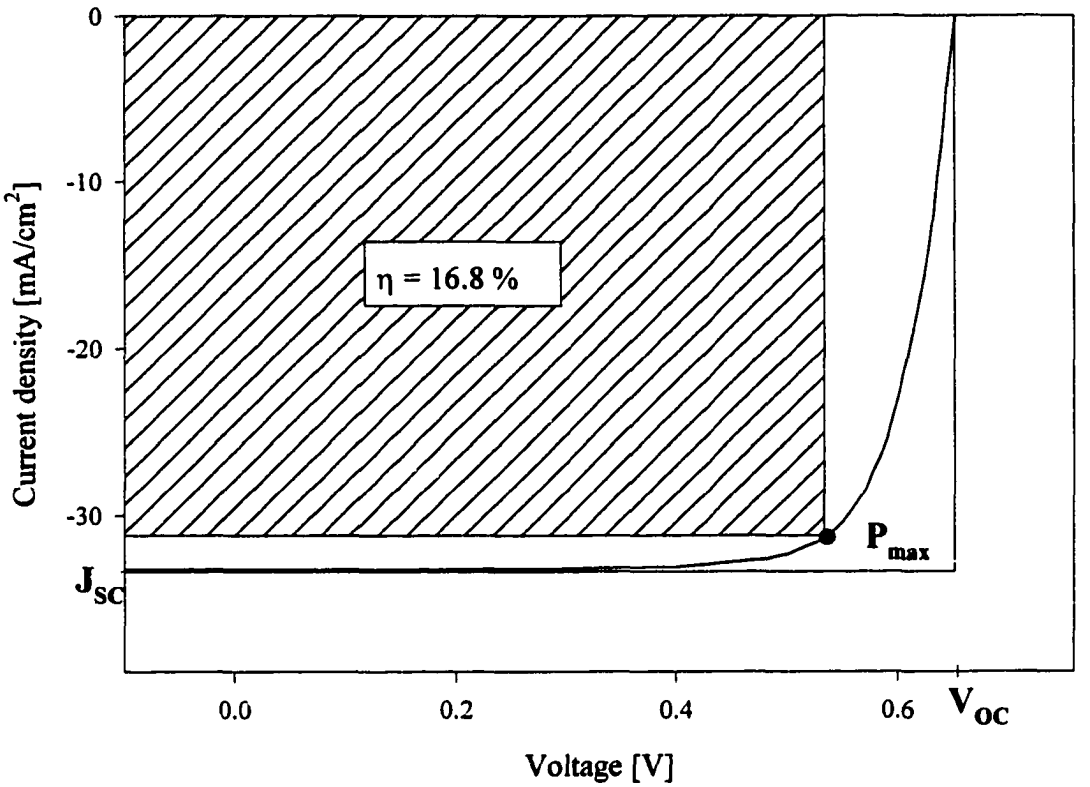

Figure 2.7. Light JV curve for a high-efficiency $CuInSe_2$ device.

The measured light-induced current at zero bias (J_{SC}) is always less than the maximum light-induced current possible, calculated by integrating the solar photon spectrum up to the bandgap of the absorber material. This difference is due in part to photon losses from reflection off the surface and from absorption in the top layers of the cell. Grid coverage is the source of another loss mechanism. In some cases, a photon excites an electron-hole pair deep in the absorber, but the lifetime is shorter than the time needed for the electron or hole to reach the depletion region. This introduces another current loss. Other mechanisms, such as high recombination rates, will decrease the current collected independent of the photon wavelength. A spectral response

measurement allows one to calculate the quantum efficiency of solar cells and extract these current losses. See reference 16 for details.

Assuming the solar cell behaves as an ideal diode, under a negative voltage or reverse bias in the dark, the electrical junction resembles a parallel-plate capacitor. The capacitance C of such a capacitor can be described by:

$$C = \frac{\varepsilon A}{x} \tag{8}$$

where ε is the dielectric constant of the medium, A the total area, and x the width of the capacitor. Using this equation, one can measure the capacitance of a solar cell and extract the width of the space-charge region. A few assumptions and mathematical rearrangement also allow an extraction of the dopant density of the absorber layer [17]. Although the values measured and calculated using this method are often subject to corrections, this method allows an accurate relative comparison between devices.

Current-voltage, quantum efficiency, and capacitance comparisons aid in understanding how solar-cell devices change with variations in fabrication parameters. These tools will be useful in determining what effect sodium has on device performance, and give insight into the mechanisms involved. For instance, an improvement in open-circuit voltage can indicate a decrease in recombination, or an increase in calculated hole density can indicate an increase in the effective acceptor concentration. The task is to optimize solar cell performance, and determine how sodium fits into this optimization using the tools available.

2.4 Current Challenges

Thus far, this chapter has outlined the basic physics of solar cells, the theory specific to $CuInSe_2$ materials, and many of the analysis techniques employed to characterize both materials and devices. Before delving into a review of the sodium issue to date, it is helpful to take a look at the general challenges and problems facing the researchers and manufacturers in the CIS photovoltaics community today.

Although CIS technology works well, the community is constantly searching for ways to improve performance, fit more applications, and be more economical. The main areas of needed improvement include the substrate, the back contact, the $CuInSe_2$, and junction quality.

As shown in Figure 2.1, a finished solar cell consists of many layers, and each plays a part in the overall performance. Ideally, the substrate can be chosen to fit the application: a low-weight substrate for use in space; a flexible substrate for roofing and siding; a conductive substrate to act as back contact; or a sturdy substrate for exposed terrestrial arrays. At this time, the choice of substrate is limited because, empirically, high-quality $CuInSe_2$ can only be grown on select substrates. It will become apparent that this is mainly due to the sodium introduced from the substrate.

As with the substrate, the back contact material should not be a limiting factor in making good $CuInSe_2$ solar cells. It is possible that Mo has worked well as a back contact material in $CuInSe_2$ devices at least in part because it allows sodium to diffuse from the substrate. The diffusion mechanism appears to be dependent on the structure of the Mo. Finding a way to remove this reliance on the back contact would allow more materials to be used which may better suit the application.

The $CuInSe_2$ layer is the most important layer in the stack because it is primarily responsible for current collection and the quality of the junction. The ability to make good-quality material inexpensively is one of the advantages of using thin-film materials such as $CuInSe_2$. There are trade-offs between single crystal and polycrystalline materials for solar cell use. Single crystals do not suffer losses due to grain boundary recombination, but polycrystalline cells are almost always more economical. Increasing grain size and improving grain boundary and surface passivation in polycrystalline materials can narrow the gap between the two types of materials while maintaining the advantages of thin film production. Large-grained material alone does not ensure high-quality cells, but a good material often improves when the grain size is enlarged. Similarly, smaller-grained material yields better cells when, even with no change in grain size, surface passivation is improved. Manufacturers can benefit from a variety of techniques that improve $CuInSe_2$ grain size, passivation, or both.

Another area that limits $CuInSe_2$ performance is secondary phase formation, as described in section 2.2. Currently, high-efficiency, single-phase material can only be produced by select methods, using select recipes. Techniques that would "open the $CuInSe_2$ processing window" would afford researchers and manufacturers greater flexibility in choosing low-cost, low-temperature $CuInSe_2$ processing methods.

In all of the processing methods currently in use, $CuInSe_2$ is grown in an ambient ranging from atmospheric pressure to 10^{-7} Torr. At any of these pressures, a significant amount of oxygen is present to affect the film growth. It has been shown that oxygen can be beneficial in surface passivation. Making better use of an element that is always present could improve performance and possibly lower costs.

Although most of the current production takes place in the $CuInSe_2$, p-n junction formation is necessary for a solar cell to work as such. One would envision that this junction forms at or near the metallurgical $CdS/CuInSe_2$ junction. If this were indeed the case, then good surface passivation would likely help form a good junction devoid of defects. Most high-quality $CuInSe_2$ cells, however, have a junction contained within the $CuInSe_2$ due to type-conversion of a thin surface layer by Cd doping [18]. Further understanding of how and where the junction forms will help improve junction quality.

These are some of the challenges facing the CIS community. As a physicist within this community, the task is to understand the underlying mechanisms and suggest and/or implement methods for improvement. This task sets the context for the work provided in this thesis.

2.5 The Sodium Issue

Now that the solar cell and materials background have been covered and the context set, the main contributions to both the experimental and theoretical aspects of understanding the sodium issue to date are presented.

J. Hedström, et al., in 1993 first suggested that the presence of sodium might affect the texture and structure of polycrystalline $CuInSe_2$ (CIS) and $Cu(In,Ga)Se_2$ (CIGS) thin films [19]. This group used four types of substrates: soda-lime glass (SLG), borosilicate glass, sapphire, and sintered alumina. They found that CIS films grown on Mo-coated SLG showed a strong preferred (112) orientation relative to the (204,220) orientation, whereas films grown on the other substrates were more randomly oriented. Also, films grown on SLG demonstrated increased grain size over those grown on borosilicate glass. They suggested two possible explanations: variations in stress due to

the different thermal expansion coefficients of the substrates, and different contaminants in the films. The films grown on SLG showed high amounts of sodium both at the surface and in the bulk of the film. Devices made with these absorbers demonstrated that those grown on SLG had higher open-circuit voltages and fill factors than those grown on the other substrates. Thus began the interest in the role of sodium in $Cu(In,Ga)Se_2$-based photovoltaic devices.

During the following year, some members of the same group attempted to separate the stress-related and impurity-related effects on CIS [20]. M. Bodegärd, et al., compared CIS grown on Mo-coated SLG both with and without an amorphous Al_2O_3 sodium diffusion barrier. They found sodium at the surface and in the bulk of the films grown on SLG. Secondary-ion mass spectroscopy (SIMS) mapping data to detect the sodium in the bulk combined with scanning electron microscopy (SEM) data to determine grain size and position showed that, for their films, the sodium is spread relatively evenly throughout the films and resides mainly in the grain boundaries. They again observed an improvement in grain structure (size and density) and an increase in the (112)-preferred orientation (texture) with the presence of sodium. A Mo back contact did not limit the sodium diffusion out of the glass. Device characterization again indicated increases in open-circuit voltage and fill factor on the sodium-containing substrate versus the sodium-free substrates. In their paper [20], the authors offered a possible mechanism: "The effect of sodium on the microstructure of the CIS films, together with the observed sodium distribution in the films, *clearly suggests that the sodium enhances the mobility of the film constituents during growth.*" This is similar to the growth model suggested by

Klenk, et al., [21] in which they argue that Cu-Se binary phases may act as a flux during CIS growth.

Another group, J. Holz et al, looked at the effects of sodium on the conductivity of CIS films [22]. They found that room-temperature conductivities of films grown on SLG were approximately two orders of magnitude greater than conductivities of films grown on sapphire. When the films grown on sapphire were implanted with sodium, the conductivities were nearly identical to those grown on SLG. This group also found that barrier layers between the SLG and the CIS, such as SiO_2 or a Mo back electrode, decrease the film conductivity relative to films grown on SLG. They state that other impurities coming from the glass, namely potassium, calcium, magnesium and aluminum, cannot be ruled out as possible suspects, but the sodium implantation experiment gives clear evidence that much of the effect noted previously can be produced by the presence of sodium. This group did see changes in electrical conductivity and photoresponse with the addition of sodium, but no changes were observed in the film morphology. They concluded that the observed higher conductivities are most likely due to "*modified potential barriers at surfaces and grain boundaries*."

The discovery that impurities diffuse out of the glass and into the film during deposition motivated additional studies of the effects of sodium, as well as the impact of the Mo back contact and substrate on film properties. Several groups began investigating the latter in 1994 [23-26], and discovered that sodium diffuses out of the glass, through the Mo and into the growing film. Some significant results concerning the role of sodium from these studies were:

(1) B. M. Basol, et al., [23] found that the degree of sodium diffusion depends on the nature of the Mo. This group also reported that efficiencies of cells fabricated on soda-lime glass are higher than those fabricated on other glass substrates and that the difference between efficiencies on soda-lime glass and other substrates is largest for the lowest CIS stoichiometries (lowest Cu/In ratios). This is an important observation, as it implies that the "*[P]resence of sodium actually increases the processing window of solar cells in terms of usable CIS stoichiometries.*"

(2) D. F. Dawson-Elli, et al., [24] observed increases in open-circuit voltage and efficiency with the presence of sodium, but no correlation of the fill factor with sodium. They speculated that the presence of sodium in CIS films increases the effective hole concentration, causing the observed increase in open-circuit voltage. Since no correlation is observed with the fill factor, they suggest that fill factor and open-circuit voltage are controlled by different mechanisms.

(3) M. Ruckh, et al., [25] added that the sodium content as a function of film composition is largest for slightly Cu-poor films, and decreases as the copper content increases. They were also among the first to publish capacitance data on devices with varying sodium levels. Their analysis of capacitance-voltage data shows a decrease in the space-charge width with increasing sodium. Increased open-circuit voltage correlates with low values of space-charge width. In this case, they found that the changes in V_{OC} could not be explained by improved morphology. They conclude by favoring the model that "*the increased V_{oc} is a consequence of a higher effective acceptor concentration in the absorber material. An explanation could be the neutralization of donor-like Se*

vacancies through a promoted chemisorption of oxygen in the presence of sodium species."

(4) J. H. Scofield, et al., [26] studied the Mo deposition technique and found that sodium impurity levels in the absorber appeared to be independent of the underlying Mo properties. They suggested that sodium impurity levels are thus determined by thermodynamic rather than kinetic factors.

Work performed by V. Probst, et al., [27] supports Scofield's statement concerning thermodynamics. Probst studied the effect of controlled sodium incorporation on rapid thermal processed (RTP) CIGS thin films and devices. RTP films are fabricated using less heat than films fabricated by co-evaporation, which most of the groups cited here thus far have used. Films made by RTP on Mo-coated soda-lime glass had no detectable sodium in them. This group then varied the properties of the Mo back electrode, namely stress, to allow an increase in sodium diffusion, even at low temperatures. They also controlled the sodium in the films by adding a sodium selenide layer between their unmodified Mo and the CIGS. The main changes observed with the presence of sodium were improved morphology (larger grains) and increased film conductivity.

In 1995, strong interest continued in the sodium issue as well as in the overall effects of the Mo back contact and substrate. Many groups recognized the incorporation of sodium in their films, even if they were not studying the issue in detail. Among these subsequent findings are:

(1) S. Zwegart, et al., [28] studied CIGS deposition by sequential deposition of precursors followed by selenization. With regard to sodium, they found that the

"*incorporation of sodium from the glass depends very strongly on the order in which the precursors were deposited in the sequential process*," and that a Cu-rich layer appears to inhibit sodium diffusion. SIMS data demonstrated different sodium signals in the same film correlated with grain size. That is, a structure with smaller grains near the bottom and larger grains on top had a SIMS sodium signal five times larger in the region of the smaller grains. From this they concluded that the enhanced grain boundary surface in the bottom layer allowed a larger amount of sodium segregation, assuming sodium segregates preferentially through the grain boundaries.

(2) R. Menner, et al., [29], studying the Mo back contact, noted that for their work, the presence of sodium did not correlate with an increased efficiency. They therefore concluded that "*above a certain concentration level of sodium incorporation, efficiency seems to be more affected by other parameters like e.g. CIGS deposition temperature*."

(3) Three groups began studying deliberate and controlled incorporation of sodium into CIGS films. C. Heske, et al., [30] compared the effects of sodium segregation from glass with evaporated metallic Na. They found that Na exists as at least two species (metallic, ionic, etc.), and both reduce the work function of the CIGS thin film surface. Also, an increasing amount of sodium increases what they refer to as a local surface photovoltage, due to surface dipoles.

(4) M. Bodegärd, et al., [31] used Na_2S and Na_2Se precursors on sodium-free substrates to study the effects of controlled sodium addition. They found, as with sodium diffusion from the glass, an increase in grain orientation and grain size.

(5) V. Probst, et al., [32] similarly used a Na compound in the precursor. They noted an increased uniformity of photocurrents when the Na precursor was used over uncontrolled sodium incorporation from the glass. They also noted an improvement in grain size. Their device work showed the most significant enhancement in fill factor and short-circuit current.

In 1996, more emphasis was placed on understanding the role of sodium. Three papers investigated the chemistry of the sodium found in CI(G)S films [33-35]. T. Tanaka, et al., [33] suggested that for relatively high sodium levels in CIGS, there is a transition to an ordered vacancy chalcopyrite structure. B. J. Stanbery, et al., [35] suggested the formation of a surface-segregated quaternary Na-Cu-In-Se compound. Other groups continued to investigate sodium's electronic effects [36-39]. T. Nakada, et al., [36] found that the addition of sodium allowed a wider range of off-stoichiometric CIGS-based devices, supporting Basol's earlier findings, and attributed the improved efficiency (relative to the same Cu/[In+Ga] ratio without Na) to an increased acceptor concentration. U. Rau, et al., [37] identified a "*Na-induced, shallow, acceptor-like defect at about 75 meV from the valence band.*" They also attributed the improved device performance to an increase in free carrier concentration by this acceptor state. Another result from their work is that "Na-rich" samples showed a decreased drift length in the space-charge region and a decreased effective diffusion length in the neutral region compared to samples with five times less sodium. This, along with Menner's observations, show that there is a limit to how much sodium is needed to improve device performance.

In 1997, interest focused on gaining an understanding of the role of sodium in CIGS materials, as well as additional information from different materials techniques. Two papers suggested, each from a different perspective, that the presence of sodium suppresses the formation of the β-phase of CIGS, allowing a wider range of useful compositions [40-41]. These findings strengthen Basol's and Nakada's findings. B. M. Keyes, et al., [42] stated that the change in V_{OC} observed in their samples cannot be explained simply by the increase in carrier concentration. Fourier transform photoluminescence data showed the removal of a low-energy peak with the addition of sodium, and defect-level trap spectroscopy data demonstrated a reduction in majority-carrier traps and an almost complete suppression of minority-carrier traps with sodium, suggesting that the presence of sodium removes midgap states. These findings take much of the previous understandings one step further. M. A. Contreras, et al., [43] found from X-ray diffraction measurements that the incorporation of sodium at high levels leads to the formation of secondary phases. From photoluminescence data they found a decrease in both high and low energy transitions when sodium was added. They suggested that "*the formation of donor point-defects (In_{Cu}) is inhibited by a finite Na substitution for the In_{Cu} antisites.*" Niles, et al., [44] used XPS and Auger techniques to determine where the sodium resides and how it is bonded. They found that sodium is bonded to selenium, the sodium concentration in the film is typically ~ 0.1 at%, and the majority of both sodium and oxygen is at the grain boundaries. Sodium and oxygen concentrations in the bulk were found to be below instrument detection limits.

In 1998, Kronik, et al., [45] proposed a model based on data presented in the literature. They proposed that sodium acts as a catalyst to oxygen at surfaces, polarizing

the O-O bond to enhance the formation of O_2^-, which in turn dissociates and fills selenium vacancies. This model is theoretical thus far.

Table 2.1 outlines the main experimental findings with regard to sodium of most of the authors mentioned above. The table is used to draw out general trends from the literature, and hence, some authors and findings are omitted. The main effects of interest presumed to be due to the presence of sodium listed here are: 1. increase in grain size; 2. increase in preferred orientation; 3. increase in conductivity; 4. increase in hole concentration (hc) and/or decrease in space-charge width (scw); 5. increase in device performance as evidenced by increases in open-circuit voltage (V_{OC}), fill factor (FF), efficiency (η), or short-circuit current (J_{SC}); 6. increase in the CI(G)S processing window; 7. a dependence of sodium incorporation on CI(G)S stoichiometry/molecularity; 8. the observation of a sodium saturation limit. A blank space in a given column indicates no information was reported regarding this effect. Effects observed are marked with a "yes" or "no" and the details are indicated where appropriate.

The combined findings with respect to the Mo back contact and sodium are not fully consistent. It appears from these data that sodium diffusion through Mo depends on both the Mo and CI(G)S deposition processes. This makes sense as the porosity of the base materials depends very strongly on the deposition processes. Much evidence points to the mechanism of sodium improving grain size and structure, but there is also evidence that shows improvements in electrical properties with no observed change in structure. Some authors discuss sodium at the surface and the effects of oxygen, yet they have not considered how this may change when the top layers are deposited to form the device

structure. Many authors suggest mechanisms affected by sodium, but none to date gives a comprehensive explanation of the observations.

This now leads to the purpose of this thesis. The evidence given above shows improvements in device performance, improvements in material quality, and possibly a widening of the Δx window for device-quality $CuInSe_2$ with sodium. It has not been clear how much sodium is needed for these changes to occur, and there is disagreement where the sodium resides. Much has been speculated as to the mechanisms involved. This work will shed light on the above three areas, and add information to other areas as well.

Table 2.1. List of main findings by author in the literature on the "sodium issue."

Author	Experimental Emphasis	GS	OR	σ	HC/SCW	Device Perf.	PW	Cu/In	SL	Other
Hedström, 1993	Substrate investigation	yes	yes			yes: V_{OC}, FF				
Bodegärd, 1994	Film stress vs. impurities	yes	yes			yes: V_{OC}, FF				
Holz, 1994	Effect of Na on conductivity	no	no	yes						
Basol, 1994	Mo structure, substrate influence					yes: η	yes	yes		
Dawson-Elli, 1994	Mo structure, substrate influence					yes: V_{OC}, η no: FF				
Ruckh, 1994	Substrate investigation	no	no		yes: scw	yes: V_{oc}		yes		
Probst, 1994	Controlled Na in RTP CIGS	yes		yes						
Zwegart, 1995	Sequential CIGS processing							yes		
Menner, 1995	Sputtered Mo					no: η			yes	
Bodegärd, 1995	Na precursors	yes	yes							
Probst, 1995	Na precursors	yes				yes: FF, J_{SC}				
Nakada, 1996	Controlled Na incorporation				yes: hc	yes: η	yes	yes		
Rau, 1996	Na incorporation				yes: hc				yes	
Herberholz, 1997	Phase segregation						yes			
Stanbery, 1997	Na compound formation						yes			
Keyes, 1997	Electro-optical properties				yes: hc	yes: V_{OC}				
Contreras, 1997	Na precursors			yes						
Niles, 1997-98	Na chemical bonding									Na at surfaces

Key: GS: Increase in grain size. OR: Increase in preferred orientation. σ: Increase in conductivity. HC/SCW: Increase in hole concentration (hc) or decrease in space-charge width (scw). Device Perf.: Increase in device performance as evidenced by V_{OC}, η, FF, or J_{SC}. PW: Increase in the CI(G)S processing window. Cu/In: Dependence of sodium incorporation on Cu/In. SL: Observation of a sodium saturation limit.

CHAPTER 3

EXPERIMENTAL METHOD

Three questions central to the sodium issue are (1) how much is needed, (2) does it affect grain boundaries, the bulk, or both, and (3) what does the sodium do? In order to answer these and other related questions, sodium was added to $CuInSe_2$ material in varying amounts, and the effect on device performance and material properties was studied. This chapter outlines the experimental methods used for solar cell fabrication, sodium incorporation, materials analysis and device analysis.

3.1 Solar Cell Fabrication

The solar cells used in this study were fabricated at the National Renewable Energy Laboratory (NREL). Six different Mo-coated substrates were used, including sodium-containing and non-sodium-containing substrates. The differences among the substrates will be outlined in the next chapter. Coevaporation of p-type $CuInSe_2$ followed the Mo-layer. A thin layer of n-CdS was then deposited, followed by a bilayer of ZnO for the transparent contact. Metallic grids finished the cell fabrication. Several solar cells were made on each substrate. Details of these processes follow.

Molybdenum: The Mo coating was put down at NREL on four of the substrates used. The standard NREL procedure begins with cleaning the substrates using a soap and

deionized (DI) water scrub. Substrates are then rinsed and soaked in DI water, spun dry, and ultrasonically cleaned. Following this cleaning procedure, a chromium layer the order of 10 nm is electron-beam deposited onto the surface for adhesion purposes. This layer is immediately followed by one layer of approximately 1 μm of Mo sputtered in an argon atmosphere at a pressure of 4 mTorr. The processes used for Mo-deposition on the substrates supplied by Siemens Solar Industries (SSI) and Solarex, Inc. are similar in nature, but the details of the processes are public information.

$CuInSe_2$: The $CuInSe_2$ absorber layers were fabricated by the author in one of the vacuum co-evaporation systems managed by the CIS group at NREL. In this system, the constituent elements - Cu, In, Se, Na-compound - were resistively heated in a bell jar, or vacuum chamber. The substrate and metals were loaded into the chamber, and the bell jar was evacuated to a pressure of approximately $2x10^{-6}$ Torr. An emissions sensor allowed control of the evaporation rates. The substrate was approximately 12 inches above the "boats" that hold the source materials, and it was heated by infrared lamps, controlled by a thermocouple feedback. A mechanical shutter was used to shield the substrate during calibration, warm-up, and cool-down of the source materials. Figure 3.1 demonstrates the configuration of the sources and substrate.

The emissions sensor was used to monitor the flux rates from the copper and indium sources. This technique is quite sensitive and material selective. The selenium source was monitored by a quartz or gold crystal oscillator, which is moderately sensitive and non-material selective. Hence, this sensor needed to be shielded from the other flux sources to accurately monitor the Se flux.

Two processes were used for $CuInSe_2$ fabrication in this study. In the "two-stage process," Cu, In, and Se were co-evaporated to form a Cu-rich layer. Then a layer of In and Se was deposited to result in a Cu-poor film, with a targeted Cu/In ratio of 0.9, approximately 3 μm thick. In the "three-stage process," an In-Se layer was deposited, followed by a Cu-Se layer to bring the film to a Cu-rich composition, and then a final In-Se layer was deposited to make the composition Cu-poor, again with a targeted Cu/In

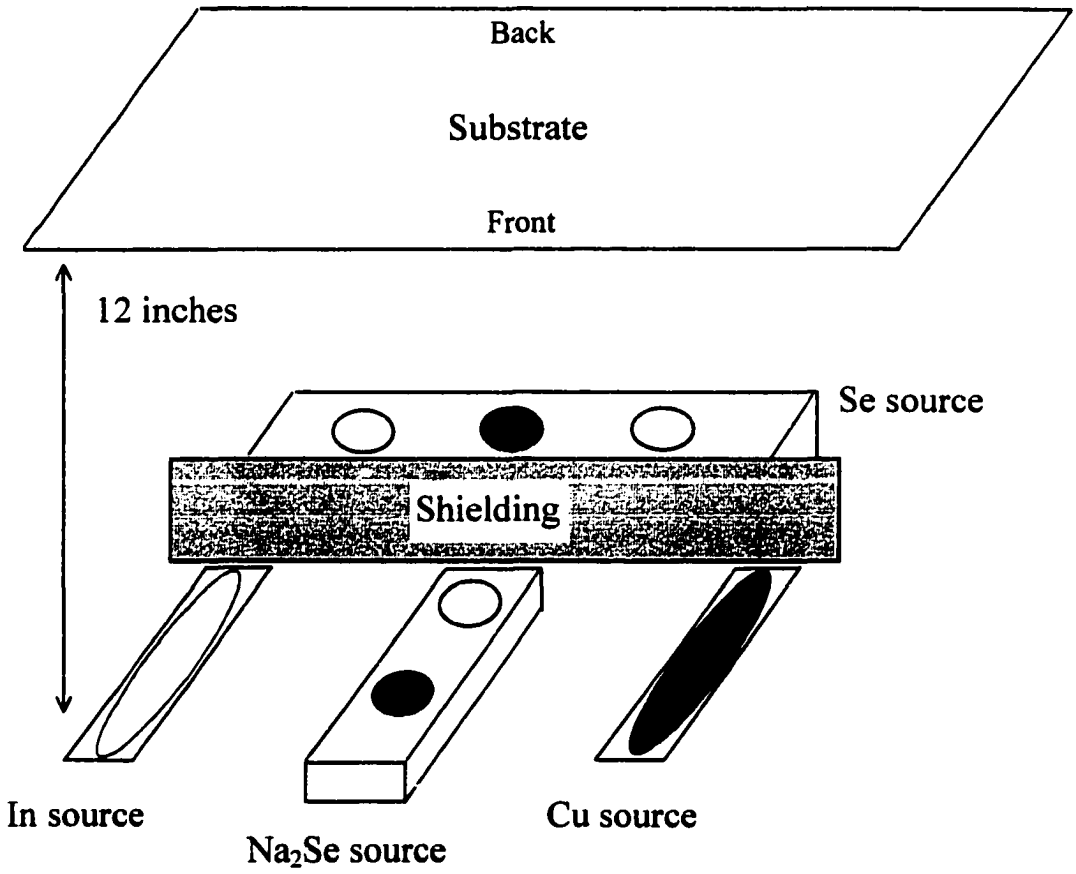

Figure 3.1. Source-substrate configuration in vacuum evaporation system. Not drawn to scale.

ratio of 0.9, approximately 2.5 μm thick. Both processes were performed in a vacuum of between 10^{-6} and 10^{-5} Torr. The exact deposition rates, temperatures, and times are given in the following chapter.

CdS: Following the $CuInSe_2$ fabrication, the CdS buffer layer was deposited. At NREL, chemical-bath deposition (CBD) was used to put down a uniform CdS layer approximately 50 nm thick. An ammonia thiourea bath was used. See reference 46 for details. Following the CBD process, the samples were quickly dried with concentrated nitrogen gas, and then further dried in air at 180 °C for two minutes.

ZnO: A bilayer ZnO transparent contact was RF-sputtered on top of the CdS. The first layer of 50 nm was an intrinsic layer, sputtered from a ZnO target. The second layer was doped with aluminum to be highly n-type. This layer was 300 nm thick and was sputtered from a ZnO target doped with 2 wt% Al_2O_3.

Top contacts: The devices were finished with a Ni/Al grid. 50 nm of Ni was deposited by ion-beam sputter deposition to form a good ohmic contact. The Ni was followed by 3 μm of Al. Typically, nine separate device grids can fit on a 2" x 1" sample.

Device isolation: Once the grids were finished, the sample had to be scribed to isolate the nine devices from one another. A razor blade was used to cut through the top materials to the Mo. Ideally, a 2" x 1" sample yielded nine solar cells, each with an area of approximately 0.43 cm^2. A strip of the top material was scraped off in an inactive region of the sample to reveal a strip of Mo to be used as the second contact. Indium metal was often placed over this strip to aid in current collection. Figure 3.2 demonstrates a schematic of a finished sample.

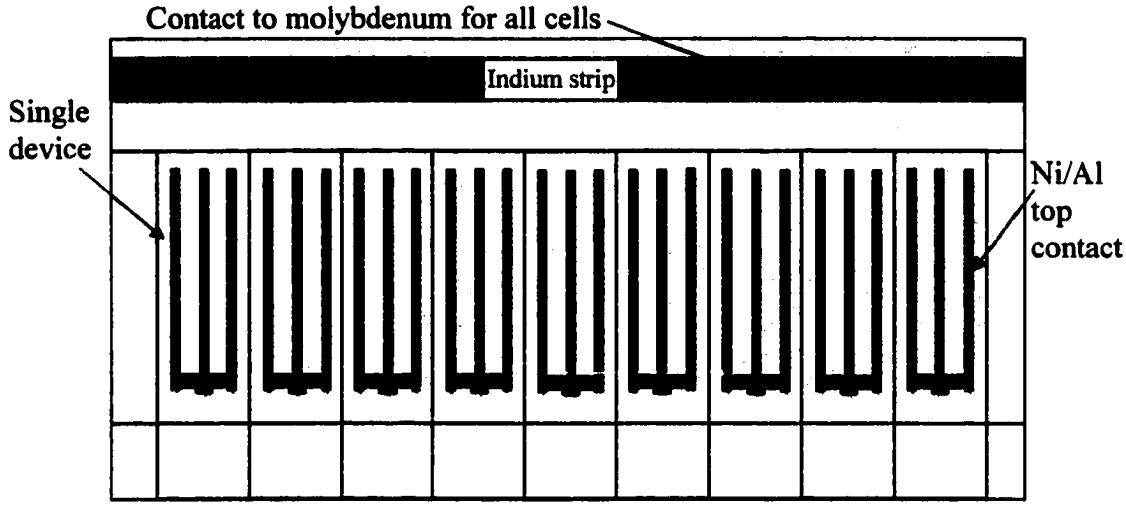

Figure 3.2. Example of a finished $CuInSe_2$ sample with nine 0.43 cm^2 solar cell devices.

3.2 Sodium Incorporation

Sodium was first introduced into $CuInSe_2$ films inadvertently because it diffused out of soda-lime glass substrates during film deposition. Although this additional sodium turns out to be helpful, it is difficult to control and quantify the sodium from such a source. By adding sodium to the film during growth, and using both sodium-containing and non-sodium-containing substrates, the amount of sodium in the film could be better controlled. The sodium source used for the experiments in this thesis was an anhydrous, powdered form of Na_2Se. Although this salt is not very stable, its usage avoids the introduction of other contaminants that using Na_2S or NaF, other readily available options, may do.

Adding the sodium controllably was a challenging task. It would have been useful to introduce a detector similar to those used to control the metals. Unfortunately, this option was unavailable at the time. Instead, a timing and weighing method was used.

A closed, baffled boat was used for the sodium source to avoid problems associated with evaporation of powders from an open boat. Such problems include incomplete evaporation or loss of material due to "popping" out of the boat. In the baffled boat configuration, the charge is placed in one side of the boat and covered. As the boat is heated and the source evaporates, the sodium compound must pass through a series of baffles before being released into the vacuum. The baffles insure that only the gaseous phase is released into the chamber. This also provides a steadier evaporation rate for Na_2Se than an open boat. See Figure 3.3.

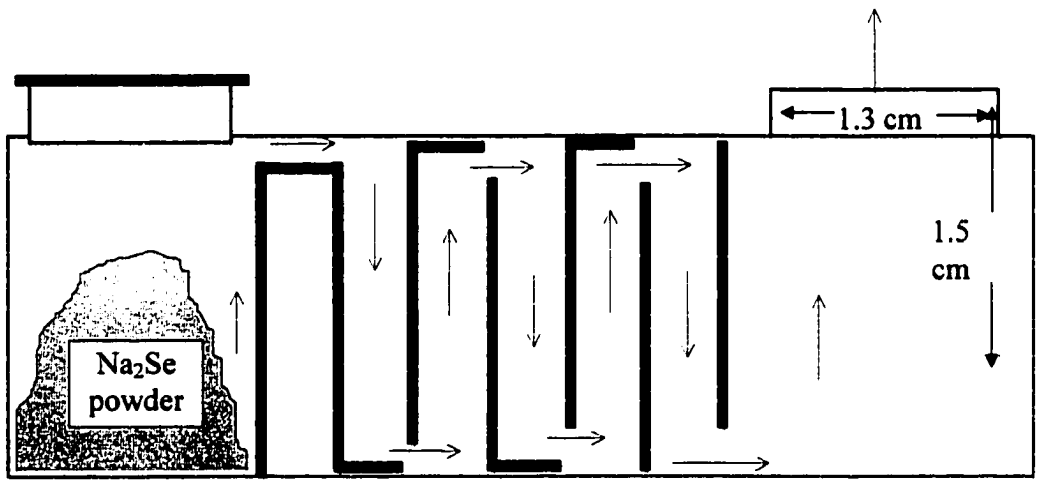

Figure 3.3. Baffled boat used for Na_2Se evaporation. The arrows indicate the path followed by the Na-Se gas.

The initial Na_2Se charge was weighed in the boat prior to the $CuInSe_2$ run. Between 500 and 700 mg were used, and a new charge was used for each run. Since the anhydrous powder absorbs water from the atmosphere easily, weighing was the final step in the run preparation process. The boat was then placed in the chamber, and evacuation begun as quickly as possible following the weighing step. It took approximately five minutes from when the charge was added to the boat until the chamber was closed. It

then took 1-2 hours to pump the chamber to $2x10^{-6}$ Torr, the usual chamber base-pressure for $CuInSe_2$ fabrication. This method allowed better reproducibility and control than other attempted methods.

One of the problems observed in the initial sodium-incorporation runs was that the Na_2Se source, if evaporated at a high rate, would flood the other detectors and make controlling the other elements difficult. To avoid this, the sodium was added at a low and steady rate. A calibration step was performed first that consisted of evaporating the sodium salt by itself in the evacuated chamber. The rate could be fairly well-controlled by observing the pressure change as the current through the boat was increased, and the amount evaporated could be controlled by maintaining a given pressure for a certain amount of time. The boat was weighed again immediately upon opening the chamber. The difference between the initial and final weights was assumed to be the amount of Na_2Se evaporated. By keeping track of the currents applied, the change in chamber pressure, and the evaporation time for a given amount of sodium, the process could be quantified during a $CuInSe_2$ deposition without requiring a sodium detection source. Once the sodium boat had been calibrated, the $CuInSe_2$ run was performed using the same sodium boat. Ideally, this run immediately followed the calibration.

Six Na_2Se addition levels were used in each sample set (Set I used the two-stage $CuInSe_2$ process and Set II used the three-stage $CuInSe_2$ process). The addition levels were chosen to give a broad range of targeted sodium concentrations.

The targeted sodium concentrations were calculated assuming the Na_2Se dissociates upon evaporation. This assumption appears to be reasonable since no evidence of Na_2Se as a compound was found in $CuInSe_2$ films made using this process.

Hence, the Na and Se ions can be treated as an ideal gas in the classical limit. The mean-free path ℓ is given by:

$$\ell = \left(\sqrt{2}\pi d^2 n\right)^{-1} \tag{1}$$

where d is the particle diameter and n is the gas density. Assuming an ideal gas:

$$PV = nRT\,. \tag{2}$$

Using these two equations, the mean-free path length for a Na ion at the working temperature and pressure in the vacuum chamber during deposition can be calculated. For a chamber temperature of 623 K and a chamber pressure of 10^{-5} Torr, the sodium mean-free path length $\ell_{Na} \sim 10$ meters. Using the same assumptions, $\ell_{Se} \sim 5$ meters. The distance between the source boats and the substrate is 35 cm. Therefore, molecular motion within the Na-Se gas will be very nearly ballistic. Using this assumption, the space into which this gas evaporates is limited by the geometry of the system. The details are unimportant, since they simply yield a working estimate of the sodium concentration. The measured sodium concentrations will prove to be much more interesting.

In each sample set, one run was performed with no added sodium. Four runs spanned low-to-moderate Na_2Se addition levels, ranging from 4 mg to 100 mg. One run had a high Na_2Se addition level of more than 200 mg. This resulted in targeted sodium concentrations ranging from 0 to 10 atomic percent sodium (at% Na). The next chapter outlines the Na_2Se addition levels used.

Following the absorber runs, part of each sample was used for materials characterization and part was made into devices, which were then characterized.

3.3 Material Characterization

It is important to probe the absorber material itself to see what changes occur as a result of sodium incorporation. The important features to probe are sodium concentration, film composition, structural and morphological changes, and any differences in junction quality.

It is important to probe the film composition for several reasons. As mentioned in Chapter 2, empirically there is a small window of values of off-molecularity (Δx) that results in good-quality solar cell material. It is important to know that the composition of the films used lies within this window, and whether sodium incorporation affects Δx. Although specific Δx values are targeted during $CuInSe_2$ film growth, run-to-run changes in the evaporation system may cause deviations from the compositional target. The physical set-up of the evaporation system also causes a spread of Δx values across the substrate. Finally, evaluating the amount of sodium incorporated into the films is imperative for this thesis. Three measurement techniques were used to determine the chemical composition of the films: electron probe microanalysis (EPMA), inductively-coupled plasma spectroscopy (ICP), and secondary-ion mass spectroscopy (SIMS).

EPMA is a non-destructive process. It can provide an average composition of a local area and can easily check spatial uniformity. Typically, a strip 2 cm x 0.20 cm from each (or one representative) substrate was used and ten points were probed along the length of the strip. Since the composition varied across the substrate, this gave both an average composition and the spread. It is important to point out the limitations of this technique. EPMA requires a highly-conductive material for accurate results. For a high quality, highly conductive $CuInSe_2$ sample, a 20 kV electron probe samples

approximately the first two microns of the film. For lighter elements (below Al), concentrations as low as 1 at% can be accurately detected. For heavier elements, the accuracy drops to approximately 2 at%. EPMA is a good technique to use for an accurate measure of Δx values, but, due to its sensitivities, it cannot be used to determine the relatively low sodium concentrations expected in the films used in this thesis.

ICP is a destructive technique. It provides a measure of the average composition for the piece of material used. The film is dissolved in an acid solution and the composition is therefore averaged over a larger area than the spot size used in EPMA. ICP is used in conjunction with EPMA since ICP has a lower detection limit of 0.1 atomic percent. This technique is used mainly to determine the sodium concentration in the absorber for concentrations greater than 0.1 at%. The same strips of material that were probed by EPMA were used for ICP analysis.

SIMS is also a destructive technique, but it can detect elements with concentrations as low as 0.00001 at%, and has the added benefit of determining the distribution of elements through the thickness of the film. Such a compositional profile is beneficial as it allows a measurement of very low sodium levels and demonstrates the distribution of sodium. The SIMS technique used for these samples uses an analysis area of approximately 60 microns in diameter, using Cs ions as the ion probe. Figure 3.4 shows the results of a typical SIMS run for one $CuInSe_2$ sample. The Cu, In, Se, and Mo counts are actually the elemental response plus the Cs ion response in that region. The elemental ion count levels do not directly translate into concentrations. For example, the

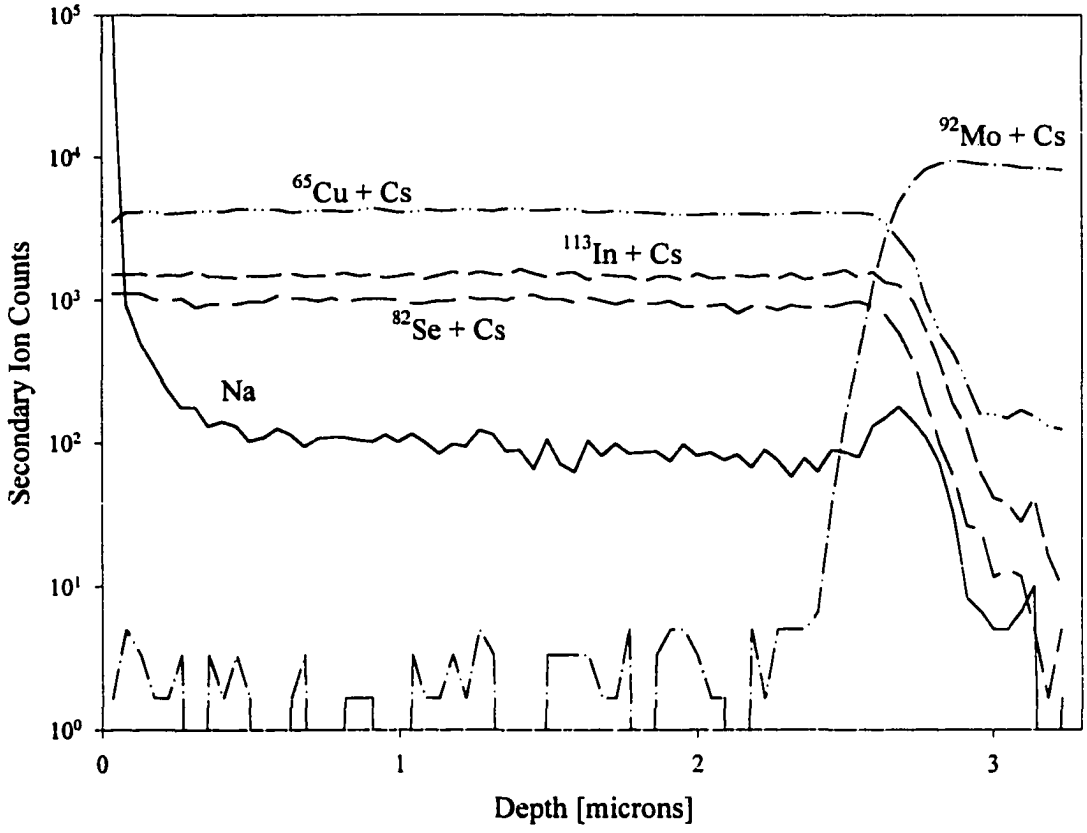

Figure 3.4. Typical SIMS results. $CuInSe_2$ sample on Mo/Alumina, no Na_2Se added.

Cu count rate in Figure 3.4 is five times higher than the Se response, but the Se concentration is more than twice that of Cu. The levels recorded during a SIMS measurement are useful in a comparative way, and an atomic concentration can be extracted if an appropriate calibration sample is used for which the concentrations are known. The Figure 3.4 sample used an alumina substrate and no sodium was added. The Na signal therefore demonstrates the background Na level of the instrument or sodium contamination during handling, and corresponds to essentially a zero sodium concentration in the $CuInSe_2$. A word needs to be said about the large Na signal near 0 μm. Due to the nature of a SIMS technique, which relies on a dynamic equilibrium between the probe beam and the analysis beam for an accurate measurement, sputtering

of the first 5-10 monolayers of the sample does not occur in equilibrium. Therefore, interpretation of the data from these first few layers is difficult and little weight is placed on data from this region in this thesis.

Chapter 2 outlined the structure of single-crystal $CuInSe_2$, and showed the differences between this ideal structure and the thin-film case. Some researchers have observed structural changes in $CuInSe_2$ with the addition of sodium [19-20, 30, and 43]. In this thesis, X-ray diffraction (XRD) was used to probe the structural and phase changes observed in the absorbers as a function of sodium incorporation. This information will help determine the role sodium plays in improving device performance. Figure 3.5 gives

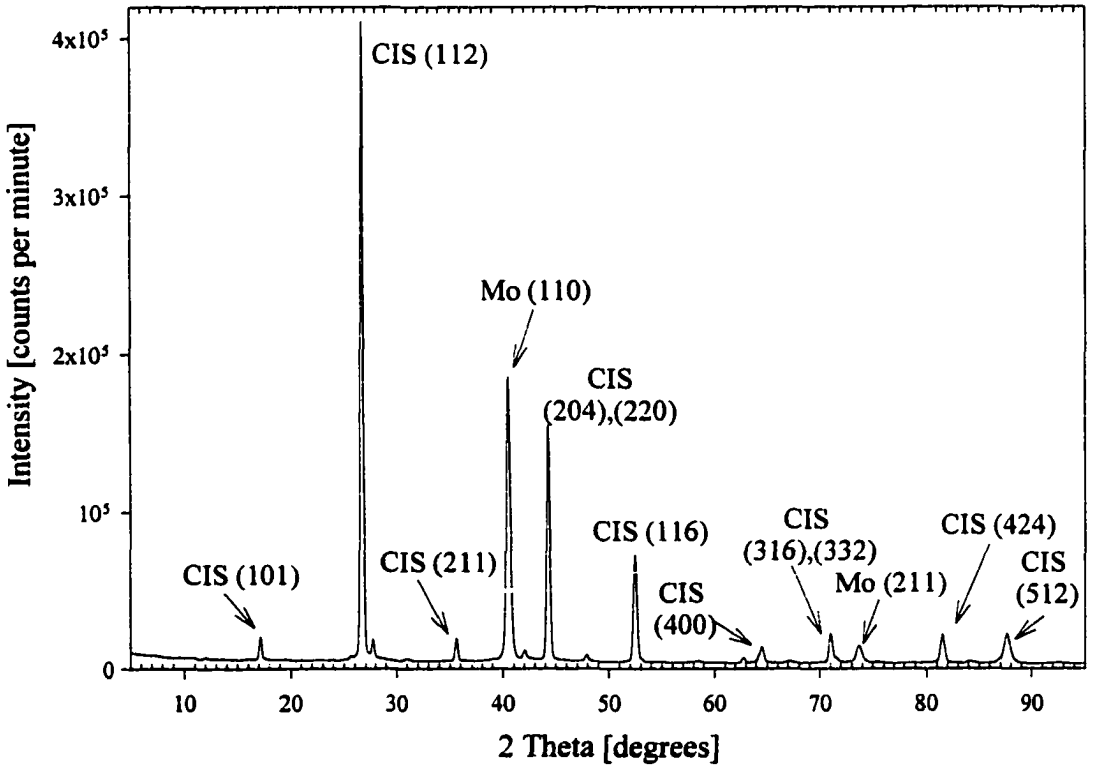

Figure 3.5. Sample XRD spectrum for $CuInSe_2$ on Mo/SLG. The main Mo and $CuInSe_2$ peaks are marked.

an example of XRD data on one absorber on soda-lime glass with no Na_2Se added. In this figure, the main $CuInSe_2$ peaks and the main Mo peaks are marked. As mentioned in the previous chapter, the (112)/[(204),(220)] ratio may indicate the degree of structure and orientation of the $CuInSe_2$ grains. Here, this ratio is approximately 2.5, indicating a more randomly oriented (or less structured) film. This is also evidenced by the relative peak heights of the other main $CuInSe_2$ peaks. In a highly structured film, these peaks are often much weaker than the (112) peak. In this figure, the Mo and α-phase $CuInSe_2$ account for nearly all the peaks. There are no Cu_2Se or $CuInSe_2$ β-phase peaks evident.

Many groups have reported the effects they observed on grain size when sodium was present in $CuInSe_2$ [19-21, 24, 26, and 30-31], but the results have not been consistent. In this study, scanning electron microscopy (SEM) was used to look at the grains, topography, and morphology on a sub-micron level. The use of SEM allows a comparison of grain size and structure as well as detection of variations in structure from the ideal $CuInSe_2$ case. It can also give an indication of the presence of impurities or new phase formation. SEM is used here to probe these characteristics as a function of sodium content.

One way to probe the junction formation is to use electron-beam induced current (EBIC) measurements. In EBIC measurements, an electron beam bombards an electrically active sample, and the induced current is measured and superimposed on an SEM cross-sectional image. This allows one not only to compare the relative strength of the response (collection efficiency), but also to locate the peak position within the sample. The peak of the signal is generally taken to be at or very near the electrical junction. This technique can therefore probe changes in junction position. By recording EBIC scans

across the sample (termed "y-modulated EBIC"), the uniformity of the junction can also be examined. Each of these responses gives insight into overall junction quality.

3.4 Device Characterization

Although material characterization is necessary to determine the effects of sodium on the overall structure and composition of the absorber, if there are no corresponding changes in device performance, then the effects of sodium incorporation do not directly impact the final product, a finished solar cell for use in the field. Therefore, probing variations in device characterization with sodium conditions is clearly necessary. Three main measurement techniques were used by the author to evaluate the solar cells used for this thesis: current-voltage, capacitance, and quantum efficiency.

Current-voltage (JV) curves were taken in the dark and in the light under one sun, air mass 1.5 conditions [6] at 25°C. The light JV curves provided values of open-circuit voltage (V_{OC}), short-circuit current density (J_{SC}), and the maximum power point ($P_{max} = V_{mp} \times J_{mp}$). From these values, the fill factor (FF) and efficiency (η) were calculated, as described in Chapter 2. From the diode curves (JV curves), values of series resistance (R_{series}), shunt resistance (r_{shunt}), and diode quality (ideality) factor A, were extracted [15]. Figure 3.6 is an example of a typical set of JV curves.

Measuring JV curves and calculating the corresponding parameters as a function of sodium incorporation serves two purposes. (1) The results of the JV analysis will help determine a sodium concentration or range of concentrations for which device performance is optimized, and (2) the affected parameters will give insight into the mechanisms influenced by the presence of sodium.

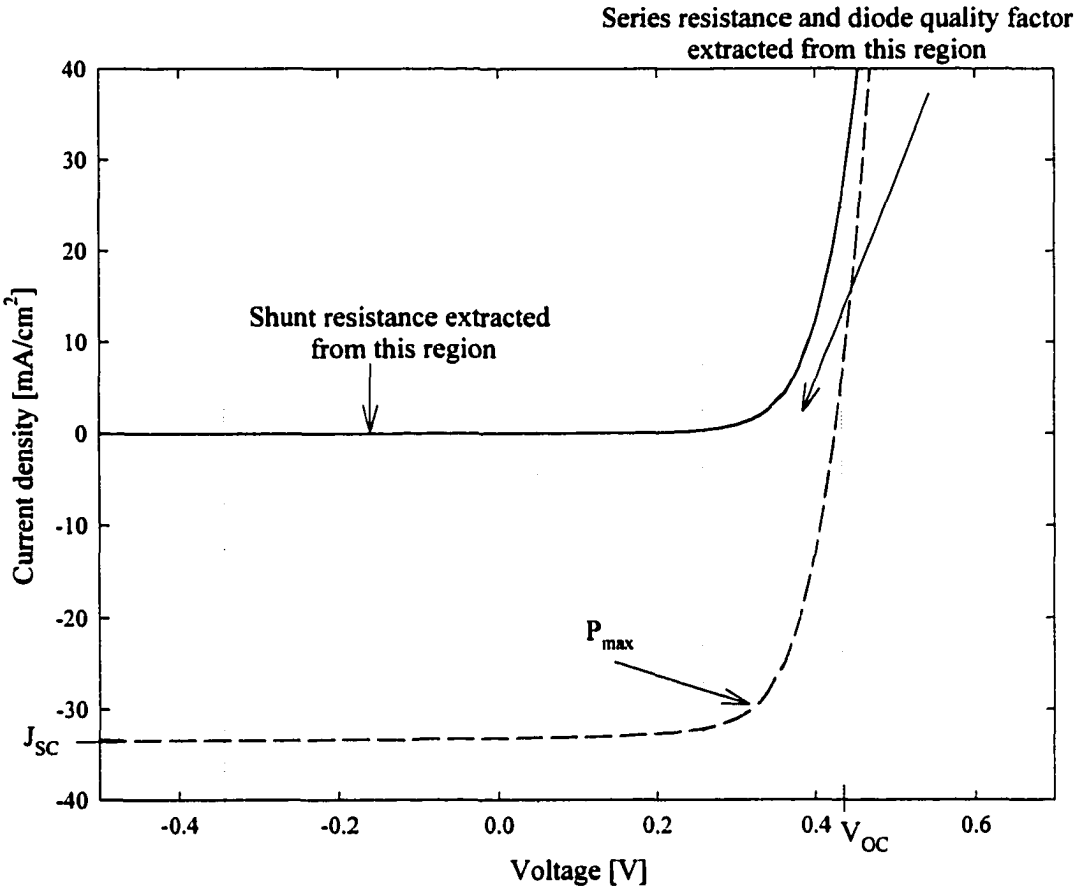

Figure 3.6. Typical $CuInSe_2$ dark (top) and light JV curves. The dotted vertical lines indicate the regions of the curves used for diode parameter calculation.

Capacitance measurements were made to calculate the effective hole or dopant density, and the effective depletion width. These parameters are important to know as a function of sodium concentration since each will give insight into the mechanisms affected by the presence of sodium.

Since thin-film $CuInSe_2$ solar cells have a high number of trap states with various time constants, capacitance versus frequency measurements at various dc bias voltages were performed first to determine a measurement frequency range over which the solar

cell acts reasonably like a parallel-plate capacitor at the bias of interest. Once a frequency in the middle of this range was determined, capacitance versus voltage measurements were performed by applying a small oscillating voltage at the ideal frequency imposed on the dc bias voltage. Depletion width and hole density were then extracted [24].

Figures 3.7.a-c give examples of these measurements and the results of the corresponding analysis for a typical $CuInSe_2$ device. Figure 3.7.a. demonstrates capacitance-frequency data on a typical $CuInSe_2$ solar cell used in this thesis at four dc bias voltages. The curves are fairly flat between 5 kHz and 400 kHz. The curvature below 5 kHz is due to charge transfer in and out of extraneous states whereas the curvature above 400 kHz is due to inductive effects in the measurement circuit. For this cell, a frequency of 75 kHz was chosen for capacitance-voltage measurements. In Figures 3.7.b. and 3.7.c., there are two curves. The one referred to as "Downsweep" indicates the voltage was swept from forward bias to reverse bias, whereas "Upsweep" indicates the voltage was swept from reverse bias to forward bias. The hysteresis observed is typical and may be an indication of the number and type of trap states. For the cells used in this thesis, all capacitance-voltage measurements were performed at an appropriate frequency. The data used is the downsweep data. All hysteresis was typical, so the data used gives an accurate comparison of capacitance and extracted hole concentration and depletion width values.

The light JV curve determines the short-circuit current, which is the light-induced current at zero voltage. As explained in Chapter 2, this value rarely matches the maximum light-induced current possible for a given bandgap. One way to gain insight into the reasons for this difference is to perform a spectral response measurement. In this

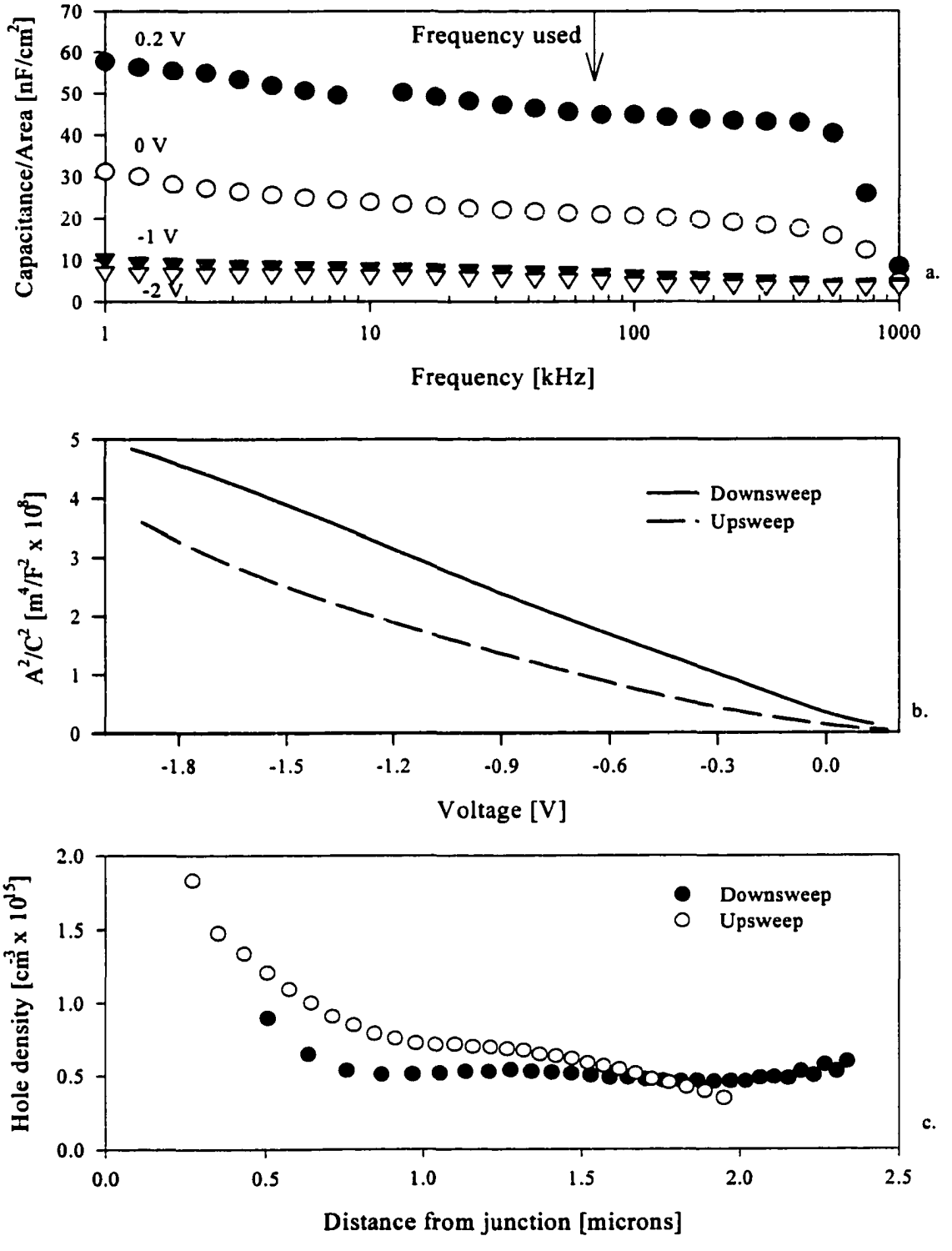

Figure 3.7. Typical capacitance-frequency curves (a.), capacitance-voltage curves (b.), and the corresponding hole density vs. distance from junction curves for thin-film, $CuInSe_2$ solar cells.

measurement, light of different wavelengths is incident upon the device and the current is collected. This measures the response of the device at each wavelength. Weighting the response by the solar spectrum [6] results in a quantum efficiency curve. See Figure 3.8 for an example for a $CuInSe_2$ test solar cell on a Mo/soda-lime glass substrate.

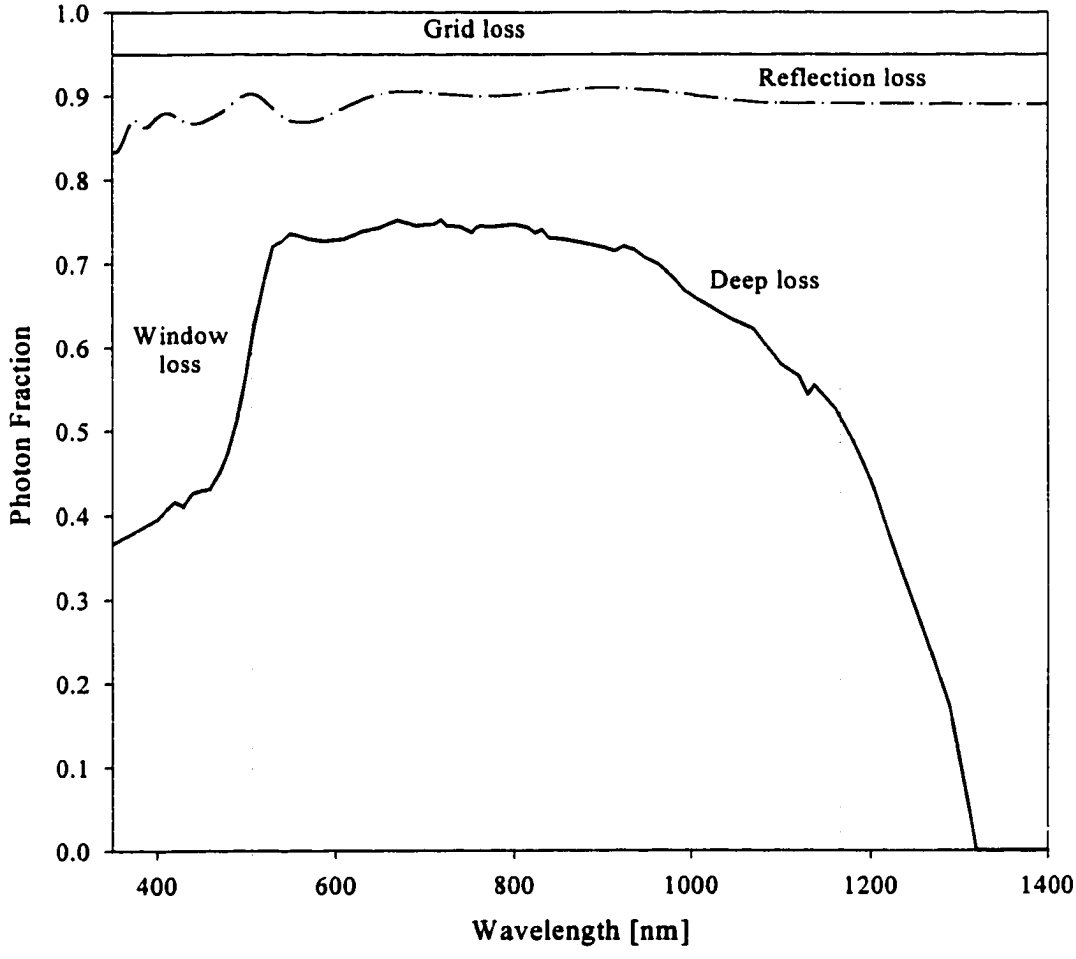

Figure 3.8. Example quantum efficiency curve for a $CuInSe_2$ device. Reflection and grid losses are also shown.

Multiplying the spectral response curve by the solar spectrum and integrating over the wavelength range of interest results in the light-induced current. This is always less than the maximum light-induced current due to various current losses. For $CuInSe_2$ solar cells, there are five main areas of current loss: grid loss, reflection loss, window loss, deep penetration loss, and wavelength-independent loss. These are shown in Figure 3.8. The grid loss is simply the percentage of the total area of the device covered by a grid. For the samples used in this thesis, grid coverage is 4-5%. Hence, up to 5% of the maximum possible current is lost. The reflection curve is obtained from a spectrometer measurement of the front surface of the solar cell, avoiding grid coverage. The window loss is a measure of the light absorbed in the top layers of the solar cell, in this case, the ZnO and CdS. Deep penetration loss refers to those photons that generate carriers toward the back of the device that recombine before reaching the depletion region.

In the ideal case, there is no separation between the reflection loss curve and the maximum of the quantum efficiency curve. Any such separation is a measure of the "wavelength-independent" loss; perhaps due to a high number of recombination centers or trap states that limit the total current.

There is some collection beyond the bandgap of the cell shown (1.0 eV, 1240 nm). This may be due to impurities or defects that introduce allowed energy levels into the normally forbidden bandgap. In this way, light with energy less than the bandgap energy may excite carriers and be collected.

As with JV and capacitance data, comparing QE data and the associated current losses as a function of sodium content will provide information about the mechanisms involved.

CHAPTER 4

THE EXPERIMENTS

Two sets of experiments were performed to investigate the effects of sodium incorporation on $CuInSe_2$ thin film material and on the resulting solar cell performance. In the first set of experiments (Set I), $CuInSe_2$ was grown by a two-stage process and Na_2Se was evaporated during the first stage. In the second set of experiments (Set II), $CuInSe_2$ was grown by a three-stage process and Na_2Se was evaporated during the second stage. Most of the materials analysis is the same for the two sets, and all device characterization is the same.

4.1 Set I

Substrates

In the first set of experiments, a total of six sodium concentrations were incorporated into the $CuInSe_2$ by adding different amounts of Na_2Se during the $CuInSe_2$ deposition onto four Mo-coated substrates: smooth alumina with NREL Mo; soda-lime glass (SLG) with NREL Mo; soda-lime glass with Siemens Solar Industries (SSI) Mo; and soda-lime glass with Solarex, Inc., Mo. The alumina substrate contains no sodium. Therefore, the only sodium present in the absorber films grown on this substrate is due to that added during deposition. The three soda-lime glass substrates allow different

amounts of sodium to diffuse out of the glass, through the Mo, and into the film, due mainly to differences in the Mo deposition processes. These amounts will be quantified in the next chapter.

The Set-Up

Eight 2" x 1" substrates can fit in the substrate holder in the S-system evaporator at NREL, which this author used to fabricate all the absorbers for this thesis. To study device and material properties, two 2" x 1" samples of each substrate type were used in each $CuInSe_2$ deposition, placed side by side. One sample was made into devices as described in the previous chapter, while the companion sample was used to study the material. Figure 4.1 illustrates the substrate configuration. The same configuration was used for each $CuInSe_2$ deposition run.

The $CuInSe_2$

The "two-stage" process was used in this set of experiments. A Cu-rich layer of $CuInSe_2$ was deposited first, followed by an In-Se layer to make the final film Cu-poor. Table 4.1 outlines a typical two-stage run. This recipe is based on the results of previous work, particularly that of Tuttle [8] and Gabor [9]. The exact rates and times are adjusted to give the desired Cu/In ratio when the deposition is complete. For p-type $CuInSe_2$, the Cu and In are deposited in an over-pressure of Se, usually 2-3 times the equivalent rate of the metals.

It is important to know the flux equivalent of a rate of 1 Å/sec for each metal to correctly manipulate the recipe, assuming the product is α-phase $CuInSe_2$. Table 4.2 gives the fluxes and densities of the metals used. The flux can be defined as the number

of atoms per unit area, per unit time, incident on the substrate. These flux equivalents were calculated and determined previously by Tuttle [8].

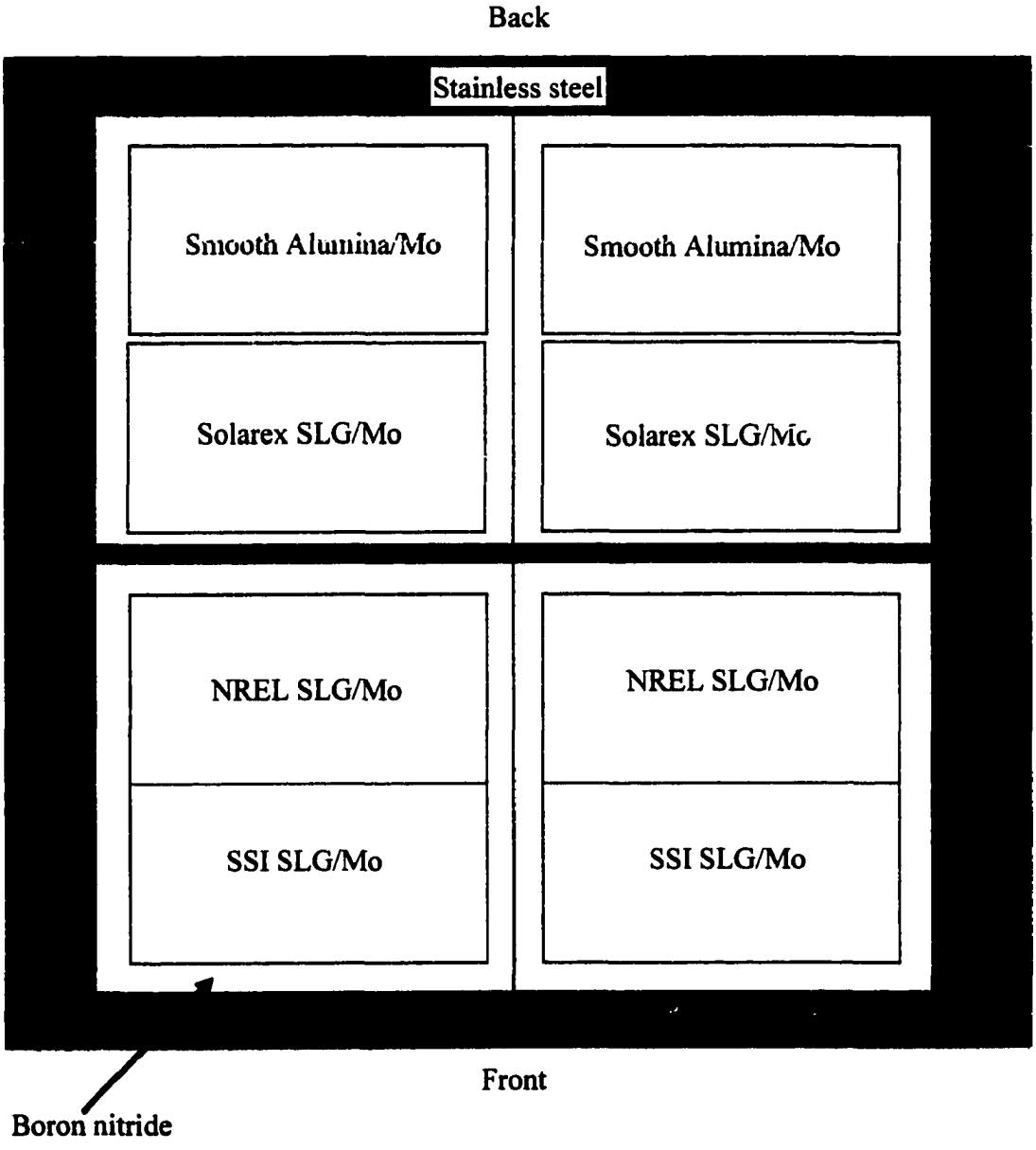

Figure 4.1. Substrate configuration for the first set of $CuInSe_2$ experiments, top view. The substrates are placed in the holder Mo-side down.

Table 4.1. Sample two-stage $CuInSe_2$ process including rates, temperatures and times.

Layer	Cu rate [Å/sec]	In rate [Å/sec]	Se rate [Å/sec]	Set Temp. [degrees C]	time [minutes]
1	3.28	6.0	30	400 to 600	18
2	--	6.0	25	600	8
finishing	--	--	20	600 to 400	3

Table 4.2. Fluxes and densities of the metals used.

	Flux (for a rate of 1 Å/sec)	Density (g/cm^3)
Cu	8.46×10^{14} atoms/sec-cm^2	8.93
In	3.83×10^{14} atoms/sec-cm^2	7.30
Se	3.68×10^{14} atoms/sec-cm^2	4.82

Once the appropriate recipe was calculated and the chamber was evacuated, the source boats were slowly warmed until the desired rates were achieved. The monitor temperature was brought up to 400°C while the substrates were shielded from the sources with a shutter. When everything was ready, the shutter was opened and the run began. The temperature was maintained at 400°C for 5 minutes, then ramped up to 600°C at a rate of 40 degrees per minute, and maintained at 600°C until the end of the second stage. At that point, the In was turned off and the temperature was allowed to drop to 400°C in an over-pressure of Se. It is commonly known that this step prevents re-evaporation of the material. The substrate was allowed to cool to room temperature in vacuum before it

was removed. Na_2Se was added during the first stage, after approximately 20% of the Cu-rich $CuInSe_2$ had been grown. Na_2Se evaporation times ranged from two to fourteen minutes.

Table 4.3 outlines the rates, temperatures, and times used for the depositions, as well as the amount of Na_2Se added, for the first set of experiments. The run numbers refer to the sequential designation system used by the CIS group at NREL.

One difficulty found in using the weighing and timing method to calibrate the Na_2Se evaporation was that residual Cu, In, and Se was left on the Na_2Se boat due to the nature of the evaporation and the geometry of the system. Calibration runs in which no Na_2Se was evaporated resulted in between 2 mg and 8 mg of metal residue, which was measured and compensated for in the Na_2Se measurement.

A word needs to be said about the changes in deposition from run to run. As stated previously, the rates were chosen to yield a desired Cu/In ratio. However, slight changes in the system, such as calibration changes or modifications in the detection system, required modifications of the rates. It was difficult to predict these changes, but they were not generally large enough to significantly affect the results. Often, compensating adjustments were made after analysis of the previous deposition. This will be evident in the comparison of the electron-probe microanalysis (EPMA) results versus the expected results, shown in the next chapter.

The temperatures quoted are the "set" temperatures. The substrate temperature is 20-40 degrees lower than the set temperature due to the placement of the thermocouple used for temperature control. Generally, a set temperature of 400°C yields a substrate temperature at the Mo surface of 380°C, whereas a set temperature of 600°C yields a

substrate temperature of 560°C. These values may vary by +/- 10 degrees depending on the substrate material.

Given the flux equivalents (Table 4.2), the deposition rates, and the deposition times, a target $CuInSe_2$ concentration can be calculated (molecules/cm^2), assuming all the Cu and In atoms incident on the substrate react to form $CuInSe_2$ molecules. Similarly, a target Cu/In ratio can be calculated. These values (targeted $CuInSe_2$ concentration and targeted Cu/In ratio) are included in Table 4.3.

4.2 Set II

Substrates

In the second set of experiments, six different amounts of Na_2Se were added during the $CuInSe_2$ deposition onto four Mo-coated substrates: smooth alumina; sodium-free borosilicate glass; soda-lime glass with a 200-nm SiO_2 sodium diffusion barrier; and soda-lime glass (SLG), all coated with Mo at NREL. In this experiment, three out of the four substrates contained little or no sodium.

The Setup

The substrate setup is similar to that used in the first experimental set, shown in Figure 4.1. The order of the substrates, from back to front: smooth alumina, borosilicate glass, NREL SLG, and SLG plus a SiO_2 sodium-diffusion barrier.

The $CuInSe_2$

The "three-stage" process was used in this set of experiments. An In-Se layer was deposited, followed by a Cu-Se layer to bring the film to a Cu-rich composition, followed

Table 4.3. Two-stage $CuInSe_2$. Six $CuInSe_2$ depositions with different Na_2Se addition levels.

Run	Layer	Cu rate [Å/sec]	In rate [Å/sec]	Se rate [Å/sec]	Set Temp. [degrees C]	time [minutes]	Targeted [$CuInSe_2$]	Targeted Cu/In ratio	Na_2Se added
S989	1	3.28	6.0	30	400 to 600	0 - 18 (Δt=18)	$3.29x10^{18}/cm^2$	0.84	none
	2	--	6.0	25	600	18 - 26 (Δt=8)			
	finishing	--	--	20	600 to 400	26 - 29 (Δt=3)			
S1005	1	3.28	6.0	30	400 to 600	0 - 18 (Δt=18)	$3.29x10^{18}/cm^2$	0.84	4 mg
	2	--	6.0	25	600	18 - 26 (Δt=8)			
	finishing	--	--	20	600 to 400	26 - 29 (Δt=3)			
S1017	1	3.28	6.0	30	400 to 600	0 - 18 (Δt=18)	$3.29x10^{18}/cm^2$	0.84	18 mg
	2	--	6.0	25	600	18 – 26 (Δt=8)			
	finishing	--	--	20	600 to 400	26 – 29 (Δt=3)			
S1024	1	3.86	6.0	30	400 to 600	0 – 18 (Δt=18)	$3.56x10^{18}/cm^2$	0.98	20 mg
	2	--	6.0	25	600	18 – 26 (Δt=8)			
	finishing	--	--	20	600 to 400	26 – 29 (Δt=3)			

S1031	1	3.81	6.0	30	400 to 600	0 – 18 (Δt=18)	$3.53x10^{18}/cm^2$	0.97	41 mg
	2	--	6.0	25	600	18 – 26 (Δt=8)			
	finishing	--	--	20	600 to 400	26 – 29 (Δt=3)			
S1023	1	3.86	6.0	30	400 to 600	0 – 18 (Δt=18)	$3.56x10^{18}/cm^2$	0.98	205 mg
	2	--	6.0	25	600	18 – 26 (Δt=8)			
	finishing	--	--	20	600 to 400	26 – 29 (Δt=3)			

by an In-Se layer to bring the film to a Cu-poor composition. Table 4.4 outlines a typical three-stage run.

Table 4.4. Sample three-stage $CuInSe_2$ process including rates, temperatures and times.

Layer	Cu rate [Å/sec]	In rate [Å/sec]	Se rate [Å/sec]	Set Temp. [degrees C]	time [minutes]
1	--	5.0	25	400	17
2	3.0	--	30	620	16
3	--	3.0	20	620	11
finishing	--	--	20	620 to 400	3

The general procedure followed was similar to that outlined for the two-stage process. There were some subtle differences. In the three-stage process, the In-Se layer was put down at a substrate set temperature of 400°C. At the end of the first stage, the In was turned off and the temperature was ramped up to 620°C in three minutes with only Se running. Once the temperature had stabilized at 620°C, the Cu rate was stabilized and the run continued. After the appropriate amount of Cu had been deposited, the Cu boat was turned off and the In was brought up to the correct rate. At the end of this stage, the In was turned off and the temperature was allowed to drop to 400°C in an over-pressure of Se. The substrate then cooled to room temperature in vacuum before it was removed. In this case, Na_2Se was added during the second stage, after approximately 10% of the Cu-Se had been evaporated. Na_2Se evaporation times ranged from one to fourteen minutes.

The most significant difference between the resulting two-stage $CuInSe_2$ and the resulting three-stage $CuInSe_2$ is grain size. Two-stage $CuInSe_2$ generally yields grains which average 1 μm across, whereas three-stage $CuInSe_2$ generally yields grains

averaging 3-4 μm across. The performance of solar cells made from the two materials is similar. The reason both methods were used was to probe any changes in sodium incorporation due to differences in growth technique, namely the differences in substrate temperature and ordering of the layers (Cu-rich to In-rich versus In-rich to Cu-rich to In-rich) during growth.

Table 4.5 outlines the rates, temperatures, and times used for the depositions, as well as the amount of Na_2Se added. The target $CuInSe_2$ concentrations and Cu/In ratios are also included. The same experimental averaging and uncertainty apply to the Na_2Se amounts quoted as in Set I.

Following the $CuInSe_2$ deposition (both sets), one 2" x 1" sample of each substrate type was made into a device, and the companion sample was used for materials analysis. Device characterization included dark current-voltage (JV) at 25°C, light JV at 25°C under AM 1.5 standard illumination, capacitance-frequency, capacitance-voltage, quantum efficiency, and optical reflection. Materials analysis included EPMA, X-ray diffraction, inductively-coupled plasma spectroscopy, scanning electron microscopy, secondary ion mass spectroscopy, and electron-beam induced current. The device and the materials data will be discussed in the following chapter.

Table 4.5. Three-stage $CuInSe_2$. Six $CuInSe_2$ depositions with different Na_2Se addition levels.

Run	Layer	Cu rate [Å/sec]	In rate [Å/sec]	Se rate [Å/sec]	Set Temp. [degrees C]	time [minutes]	Targeted [$CuInSe_2$]	Targeted Cu/In ratio	Na_2Se added
S1149	1	--	5	25	400	0 - 16:40 (Δt=16.6)	$2.58x10^{18}/cm^2$	0.96	None
	2	3	--	30	620	23-40 (Δt=17)			
	3	--	3	20	620	41-51:30 (Δt=10.5)			
	Finishing	--	--	20	620 to 400	51:30-55:30 (Δt=4)			
S1153	1	--	5	25	400	0 - 16:40 (Δt=16.6)	$2.60x10^{18}/cm^2$	0.95	4 mg
	2	3	--	30	620	23:40-40:20 (Δt=16.6)			
	3	--	3	20	620	42:30-53:30 (Δt=11)			
	finishing	--	--	20	620 to 400	53:30-57:30 (Δt=4')			
S1174	1	--	5	25	400	0 - 16:40 (Δt=16.6')	$2.55x10^{18}/cm^2$	0.91	8 mg
	2	3	--	30	620	23:20-39:20 (Δt=16')			
	3	--	3	20	620	41:50-52:30 (Δt=10.6)			
	finishing	--	--	20	620 to 400	52:30-56 (Δt=3.5)			

S1151	1	--	5	25	400	0 - 16:40 (Δt=16.6)	$2.58x10^{18}/cm^2$	0.96	39 mg
	2	3	--	30	620	24-41 (Δt=17)			
	3	--	3	20	620	42:30-53 (Δt=10.5)			
	finishing	--	--	20	620 to 400	53-57 (Δt=4)			
S1183	1	--	5	25	400	0 - 16:40 (Δt=16.6)	$2.55x10^{18}/cm^2$	0.91	99 mg
	2	3	--	30	620	23:40-39:40 (Δt=16)			
	3	--	3	20	620	41:40-52:40 (Δt=11)			
	finishing	--	--	20	620 to 400	52:40-56:20 (Δt=3.5)			
S1177	1	--	5	25	400	0 - 16:40 (Δt=16.6)	$2.55x10^{18}/cm^2$	0.91	235 mg
	2	3	--	30	620	23:40-39:40 (Δt=16)			
	3	--	3	20	620	42:30-53:30 (Δt=11)			
	finishing	--	--	20	620 to 400	53:30-57 (Δt=3.5)			

CHAPTER 5

EXPERIMENTAL DATA AND RESULTS

The experiments were designed to systematically incorporate different concentrations of sodium into the absorber to determine the effects of sodium on materials and devices. Electron-probe microanalysis (EPMA) measurements determined the composition of the films. Secondary ion mass spectroscopy (SIMS) and inductively coupled plasma spectroscopy (ICP) were used to determine the concentrations of sodium actually incorporated into the films. X-ray diffraction (XRD) and scanning electron microscopy (SEM) were compared to examine the effects of sodium on the structure and morphology. Electron beam induced current (EBIC), current-voltage (JV), capacitance-voltage (CV), and quantum efficiency (QE) measurements on finished solar cells were examined with regard to the measured sodium concentrations to determine the impact of sodium on device performance.

5.1 Film Composition

5.1.1 EPMA

Immediately after completing the $CuInSe_2$ run, a representative strip of $CuInSe_2$ was taken from the samples and submitted for electron probe microanalysis. This technique determines the composition of a film in terms of the atomic percentage of each

constituent. Table 5.1 presents the results for the 20 kV probe for both sets averaged over all the substrates in each $CuInSe_2$ deposition run. These values correspond to the average absorber composition of the devices.

Table 5.1. EPMA results for $CuInSe_2$ experiments, Sets I (two-stage process) and II (three-stage process).

$CuInSe_2$ run, Set I	*Na_2Se added*	*at% Cu*	*at% In*	*at% Se*	*Cu/In ratio*	*Cu/In target*
S989	None	20.83	28.17	51.00	0.74	0.84
S1005	4 mg	21.16	27.74	51.10	0.76	0.84
S1017	18 mg	20.74	27.64	51.62	0.75	0.84
S1024	20 mg	19.18	28.64	52.17	0.67	0.98
S1031	41 mg	22.44	26.87	50.69	0.84	0.97
S1023	205 mg	21.51	26.62	51.87	0.81	0.98

$CuInSe_2$ run, Set II	*Na_2Se added*	*at% Cu*	*at% In*	*at% Se*	*Cu/In Ratio*	*Cu/In target*
S1149	None	21.39	28.00	50.62	0.76	0.96
S1153	4 mg	23.98	25.97	50.04	0.92	0.95
S1174	8 mg	23.52	26.35	50.13	0.89	0.91
S1151	39 mg	22.63	26.75	50.62	0.85	0.96
S1183	99 mg	22.09	26.63	50.48	0.83	0.91
S1177	235 mg	21.00	27.29	51.71	0.77	0.91

Figure 5.1 graphs the ratio of the measured to the targeted Cu/In ratio versus Na_2Se addition level. Aside from some outlying points, there appears to be a trend toward lower Cu/In ratio with increasing sodium. This suggests that the presence of sodium may increase the α-phase window by incorporating more indium into the film (less indium rejection in the final growth stage). It is also possible that sodium forces

copper rejection. Although this behavior is only prevalent at the high sodium addition levels, it may indicate similar behavior at the low/moderate levels, but may be overpowered here by run-to-run variations.

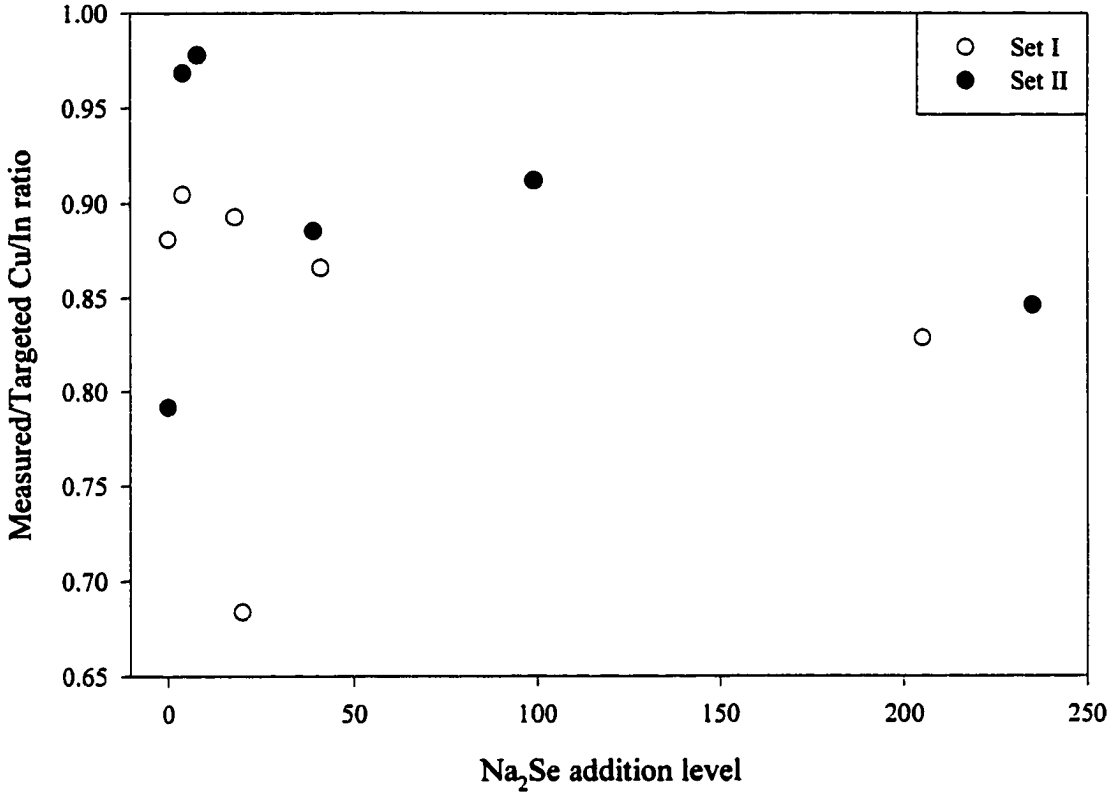

Figure 5.1. Ratio of measured to targeted Cu/In ratio versus Na_2Se addition level.

5.1.2 Sodium Concentrations

The atomic percentage of sodium in $CuInSe_2$ is defined as follows:

$$at\%Na = \frac{[Na]}{[Na]+[Cu]+[In]+[Se]} \quad (1)$$

where [X] denotes the concentration in cm^{-2}. A concentration per unit area is used to allow comparisons with other techniques that average throughout the sample. For practical purposes, [Cu] + [In] + [Se] can be approximated by four times the targeted $CuInSe_2$ concentration. This is not exact, since the films are usually not exactly 1-1-2 $CuInSe_2$. However, since the films are Cu-poor, it is assumed that the excess indium roughly replaces the deficient copper. Therefore, to first order, the number of $CuInSe_2$ molecules expected to form is equal to the average of the cations hitting the substrate. The targeted added sodium concentrations calculated in this way ranged between 0.1 and 10 at% Na.

ICP and SIMS data were used to measure the sodium concentration in the films. In Set I, reliable ICP data were only achievable for the 205 mg case, which resulted in a sodium concentration of 5.6 at%, similar to that expected. In Set II, the 235 mg case resulted in a sodium concentration of 0.31 at% for $CuInSe_2$ on 7059/Mo, 0.32 at% on Alumina/Mo, 0.39 at% on SLG/SiO_2/Mo, and 0.53 at% on NREL SLG/Mo, all considerably less than expected. Comparing the ICP values with corresponding SIMS data allows the remaining sodium concentrations to be estimated from SIMS data.

5.1.2.1 SIMS Data

Secondary ion mass spectroscopy data were taken on both sets of samples to probe the sodium concentrations in the films. By comparing the highest sodium levels to ICP results, the lower sodium concentrations are extrapolated from the SIMS data.

SIMS availability was limited when the first set of samples was finished. Therefore, only some of these films were chosen for analysis. Since no sodium is present in the alumina substrates, the films made on these substrates were analyzed and assumed

to be representative. SIMS analysis was performed on as-deposited $CuInSe_2$/Mo/Alumina samples for each Na_2Se addition level. The analysis area was a 60-micron diameter spot on the sample. The films were analyzed with a Cs ion probe, and positive secondary ion counts were recorded for Na, $^{65}Cu+Cs$, $^{82}Se+Cs$, $^{92}Mo+Cs$, and $^{113}In+Cs$. The SIMS data as plotted corresponds to the signal from the $CuInSe_2$ surface (at zero depth) to the Mo/$CuInSe_2$ interface.

For all samples in Set I, except the 205 mg sample, multiple SIMS runs on the same sample showed that the sodium was not incorporated uniformly across the film in every case. As various spots were measured on the same sample, the base metal signals of $^{65}Cu+Cs$, $^{82}Se+Cs$, $^{92}Mo+Cs$, and $^{113}In+Cs$ remained constant within the error of the measurement, but the sodium signal changed. Figure 5.2 shows an example of the point to point variations, which ranged from a factor of 2 to a factor of 40. An average sodium profile was calculated for all of the samples and used as the measured level in the following analysis. The average signal in the no-sodium-added case was considered to be the instrument detection limit for this sample set.

Each of the soda-lime glass (SLG) samples had sodium diffusing out of the glass. It was therefore necessary to measure this "background" level. SIMS data were taken on the three $CuInSe_2$/Mo/SLG samples with no sodium added. The base metal counts did not vary from the alumina samples, so calibrating to the Se signal gives an accurate comparison. Figure 5.3 graphs the baseline sodium levels coming from the glass. The resulting measured sodium concentrations were then assumed to be this background level plus the average level measured on the alumina substrates.

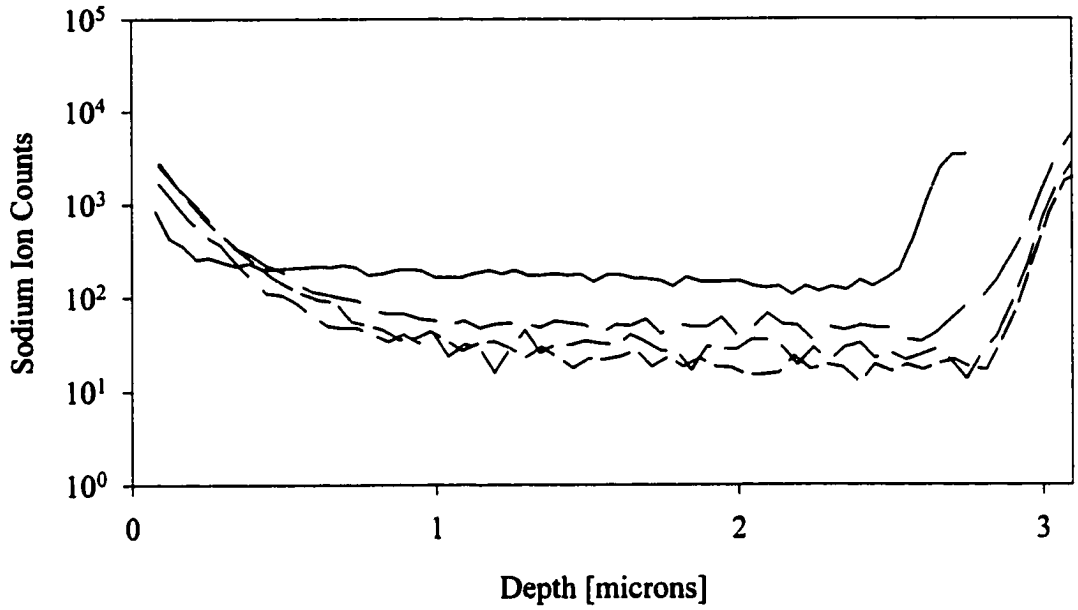

Figure 5.2. Comparison of sodium signals at different places on the sample $CuInSe_2$ on Alumina/Mo, 4 mg Na_2Se (Set I).

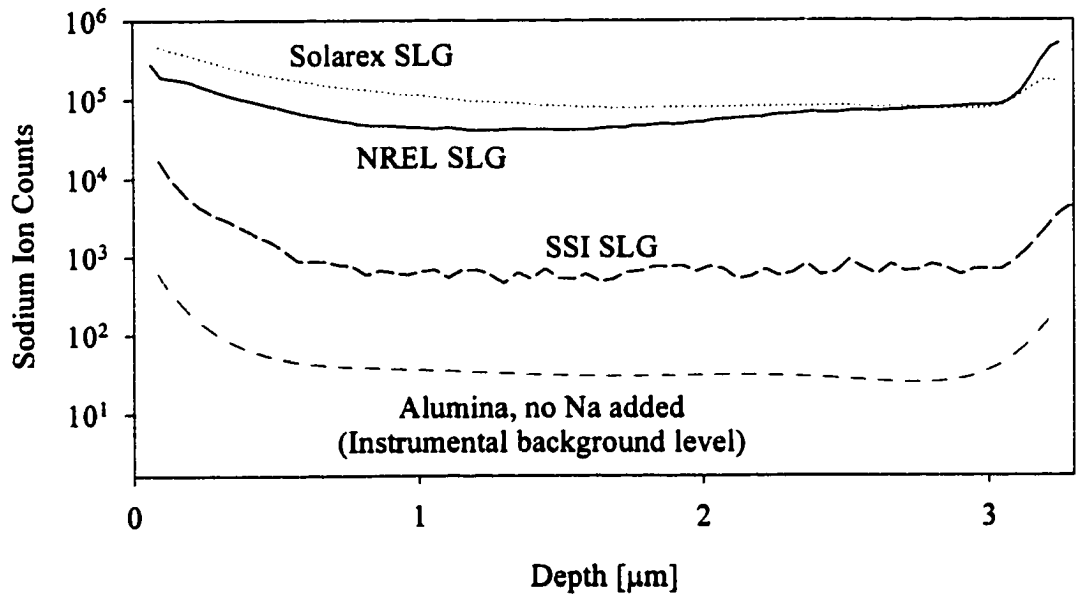

Figure 5.3. Comparison of SIMS sodium responses from $CuInSe_2$ on three different Mo-coated soda-lime glass substrates. The instrumental background sodium level is shown for reference.

For the Set II samples, more SIMS time was available. This allowed the samples on all substrates to be analyzed. There was also enough time and resources to probe the negative ion counts as well as the positive ion counts. Only one spot was analyzed on each sample. Positive secondary ion counts were recorded for Na, ^{65}Cu+Cs, ^{82}Se+Cs, ^{92}Mo+Cs, and ^{113}In+Cs. Negative secondary ion counts were recorded for ^{18}O.

As with the Set I samples, all the base metal responses were nearly identical for the different Na_2Se addition levels on a given substrate. Figure 5.4 shows the base metals, the Na comparison, and the ^{18}O comparison for $CuInSe_2$/Mo/SLG as an example. The Se level is shown for reference in both the Na and ^{18}O comparisons. In general, the sodium responses were clustered fairly close together, except for the highest sodium level in each case. The results on alumina and 7059 BSG were similar, with low response levels for the low/moderate sodium addition levels, in some cases within the background. The results on SLG/SiO_2 were the only ones that showed a monotonically increasing sodium signal with increasing Na_2Se addition level. The observed plateau in sodium incorporation with evaporated Na_2Se suggests a saturation limit for Na in $CuInSe_2$. This is important as it demonstrates that for low/moderate sodium levels, the $CuInSe_2$ takes what sodium it needs, and expels the rest. This would reduce constraints on fabrication control for manufacturers.

As with the Set I samples, the no-sodium-added case on alumina was taken as the instrumental detection limit for this sample set.

Although the sodium is not necessarily incorporated uniformly across the film, it is uniform in the growth direction, except for higher signals at the interfaces. This

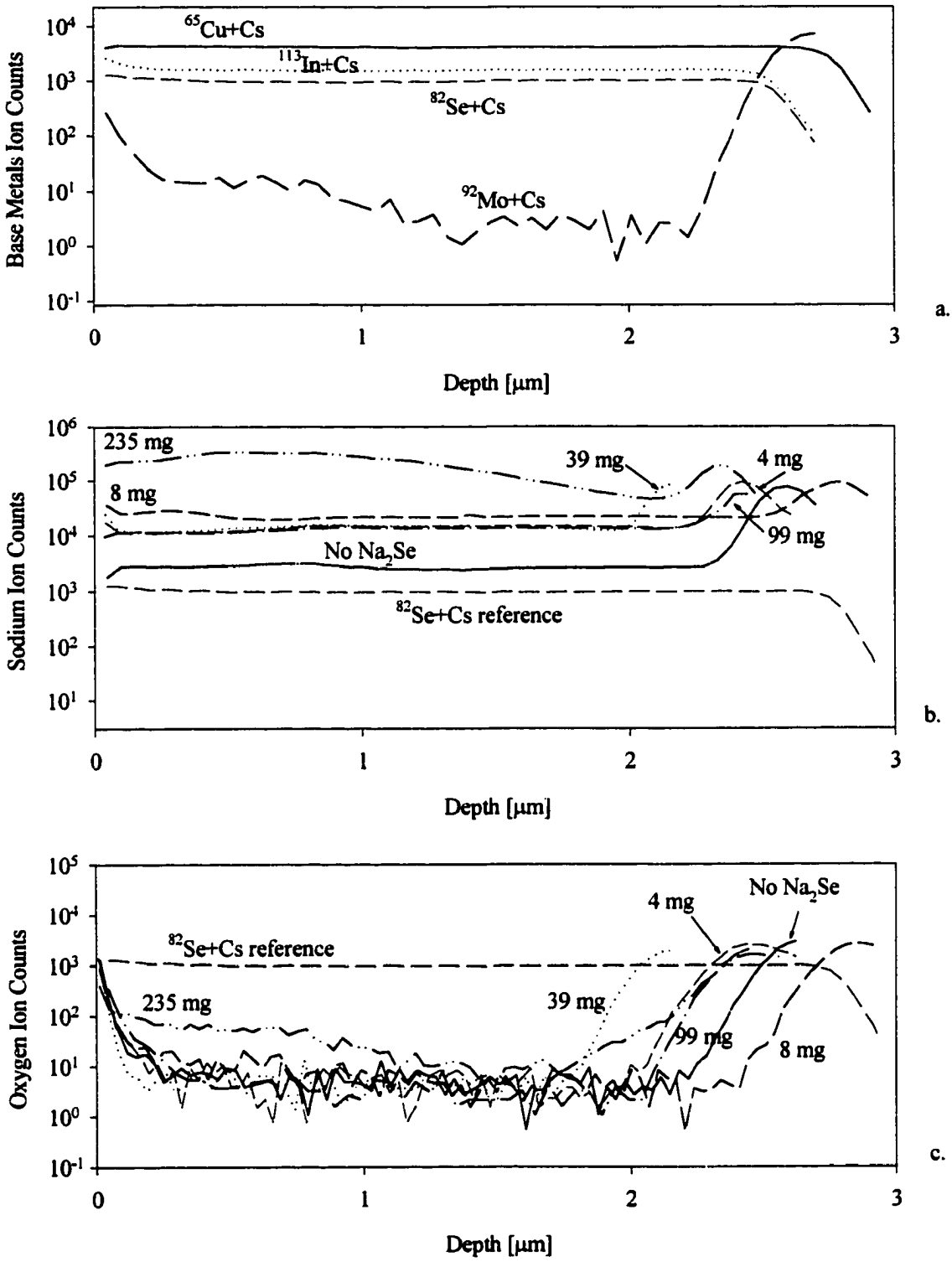

Figure 5.4. SIMS data on $CuInSe_2$/Mo/SLG, Set II. Shown are a.) sample base metal levels; b.) sodium levels on all six samples; and c.) oxygen levels on all six samples.

demonstrates that even when sodium is added in the middle of a deposition, it distributes itself evenly throughout the depth of the film, with accumulation at surfaces.

The ICP data were used to calibrate the SIMS sodium levels to atomic concentrations. An order of magnitude difference in ion counts closely corresponded to an order of magnitude difference in atomic concentration. The remaining sodium concentrations were calculated by taking the ratio of the average signal of the measured level in the $CuInSe_2$ to the average measured level of the 5.6 at% Na case. Table 5.2 shows the measured at% Na values for all samples in both data sets. It is important to know that sodium ionizes at nearly a 100% level. Therefore, the comparative SIMS sodium levels are highly accurate.

As mentioned earlier, the measured sodium concentration was limited by the SIMS detection limit. For Set I data, this limit corresponds to a calculated sodium concentration of 10^{-4} at% Na. In between the Set I and Set II analysis, the SIMS system was cleaned and the detection limit went down to $4x10^{-5}$ at% Na. In the following analysis, the most appropriate detection limit is marked.

5.1.3 Oxygen Content

SIMS oxygen data were available for Set II samples, as shown in Figure 5.4. The average oxygen level in the $CuInSe_2$ was fairly constant both throughout the samples, and from sample to sample. The one exception was the 0.3 – 0.5 at% Na case. In this case, the oxygen level was as much as ten times higher than in the other samples in the first micron. Beyond one micron, the oxygen level fell below that of the other samples. Figure 5.5 shows the average oxygen level as a function of the average sodium level. Raw data counts are used here since no oxygen concentration calibration was performed.

There is no discernible pattern of increased or decreased oxygen with increased sodium level for this sample set. The scatter in the oxygen level is most likely due to variations in the fabrication details. This is an important result, as it shows no direct correlation of oxygen with sodium. If oxygen and sodium are correlated, it is likely in regard to their interaction.

Table 5.2. Measured atomic percent sodium in $CuInSe_2$ films, Sets I and II.

Na_2Se added, Set I	0 mg	4 mg	18 mg	20 mg	41 mg	205 mg
Alumina Measured at% Na	$2x10^{-4}$	$9x10^{-4}$	$1x10^{-3}$	$3 x10^{-3}$	$4 x10^{-4}$	5.6
Solarex SLG Measured at% Na	0.15	0.15	0.15	0.15	0.15	5.7
NREL SLG Measured at% Na	0.1	0.1	0.1	0.1	0.1	5.7
SSI SLG Measured at% Na	$2x10^{-3}$	$3x10^{-3}$	$3x10^{-3}$	$5x10^{-3}$	$2x10^{-3}$	5.6

Na_2Se added, Set II	0 mg	4 mg	8 mg	39 mg	99 mg	235 mg
NREL SLG Measured at% Na	0.02	0.06	0.08	0.05	0.04	0.53
7059 BSG Measured at% Na	$6x10^{-5}$	$6x10^{-5}$	$7x10^{-5}$	$2x10^{-4}$	$5x10^{-4}$	0.31
Alumina Measured at% Na	$4x10^{-5}$	$8x10^{-5}$	$7x10^{-5}$	$2x10^{-4}$	$2x10^{-4}$	0.32
SLG/SiO_2 Measured at% Na	$6x10^{-5}$	$2x10^{-4}$	$5x10^{-4}$	$3x10^{-3}$	0.01	0.39

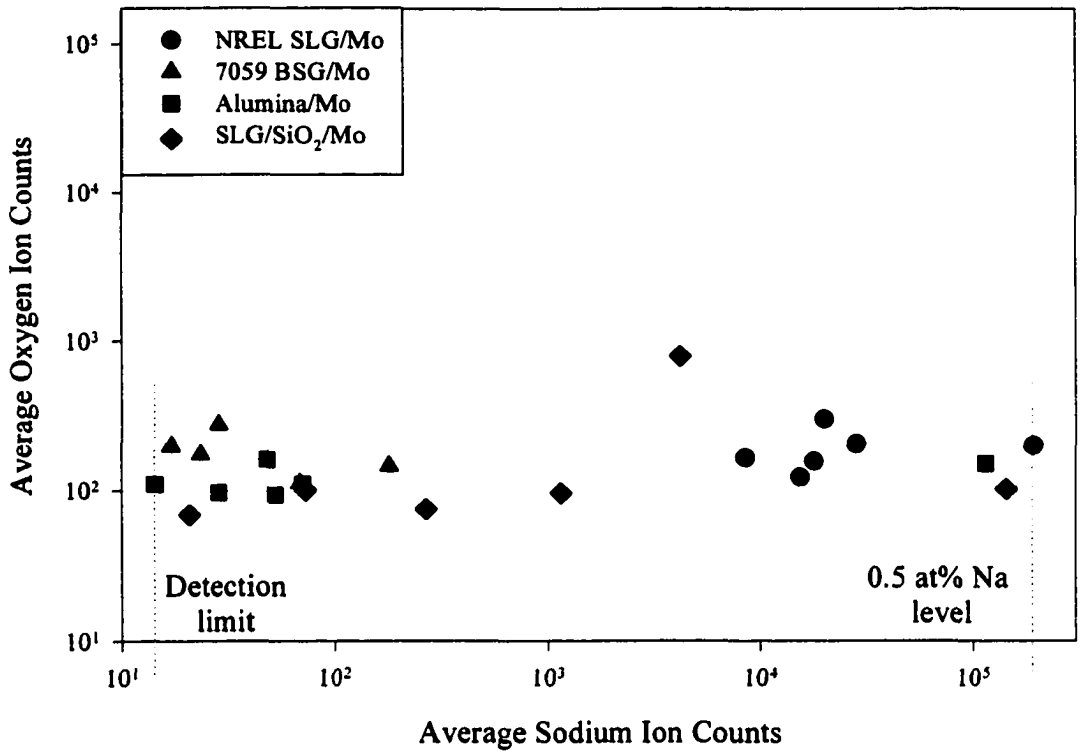

Figure 5.5. Average oxygen ion counts versus average sodium ion counts, Set II.

5.2 Materials and Device Analysis

5.2.1 X-ray Diffraction

X-ray diffraction data were taken on all the as-deposited $CuInSe_2$ to determine the structure and orientation of the $CuInSe_2$. Data points were taken every 0.03° between 5° and 95° 2θ. There are three regions of interest for this thesis: the main $CuInSe_2$ peak, (112), theoretically at 26.58° 2θ; the secondary $CuInSe_2$ peaks, [(204),(220)], theoretically at 44.12° 2θ and 44.23° 2θ; and the region between 5° and 24° 2θ, where the β-phase peak occurs and where unidentified phases have been observed. Figure 5.6 graphs these three regions for all the Na_2Se addition levels on the NREL SLG substrates in Set I. Figure 5.7

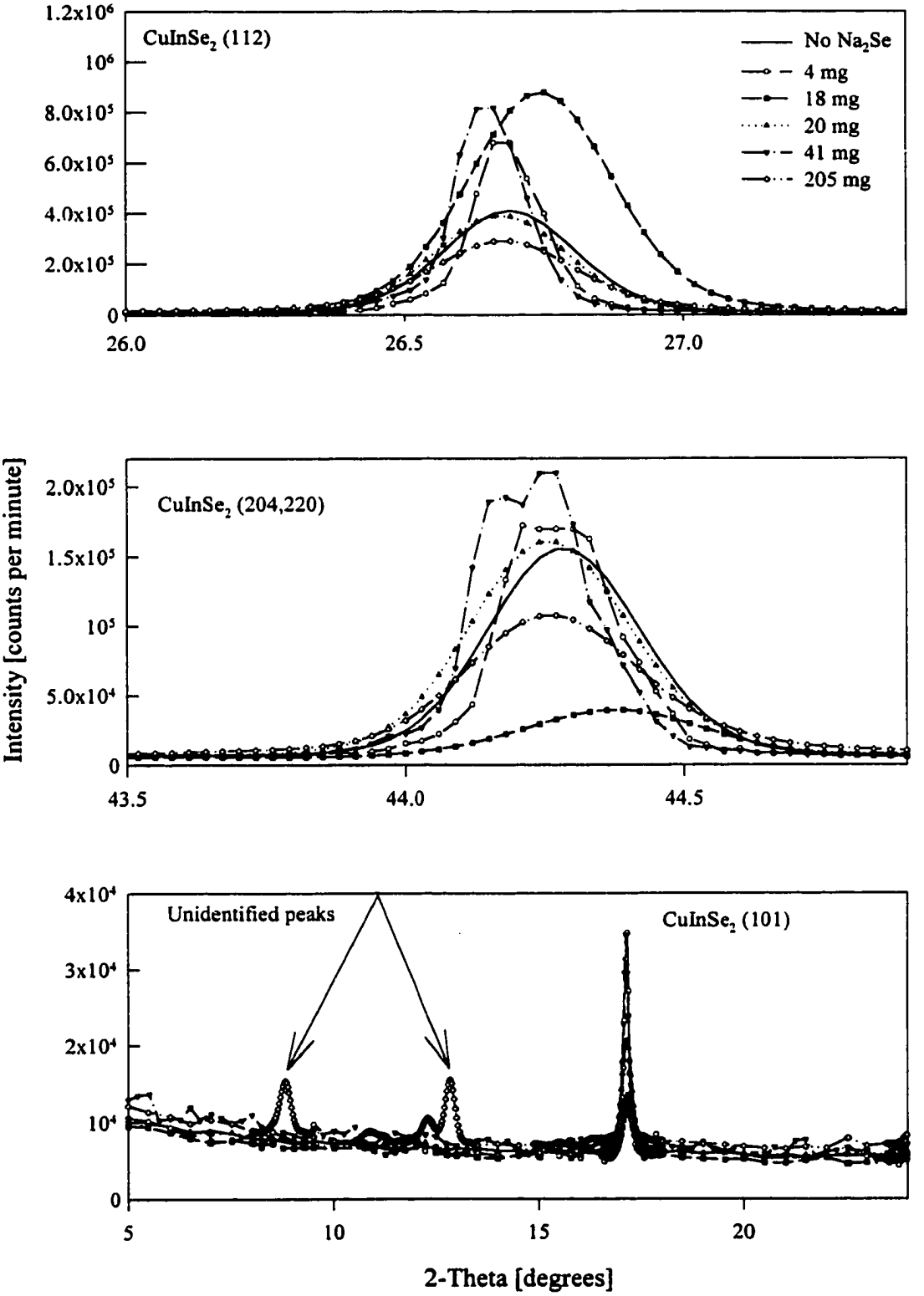

Figure 5.6. XRD data. $CuInSe_2$ on NREL SLG/Mo (Set I).

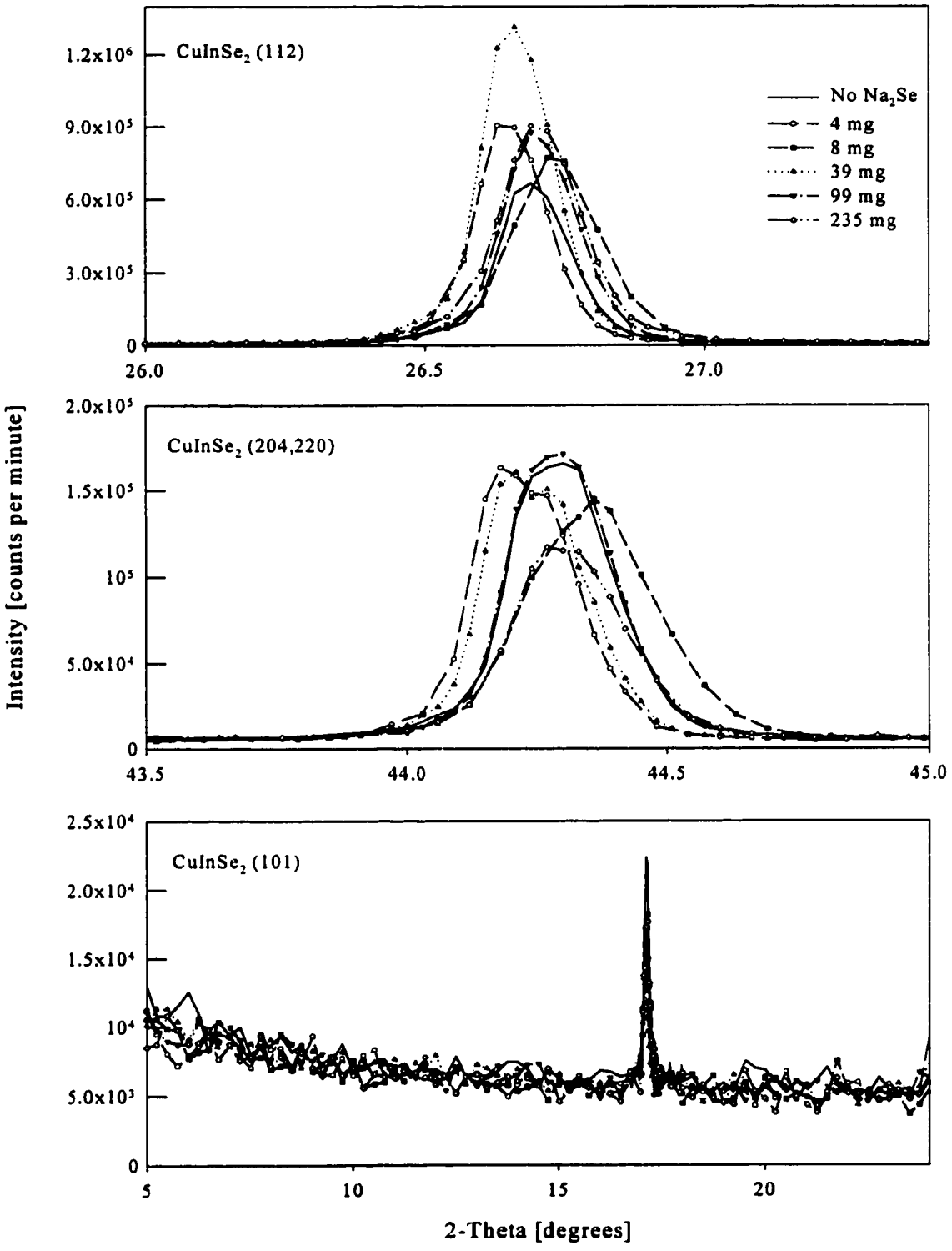

Figure 5.7. XRD data. $CuInSe_2$ on NREL SLG/Mo (Set II).

does the same for the NREL SLG substrates in Set II. These samples are used as examples. The results on all substrates were qualitatively similar.

The $CuInSe_2$ (112) peak height is compared to the $CuInSe_2$ [(204),(220)] peak height, as is the custom to determine orientation. The ratios are plotted versus measured sodium concentration in Figure 5.8. This figure shows no distinguishable pattern with measured sodium incorporation.

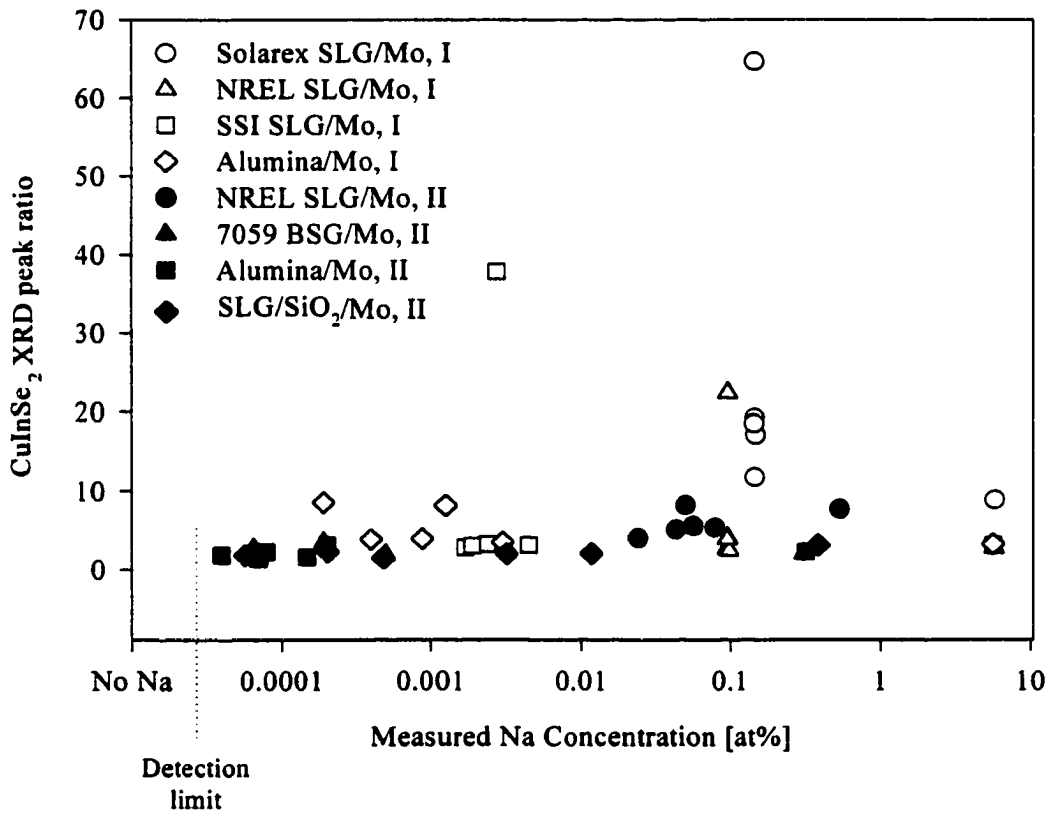

Figure 5.8. Ratio of measured X-ray diffraction $CuInSe_2$ (112) and [(204),(220)] peaks plotted versus the measured Na concentration for Sets I and II.

A word needs to be said about some of the details of the XRD data. For the Set I data, three distinct peaks appear between 5° and 15° 2θ for the 5.6 at% Na (205 mg) case. These peaks do not match any known peaks in the JCPDS database. The details of the possible structure or structures represented by these peaks will not be discussed here. Their importance is discussed in the following section. For both sets of samples, a small peak is apparent just above noise level in the region between 21.5° and 22.5° 2θ, indicating the presence of a secondary phase, commonly referred to as the $CuInSe_2$ β-phase. For Set I samples, this peak is most apparent for the two highest sodium addition levels. For Set II samples, the peak is generally largest for the highest sodium addition level.

In summary, for these $CuInSe_2$ processing methods, the presence of sodium at moderate levels does not affect the structure of the films on a detectable level. Any differences observed are likely due to variations during processing such as Cu/In ratio, substrate temperature, or differences in the Mo layer. The deposition methods used here tend to give highly- structured $CuInSe_2$. It is possible that any structural changes induced by sodium are obscured by the nature of these films. It also appears that high sodium levels induce secondary-phase formation.

5.2.2 SEM

To probe both the grain growth and the effect of sodium on it, scanning electron microscope images of the as-deposited $CuInSe_2$ samples were used. Figures 5.9.a-f demonstrate both a top view and a cross-sectional view of the films on Alumina/Mo substrates for Set I for all six sodium levels. Figures 5.10.a-f show the cross-sectional images taken on the Set II films on NREL SLG/Mo. These two sample sets are

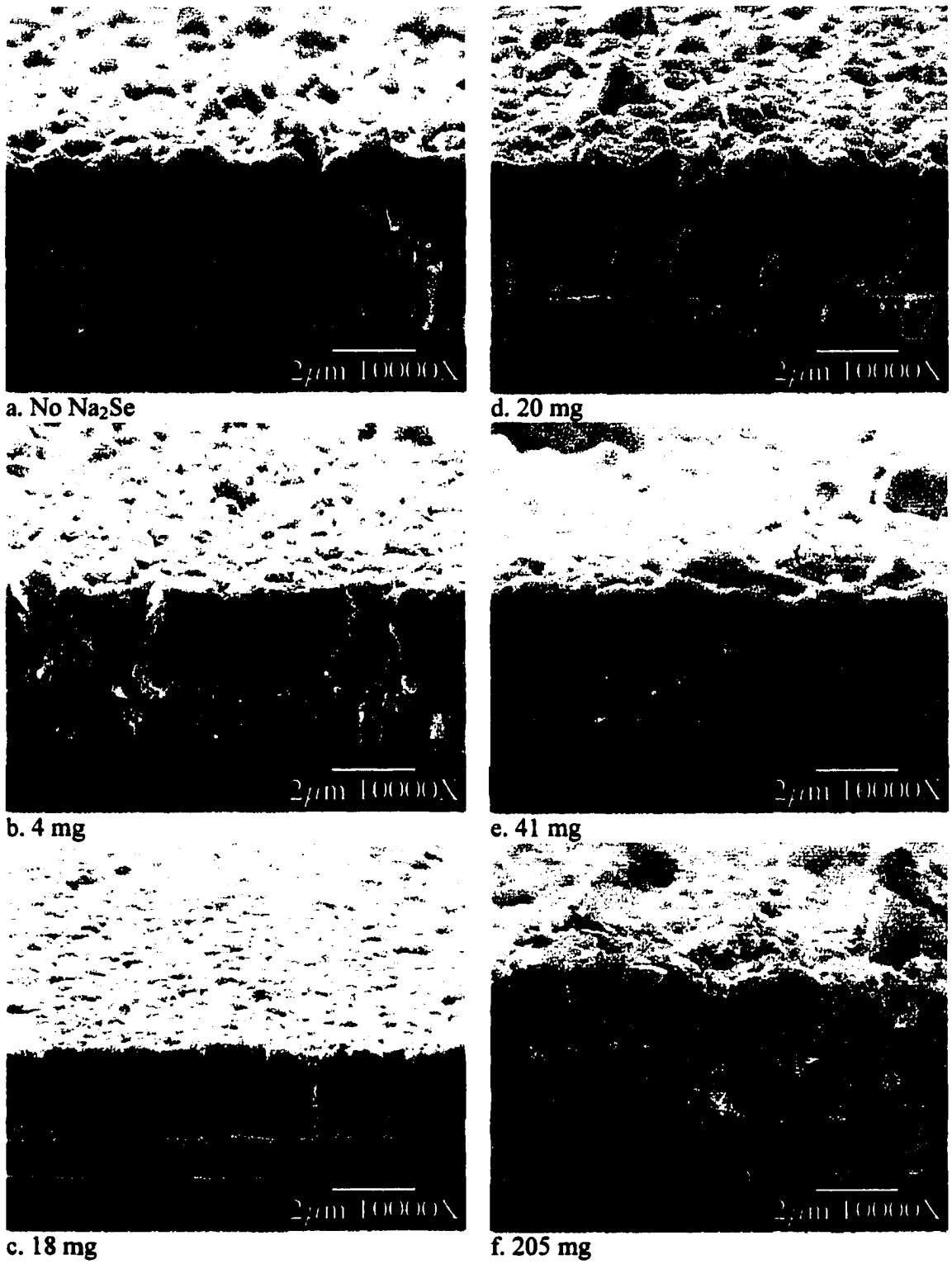

Figure 5.9.a-f. SEM images on as-deposited $CuInSe_2$ on Alumina/Mo, Set I.

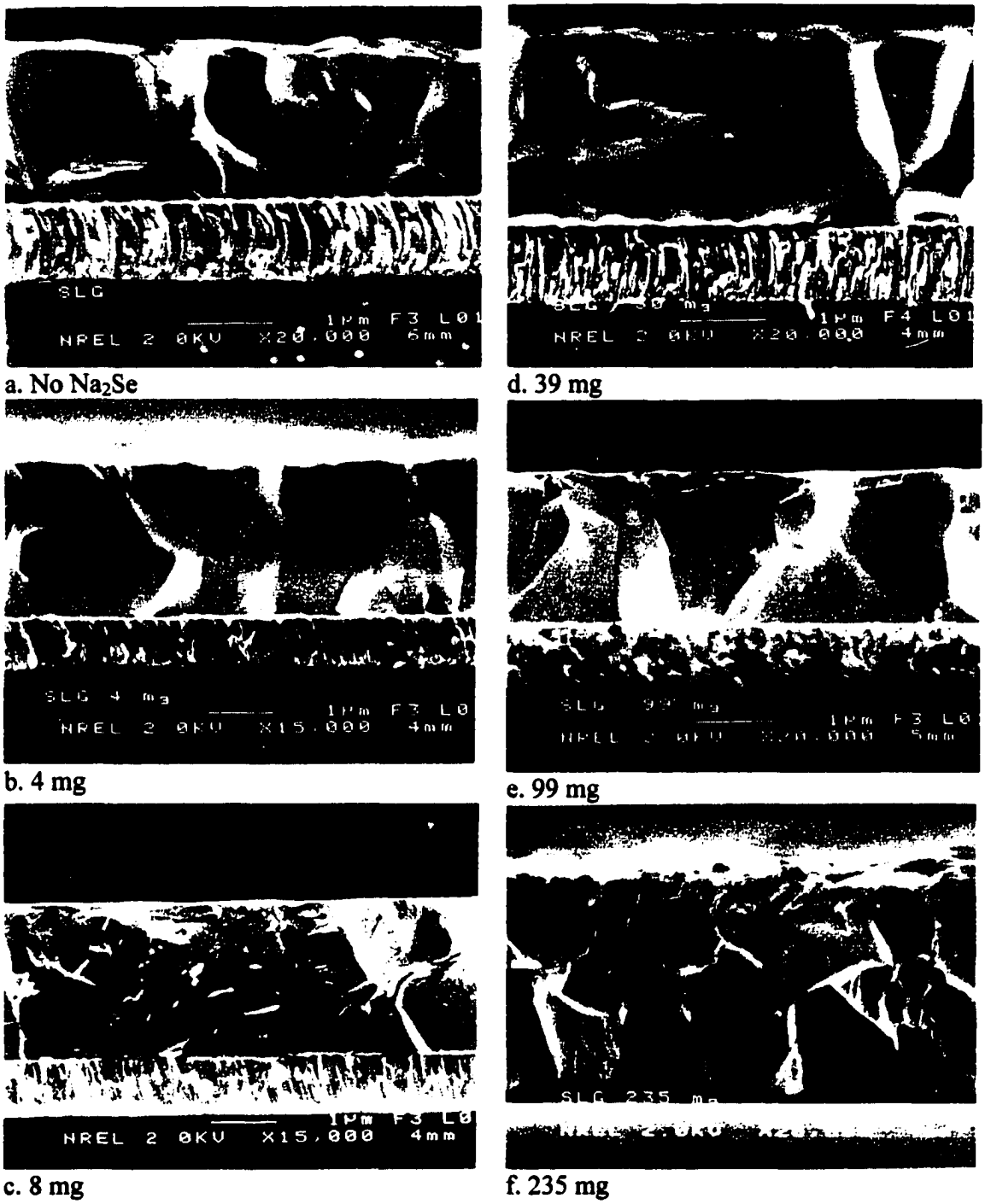

Figure 5.10.a-f. SEM images on as-deposited $CuInSe_2$ on NREL SLG/Mo, Set II.

representative of all the films in each set. The length scale and magnification are marked. In all images, the bottom layer is the Mo layer, and the $CuInSe_2$ is on top.

SEM measurements were performed to look for changes in grain size and morphology as sodium is added. Typically, an increase in grain size reduces the effects of grain boundaries and tends to improve device performance. The data from Set I show no pattern of improvement in morphology or grain size for the lower sodium levels. At the highest sodium level, the films become porous and the grains are much smaller than in all the other samples. This is clear in Figure 5.9.f. The companion figures for Set II similarly show only slight systematic changes below 100 mg, but at the 235 mg level, there is a visible difference. Again, the films become porous and the grain structure changes. It is interesting to note that in Set II, for some samples, a bilayer structure is detectable. This becomes obvious on all substrates for the 0.3 – 0.5 at% Na case. The bottom layer is made up of large-grained material, but the top layer is much smaller-grained. This may indicate that high sodium levels interfere with the Cu_2Se flux.

No significant changes in grain size and morphology were detected for low/moderate sodium levels here. The $CuInSe_2$ recipes used for this work have already been optimized for large grain structure. The process used may mask any changes induced by small concentrations of sodium.

5.2.3 EBIC

EBIC data were taken on finished devices on both sample sets to probe the effects of sodium on junction depth and uniformity. The results for each Na_2Se addition level on Alumina/Mo substrates for both sets are shown in Figures 5.11 and 5.12. The electronic

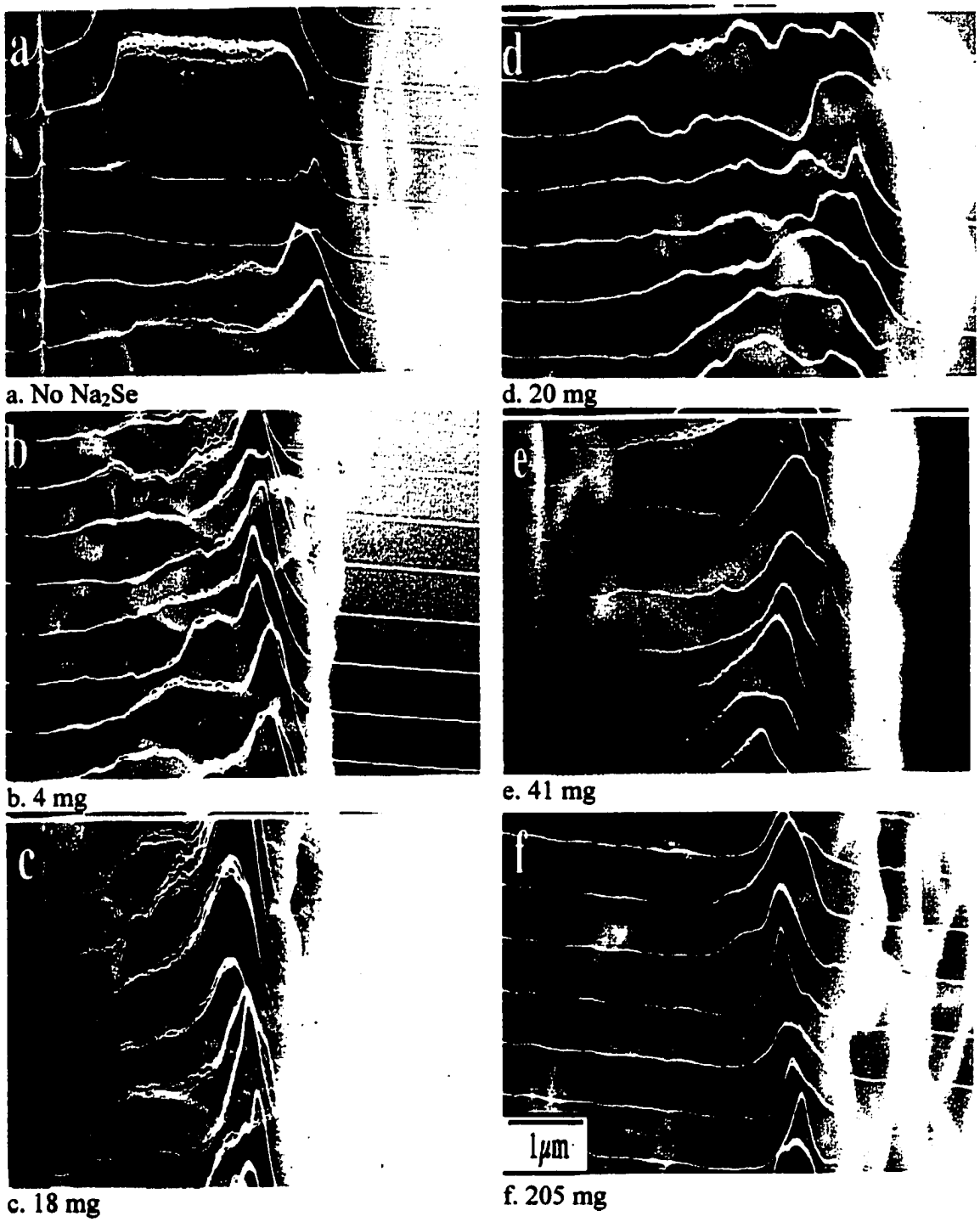

Figure 5.11.a-f. EBIC data on ZnO/CdS/$CuInSe_2$/Mo/Alumina, Set I.

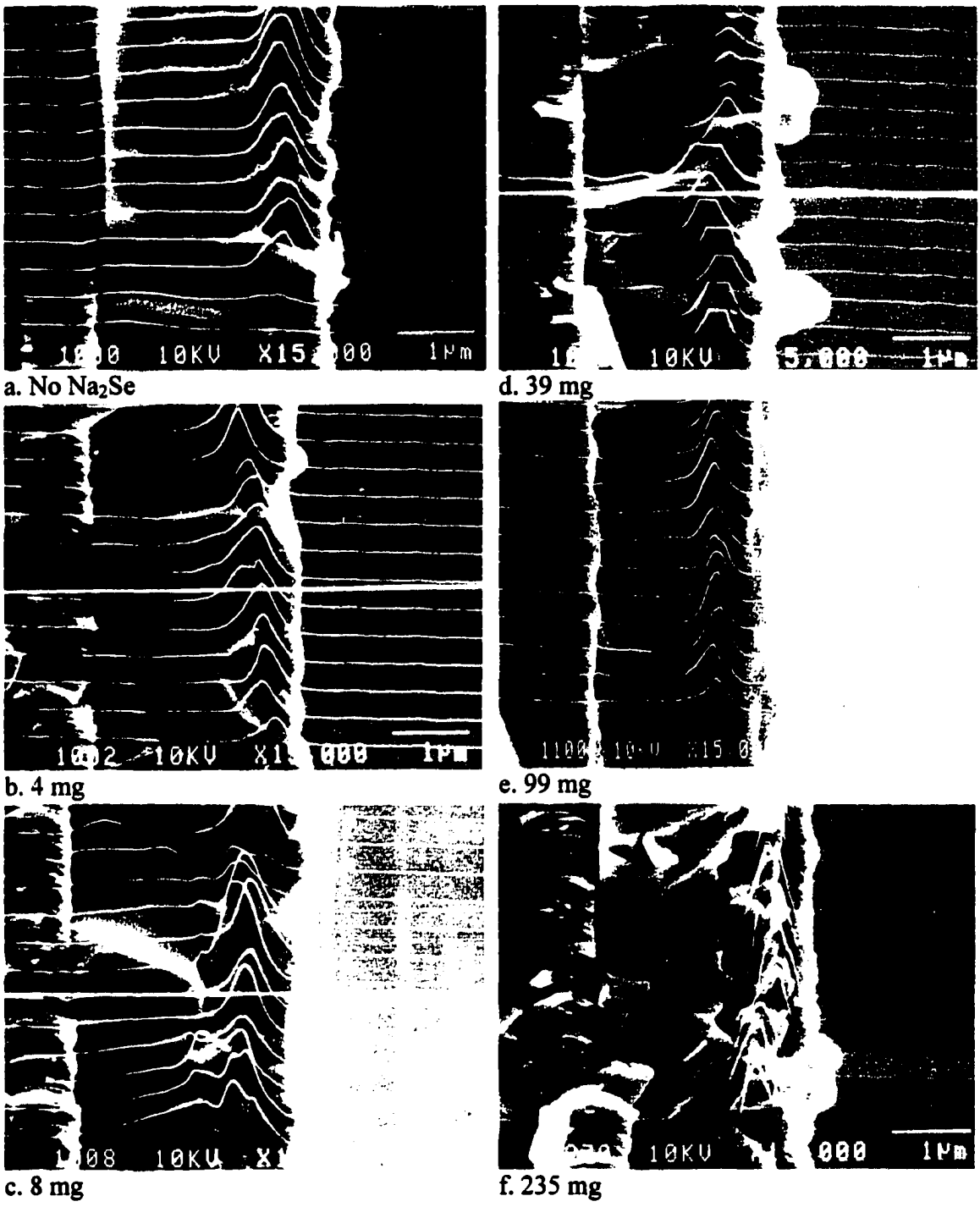

Figure 5.12.a-f. EBIC data on $ZnO/CdS/CuInSe_2/Mo/Alumina$, Set II.

response is superimposed on a SEM cross-section. The layers, from left to right, are as follows: Mo, $CuInSe_2$, CdS, and ZnO. Since the CdS layer is only 50 nm thick, it is difficult to distinguish as a separate layer. In all cases, the distance scale is marked. Magnification is either 15kX or 20kX.

In general, for the low sodium concentrations, both uniformity and collection efficiency improved over the no sodium case. At the highest sodium levels, the collection efficiency dropped, and in most cases, the signal moved closer to the metallurgical junction.

5.2.4 Device Analysis

Following $CuInSe_2$ deposition, one $CuInSe_2$-coated substrate of each type was made into solar cell devices as described in Chapter 3. In all cases, between three and seven working devices were made. Current-voltage (JV) data were taken on every solar cell on each substrate, and one cell was chosen as a representative sample for capacitance and spectral response measurements.

Figures 5.13.a-b compare dark and light JV data on a representative device for the samples on NREL SLG/Mo and Alumina/Mo, Set I. Data from each Na_2Se addition level are shown. The results on Solarex SLG/Mo are similar to those on NREL SLG/Mo, and the results on SSI SLG/Mo are similar to those on Alumina/Mo. The general trend observed with the addition of low/moderate sodium is an increase in open-circuit voltage as seen by a shifting of the light JV curves to the right, and an increase in fill factor, seen as an improvement in the knee region. At the highest sodium level, short-circuit current drops significantly, and series resistance increases, as evidenced by the change in slope in forward bias.

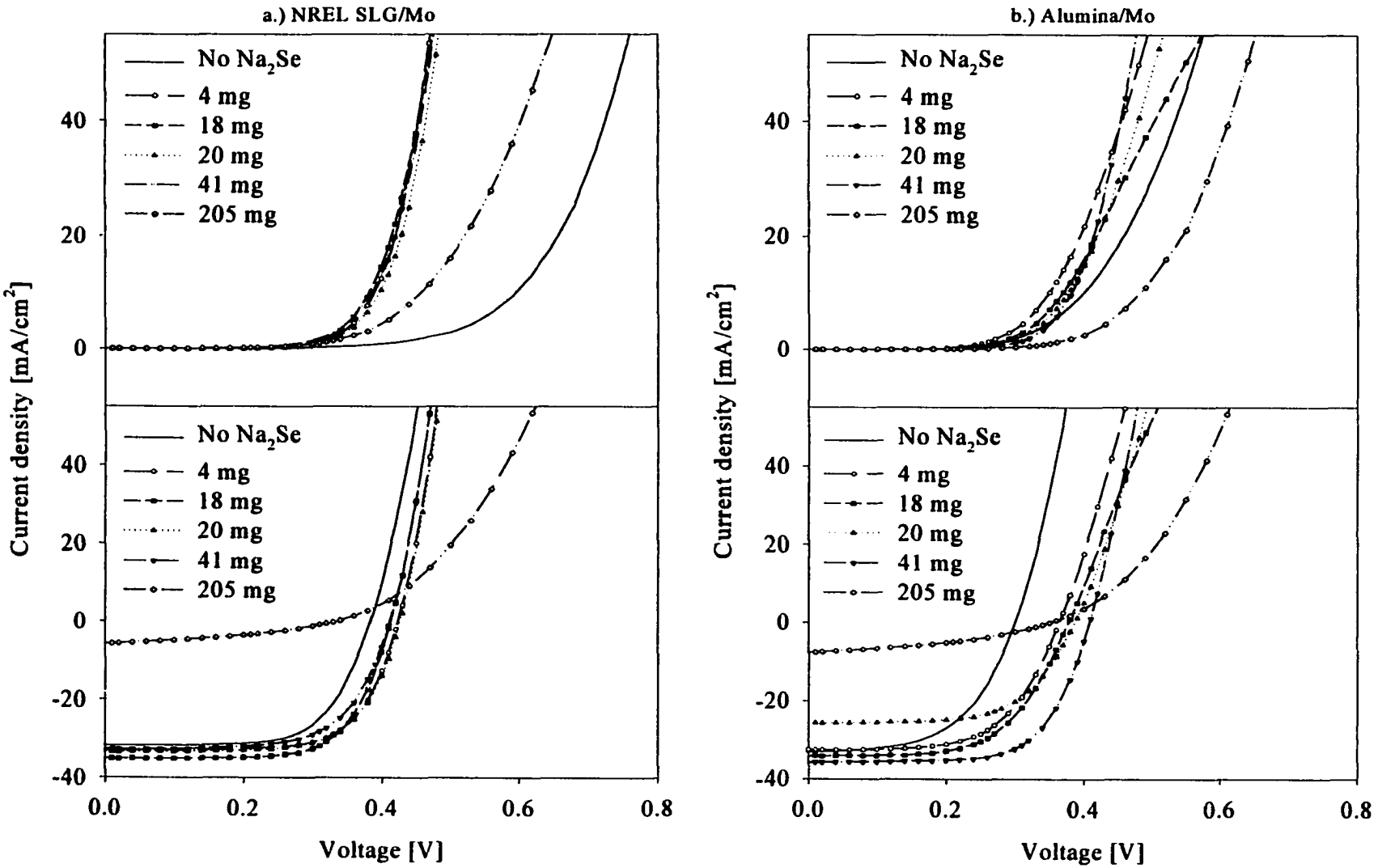

Figure 5.13.a-b. Dark (top) and light JV comparison for all Na_2Se addition levels for $CuInSe_2$ on a.) NREL SLG/Mo, and b.) Alumina/Mo (Set I).

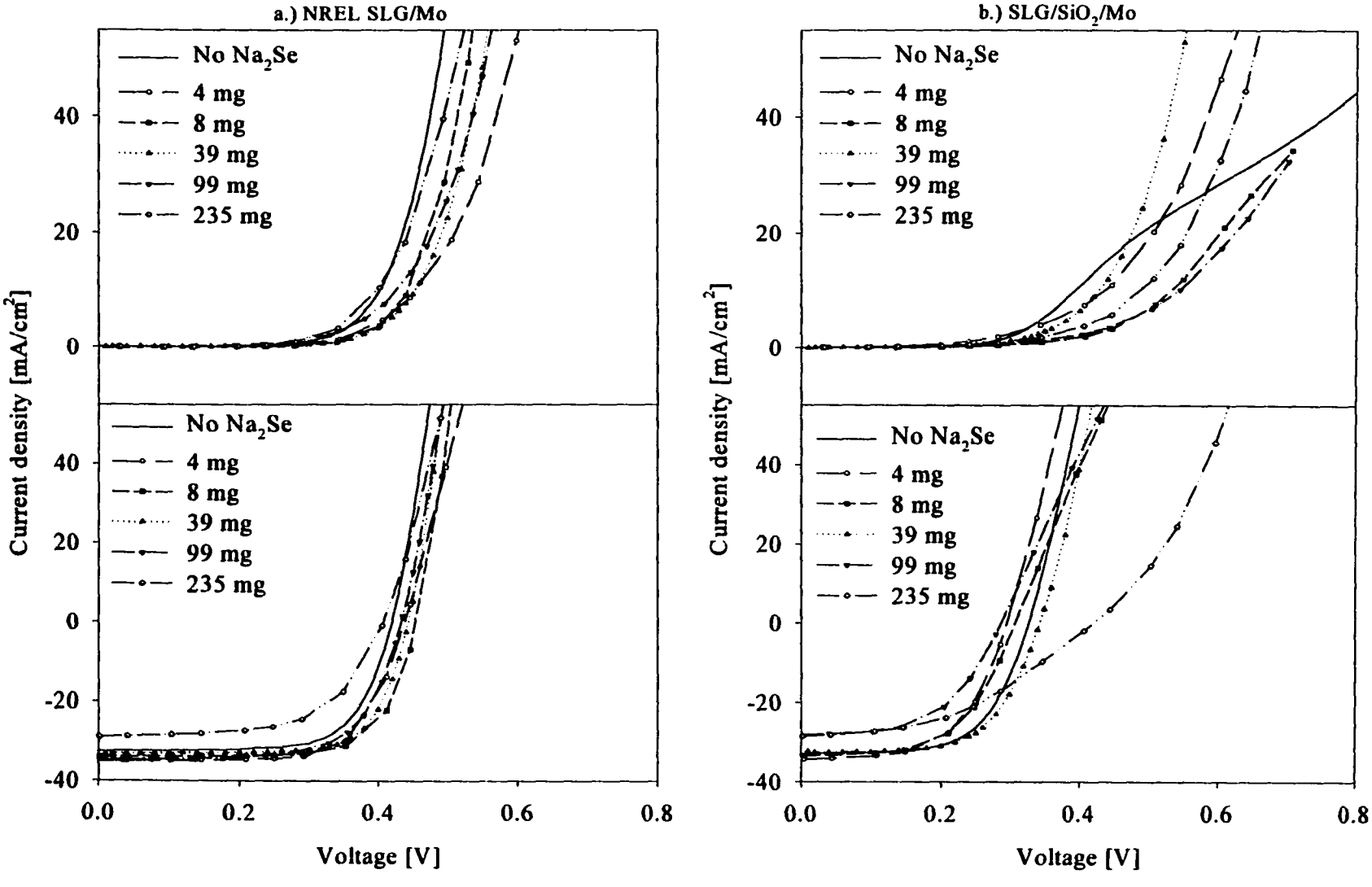

Figure 5.14.a-b. Dark (top) and light JV comparison for all Na_2Se addition levels for $CuInSe_2$ on a.) NREL SLG/Mo, and b.) SLG/SiO_2/Mo (Set II).

Figures 5.14.a-b show the same for Set II devices on SLG and SLG/SiO_2 substrates. The results on both Alumina and 7059 BSG substrates are similar to those on SLG/SiO_2. The general trend is again an increase in open-circuit voltage, and a slight improvement in the knee region, for the low/moderate sodium levels. In some cases, the presence of sodium appears to lessen or remove non-diode-like behavior such as rollover in the first quadrant. At the highest sodium level, short-circuit current and fill factor drop, although not as significantly as in Set I.

The important parameters directly measured from the current-voltage curves were open-circuit voltage (V_{OC}) and short-circuit current density (J_{SC}). Fill factor (FF) and efficiency were calculated from the data. Diode quality factor A, series resistance (R_{series}), and shunt resistance were extracted from the JV curves. The parameters most relevant to this discussion are plotted versus measured sodium concentration in Figures 5.15 through 5.19.

Figure 5.15 graphs V_{OC} versus measured sodium concentration for devices from Sets I and II. The sample sets are graphed separately with the most appropriate concentration scale. In both sample sets, V_{OC} increases when sodium is added, and plateaus for the lower sodium concentrations. This plateau matches the earlier observation of the plateau in measured sodium concentration with evaporated Na_2Se. In Set I, V_{OC} drops at 5.6 at% Na. In Set II, the pattern is similar, but there is more scatter in the data. A similar drop occurs at 0.3 at% Na. Figure 5.15 demonstrates that the low and moderate sodium addition levels yield a narrow range of concentrations for each substrate, except SLG/SiO_2, which shows a broader range.

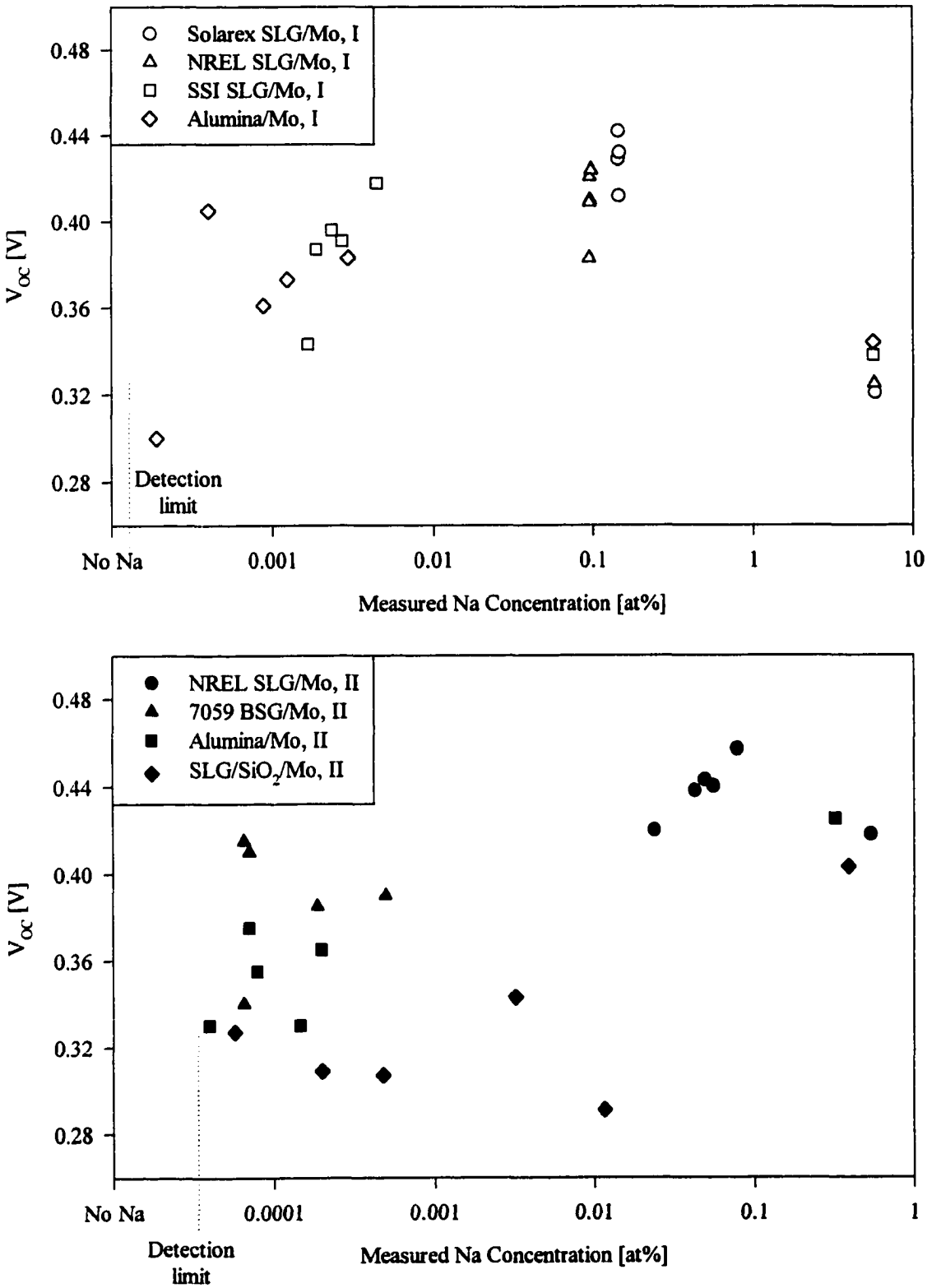

Figure 5.15. Open-circuit voltage versus measured sodium concentration for Sets I (top) and II.

Short-circuit current trends are clear in the JV data. There appears to be little change in J_{SC} that cannot be accounted for by measurement uncertainties for the low and moderate sodium concentrations. There is however a definite drop in J_{SC} in Set II at 0.3 at% Na and in Set I beyond 1 at% Na. This drop at 0.3 at% Na demonstrates the beginning of degradation in device performance. This shows that 0.3 at% Na is beyond the range of sodium concentrations that yield good performance.

Figure 5.16 shows the trends observed in fill factor. The results for Set I follow the same trends observed in V_{OC}, although the effects for the low/moderate sodium concentrations are not as dramatic. Set II samples show little or no systematic changes in fill factor with increasing sodium concentration, except for a general drop at 0.3 at% Na. This also demonstrates that 0.3 at% is beyond the optimal range of sodium concentrations.

Trends in efficiency (Figure 5.17) follow V_{OC} and FF, as expected: an initial increase once sodium is added, a general plateau up to 0.15 at% Na, and then a systematic decrease beyond 0.3 at% Na.

The series resistance was extracted from the JV curves in both the dark and the light. See Figure 5.18. The series resistance deduced from the dark JV curves shows an overall trend of either a drop or a plateau for low sodium levels, and then an increase beyond 0.3 at%. In the light, the changes in series resistance with increasing sodium concentration appear to be more substrate-dependent. An overall drop with sodium is observed, with an increase beyond 0.15 at%.

The diode quality factors were also extracted from the JV curves. The samples in Set I showed a strong trend in the dark for which A decreases with the initial addition of

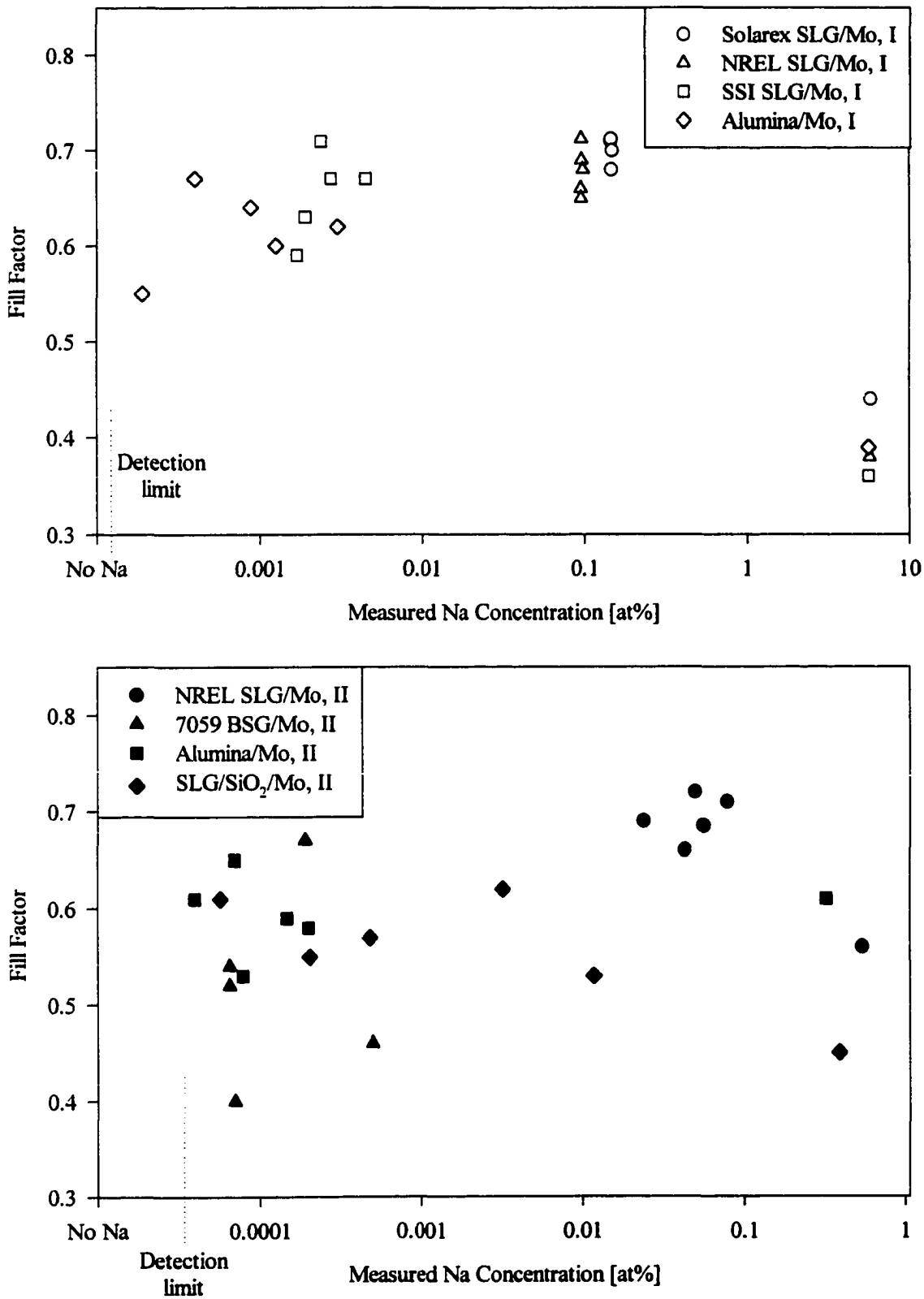

Figure 5.16. Fill factor versus measured sodium concentration for Sets I (top) and II.

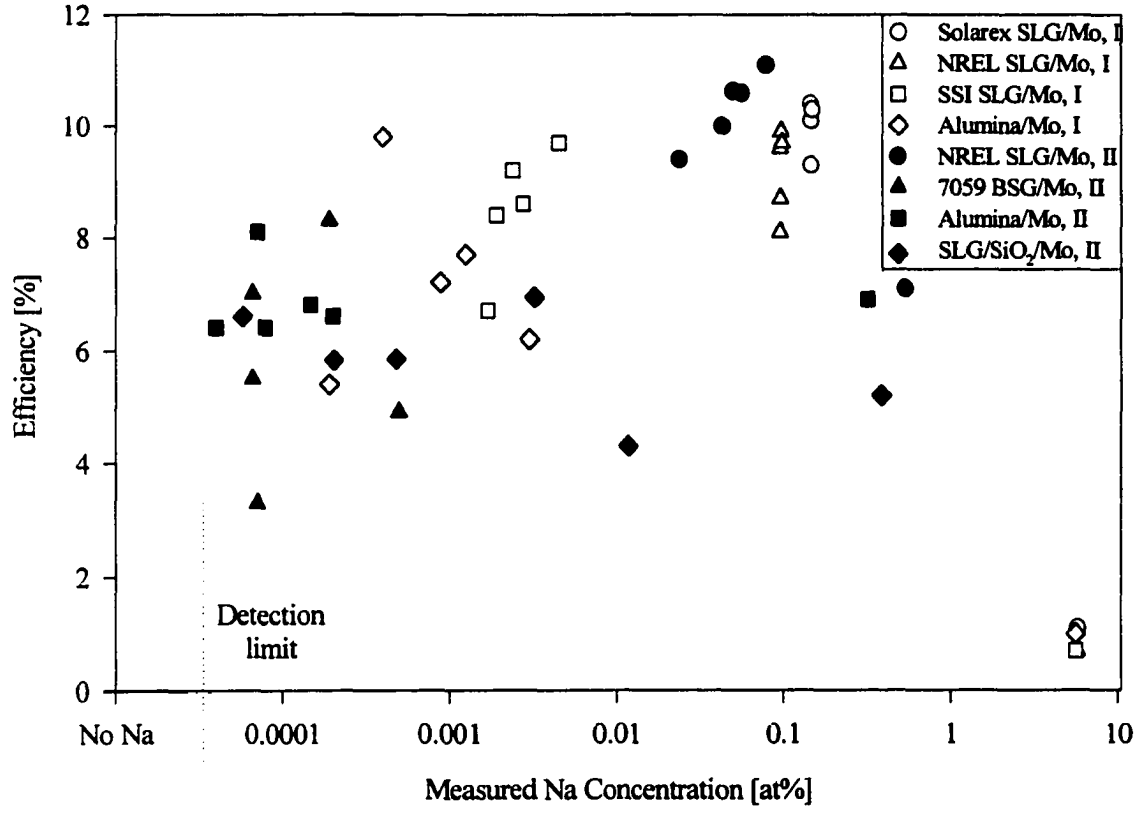

Figure 5.17. Efficiency versus measured sodium concentration for Sets I and II (plotted together).

sodium, remains fairly constant, and then increases for the highest sodium concentration. The trend in the light is the same, although the initial A-values are lower than in the dark. Figure 5.19 plots the results for Set I. The samples in Set II showed no systematic changes in the diode factor in the dark with the addition of sodium. The values in the light stayed fairly constant to within error and averaged 1.6 for all the substrates except the 7059 BSG, which averaged 2.7.

Shunt resistance is extracted from the JV curves and is proportional to the slope of the curve in reverse bias. Shunt resistance is typically higher in the dark, often above 10000 Ω-cm^2. For these two sample sets, the dark shunt resistance was above

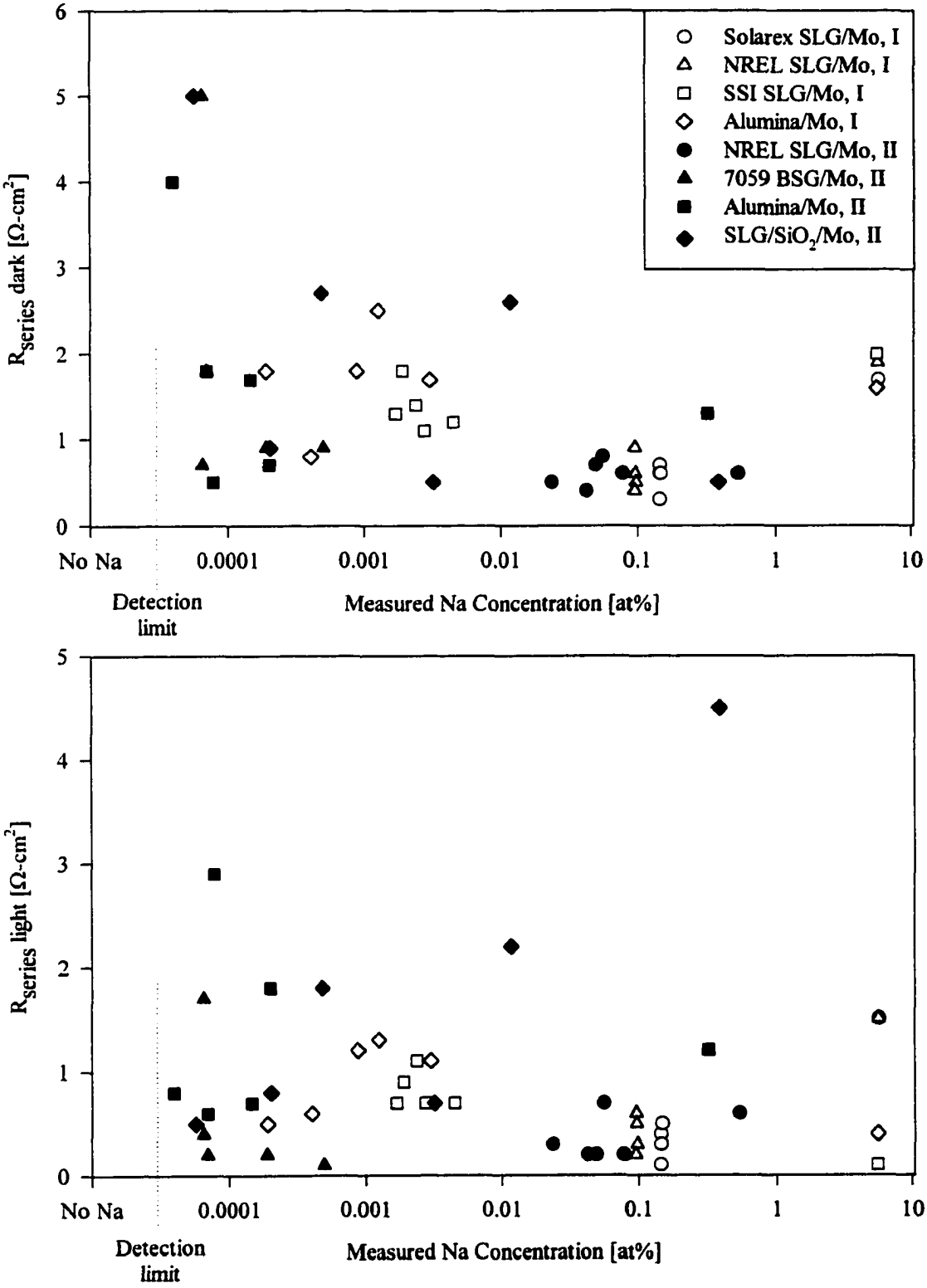

Figure 5.18. Series resistance in the dark (top) and light versus measured sodium concentration for Sets I and II (plotted together).

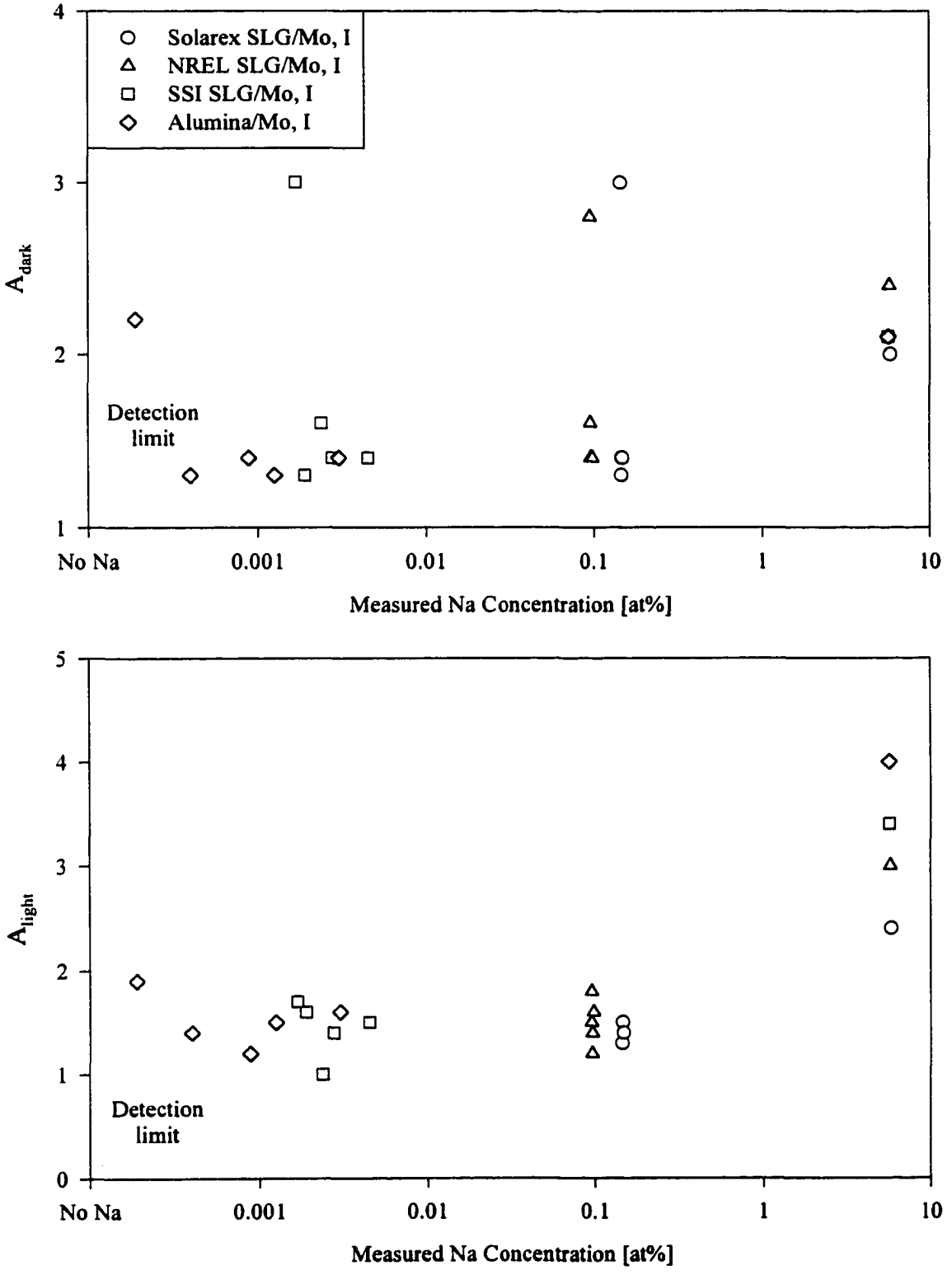

Figure 5.19. Diode quality factor in the dark (top) and light versus measured sodium concentration for Set I.

1000 Ω-cm^2 in most cases. The devices in Set I showed good shunt resistance with a systematic drop beyond 1 at% Na. The devices in Set II showed no systematic changes in dark shunting with sodium. The shunt resistance in the light showed similar patterns in both data sets: shunt resistances between 400 and 2500 Ω-cm^2 with no systematic changes for the low and moderate sodium levels, and a drop beyond 0.3 at% Na. The shunt resistance appears to be affected only by high sodium concentrations. This may be due to the changes in morphology observed at 0.3 at% Na and beyond.

Capacitance data were taken in order to extract the effective carrier concentration and depletion width. Figures 5.20.a-b show the capacitance-voltage data and the calculated hole density versus distance from junction curves for representative devices on NREL SLG/Mo substrates for Sets I and II. The general trends observed here are representative of the devices on all substrates. The capacitance at zero bias is plotted versus sodium concentration for all samples in Figure 5.21.a. The capacitance increases with increasing sodium concentration in all cases, with a significant increase at or beyond 0.3 at% Na. Figure 5.21.b plots hole density versus sodium concentration for both sets of data. In Set I, for low sodium concentrations, the hole density increased by factors of 1.1 to 10 (substrate-dependent), and then increased by two to four orders of magnitude at 5.6 at% Na. In Set II, the increases were fairly consistent and ranged from a factor of 1 to 2 for low sodium levels. At the 0.3 at% Na level, hole density increased by a factor of 10 to 30. The depletion width is calculated from the extrapolated capacitance near zero bias on the CV curve. For low sodium concentrations, there is a general decrease in depletion width below the no sodium added value. For both sets of data, the depletion width shows a significant drop in all cases for the highest sodium concentrations. This data is

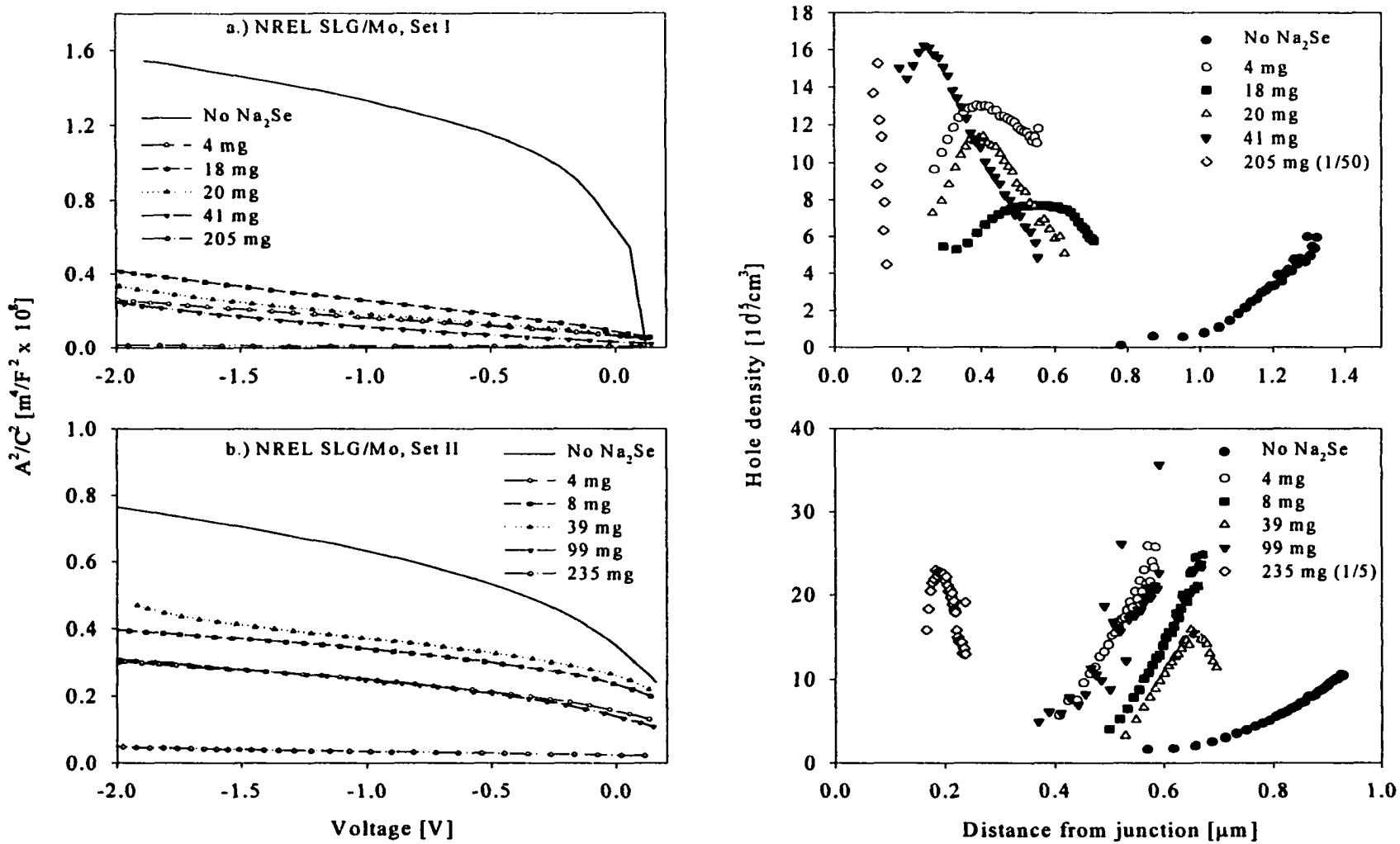

Figure 5.20.a-b. Capacitance-voltage (left) and hole-density data for all six Na_2Se addition levels on a.) NREL SLG/Mo, Set I and b.) NREL SLG/Mo, Set II.

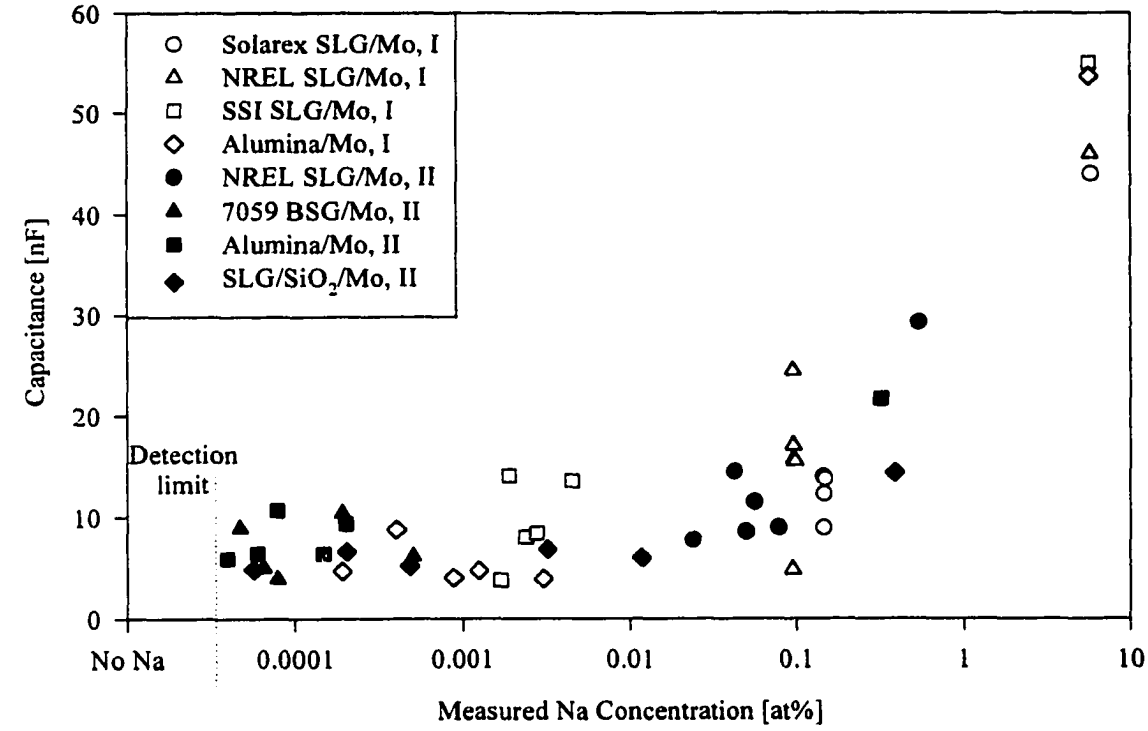

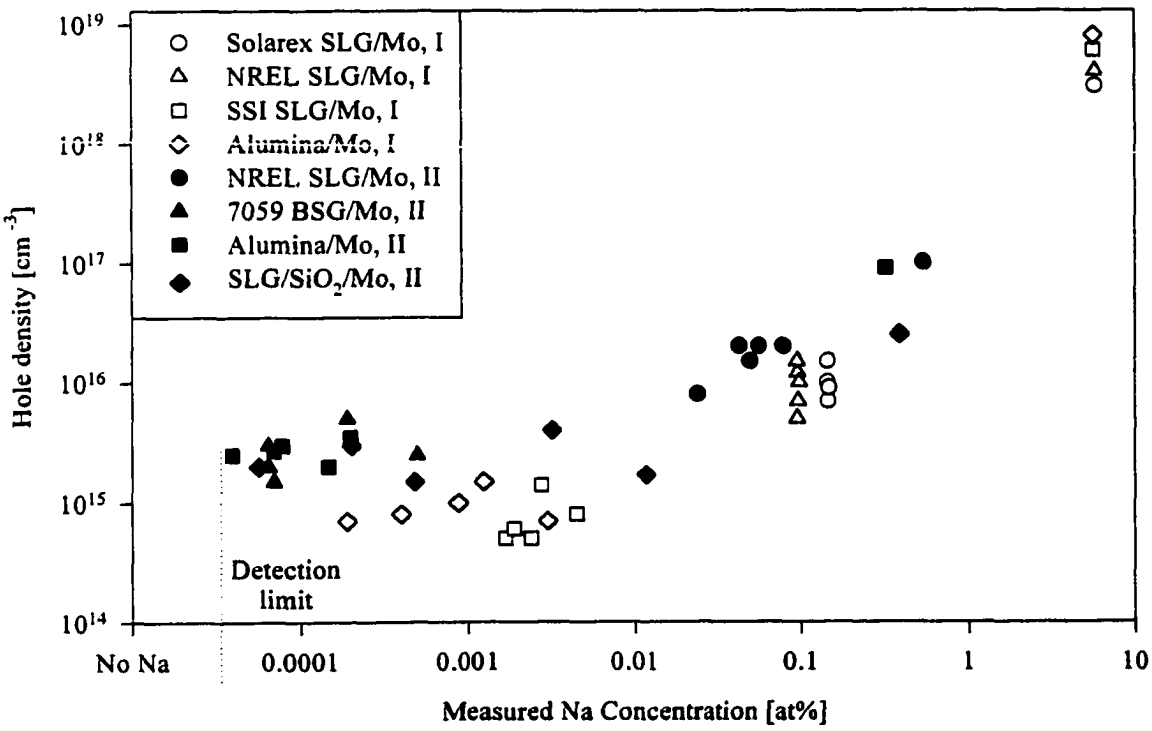

Figure 5.21.a-b. Capacitance at zero bias (a) and hole density (b) versus measured sodium concentration for Sets I and II (plotted together).

consistent with the observed changes in dopant density (large dopant densities generally correspond to narrower depletion widths). It also matches the tightening of the EBIC signal and movement of the EBIC signal closer to the metallurgical junction for the highest sodium levels.

Spectral response and reflection data were taken to probe changes in the collection efficiency at each wavelength. Figures 5.22.a-b present the calculated quantum efficiency curves and the reflection data for all Na_2Se addition levels on NREL SLG/Mo substrates for both data sets. These data are representative of the devices on all substrates in each data set. The reflection data is limited to 1100 nm by the silicon detector in the spectrometer used. One systematic change observed is a small decrease in collection in the red as the sodium level increases. This is consistent with a shrinking depletion width. For high sodium concentrations, the red loss becomes significant. There is also a small increase in short-wavelength collection. The overall drop in the maximum of the QE curve is due to an overall drop in J_{SC} at the higher sodium concentrations.

The results of the materials and device analysis are summarized in Table 5.3.

5.3 Observations

In both sets of data, the measured sodium incorporation proved not to be linear with Na_2Se addition level. The changes in cell parameters also displayed this nonlinear behavior. The relevant parameters demonstrated an initial change when sodium was added, then a general plateau for all the low and moderate sodium addition levels, and finally a more significant change at the highest sodium addition levels. This points to two thresholds. The first threshold is simply growing $CuInSe_2$ in a sodium atmosphere, as evidenced by the initial improvements in device quality when grown in the presence of

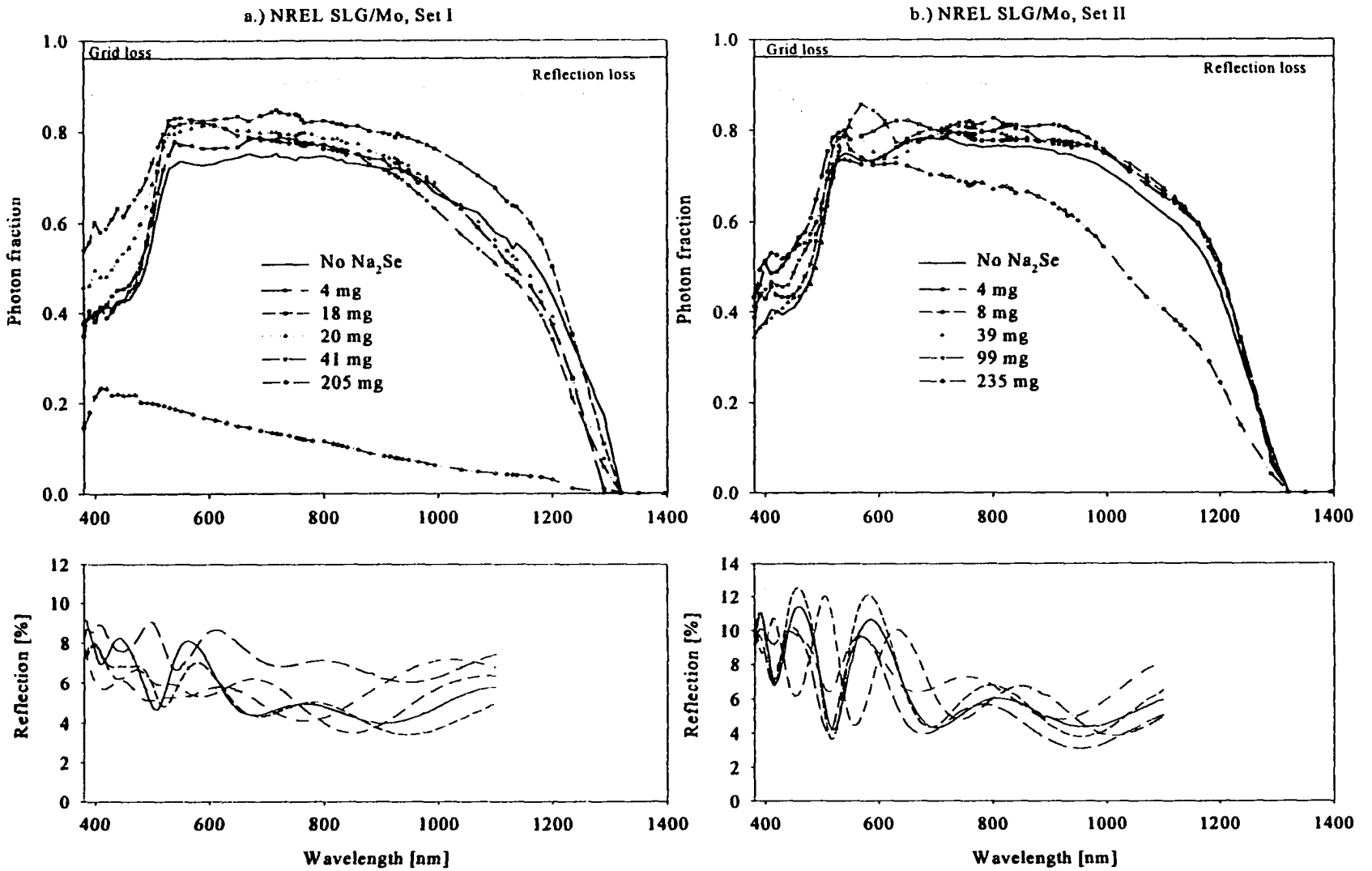

Figure 5.22. Quantum efficiency (top) and reflection data for all six Na_2Se addition levels on a.) NREL SLG/Mo, Set I and b.) NREL SLG/Mo, Set II.

Table 5.3. Summary of material and device effects observed with increasing sodium concentration (general trends).

Measurement	Effects observed					
	Set I			**Set II**		
Added Na	None	Low/Moderate	High	None	Low/Moderate	High
XRD	Orientation is substrate-dependent	Orientation changes are substrate-dependent, not Na-dependent	General decrease in all peak heights, three new unidentified peaks	Orientation is substrate-dependent	Orientation changes are substrate-dependent, not Na-dependent	General decrease in all peak heights
SEM	Grain size ~ 1 μm	Slight increase in grain size	Decrease in grain size, increase in porosity	Grain size ~ 3 - 4 μm	Slight increase in grain size	Definite bilayer observed, smaller grains on top
EBIC	Collection efficiency (c.e.) moderate	Increase in c.e., improvement in uniformity	Space-charge width decreases	Collection efficiency (c.e.) moderate	Increase in c.e., improvement in uniformity	Space-charge width decreases
V_{OC}	Baseline	Increase over baseline	Decrease from baseline (except on alumina)	Baseline	Increase over baseline	Decrease to value between no Na and low/moderate Na
FF	Baseline	Increase over baseline	Decrease from baseline	Baseline	Slight increase over baseline	Decrease from baseline (except on alumina)
J_{SC}	Baseline	No change	Significant decrease	Baseline	Changes not Na-dependent	Moderate decrease from baseline
Efficiency	Baseline	Increase over baseline	Decrease from baseline	Baseline	Increase over baseline	Decrease from baseline
Series Resistance	Baseline	Decrease from baseline	Increase over low/moderate Na	Baseline	Decrease from baseline	Increase over low/moderate Na

Measurement	Effects observed					
	Set I			Set II		
Added Na	None	Low/Moderate	High	None	Low/Moderate	High
Shunt Resistance	Baseline	No systematic changes	Significant decrease, light and dark	Baseline	No systematic changes	Moderate decrease, light
Diode Quality Factor	Baseline	Decrease from baseline	Significant increase	Baseline	No systematic changes	Slight increase over baseline
Hole density	Baseline	Increase by factor of 1.1 to 10	Increase by factor of 10^2 to 10^4	Baseline	Increase by factor of 1 to 2	Increase by factor of 10 to 30
Depletion Width	Baseline	Decrease by ~ 0.5 μm from baseline (except on alumina)	All decrease to 0.2 μm	Baseline	Decrease by 0.1 to 0.5 μm from baseline	All decrease to ~ 0.3 μm
Quantum Efficiency	Baseline	Slight changes	Significant red loss	Baseline	Slight changes	Moderate red loss

sodium, even though little or no sodium could actually be detected in the film. This was seen most clearly for cells grown on alumina and 7059 BSG substrates in Set II. The second threshold is incorporating enough sodium into the film to begin changing the material and device properties adversely. This most likely occurs when the sodium deposition rate is high enough to compete for space in the lattice.

For similar Na_2Se addition levels, great differences were observed in measured sodium concentrations between the two data sets. This leads to the possibility that sodium incorporation may indeed be dependent upon fabrication method, as suggested in the literature. Although the two methods employed for this thesis yield similar $CuInSe_2$, there are differences between the two processes that may be significant with regard to sodium incorporation. These include substrate temperature, ordering of the layers during growth, and the film composition at the time of sodium incorporation. The differences in measured sodium incorporation also give insight into the mechanisms involved. The two-stage process (Set I) yields smaller grains and, hence, an increase in the number of grain boundaries and grain surfaces as compared to the three-stage process (Set II). The higher sodium concentrations observed in the films from Set I for a given targeted sodium concentration as compared to Set II suggest that sodium resides in grain boundaries. However, since all the low sodium levels show approximately the same sodium incorporation levels, this suggests a miscibility limit for sodium in $CuInSe_2$. It appears that only a small amount of sodium can be incorporated when the sodium deposition rate is low. For higher sodium rates, sodium may compete more vigorously for a cation site, perhaps forming a new phase or a new compound. The effectiveness of this mechanism

may be tied to the $CuInSe_2$ phase (Cu-rich or Cu-poor) when sodium is added. These and other observations and possible mechanisms are explored in the next chapter.

CHAPTER 6

DISCUSSION

The many challenges facing the CIS community, outlined in Chapter 2, include: a need for flexibility in choosing substrate and back contact materials; reducing constraints on $CuInSe_2$ fabrication control; improving grain-boundary and surface passivation; improving junction quality, and understanding the underlying mechanisms. Several relevant questions relating to the sodium issue were presented in Chapter 1. These were (1) How much sodium is needed for optimal device performance? (2) Does the sodium mainly affect grain boundaries and surfaces, or the bulk, and where does it reside? (3) How does the sodium affect the junction quality? (4) What basic mechanisms are involved? The answers to these questions can now be discussed in the context of the challenges facing the photovoltaics community.

6.1 Optimal Performance

The first question to be answered is how much sodium is needed for optimal device performance? Optimal cell performance for a given set of conditions includes achieving high efficiency, high fill factor, high dopant density, low series resistance, and good diode behavior. The results in Chapter 5 demonstrated improvements in each of these parameters from the no-sodium-added case for sodium concentrations ranging

between 0.001 and 0.15 at% Na. At 0.3 at% Na and beyond, both material and solar cell properties degrade. The initial implication for researchers and manufacturers is the addition of sodium in small doses can improve efficiency and overall device performance. The improvements are relatively insensitive to the amount of sodium in the film over a broad range. The results on both soda-lime glass and non-sodium-containing substrates further demonstrate that the ability to add sodium enhances the flexibility in choosing substrates, since efficiencies on non-SLG substrates approached the SLG baseline efficiency when low to moderate amounts of sodium were added.

6.2 Grains and Grain Boundary Surfaces

The next question to be answered is how does sodium affect the grain boundaries and the bulk, and where does the sodium reside. The answer to this question lies in the analysis of some device and materials data, namely hole density, open-circuit voltage, capacitance, secondary ion mass spectroscopy (SIMS), X-ray diffraction (XRD), and scanning electron microscopy (SEM).

Among the strongest observed correlations with sodium is the increase in hole density as sodium is added (Figure 5.21.b). This correlation suggests the presence of sodium increases the effective acceptor concentration, directly or indirectly. In general, an increased acceptor concentration correlates with an improved device performance. This may occur by a passivation of grain boundary surfaces, known to have numerous defects and trapping states. It is also possible that this increase in hole density is due to reduced compensation within the bulk.

In this, as in most, CIS studies, an increase in hole density was accompanied by an increase in open-circuit voltage, which also improves overall device performance. In

some cases (for example, SSI in Set I or alumina in Set II), V_{OC} increased even when hole density remained constant or showed only a small increase. These V_{OC} increases may be due to a reduction in grain boundary recombination, or an improvement in junction uniformity. Junction uniformity may be due to surface passivation, or to changes in the surface layer that occurred during growth. An increase in capacitance, as observed here, may also result from improved junction uniformity, or from grain boundary passivation. The increases in both V_{OC} and capacitance with increasing sodium suggest sodium affects both grain boundary and bulk properties.

Strong support for sodium residing in the grain boundaries is given by the change in SIMS sodium signal for small grains versus large grains. See Figure 6.1. For the bilayer structures observed with approximately 0.3 at% Na in Set II, the SIMS data showed a higher concentration of sodium in the first micron of the film than in the region between one micron and the Mo/$CuInSe_2$ interface. The region of higher Na response corresponds to the region of smaller grains. This implies that a major fraction of the sodium resides in the grain boundaries, since the smaller-grained material has more grain boundary area. Similarly, Set I material was smaller-grained than Set II material. Comparing the measured sodium concentrations on both NREL SLG/Mo and Alumina/Mo for similar sodium addition levels between the two sets (see Table 5.2) demonstrates that more sodium was incorporated into the smaller-grained material in Set I. This further demonstrates the effects of sodium incorporation for different sized grains.

There is another possible explanation for the changes observed in sodium signal in the smaller-grained material. If the incorporated sodium forms a new phase, the SIMS

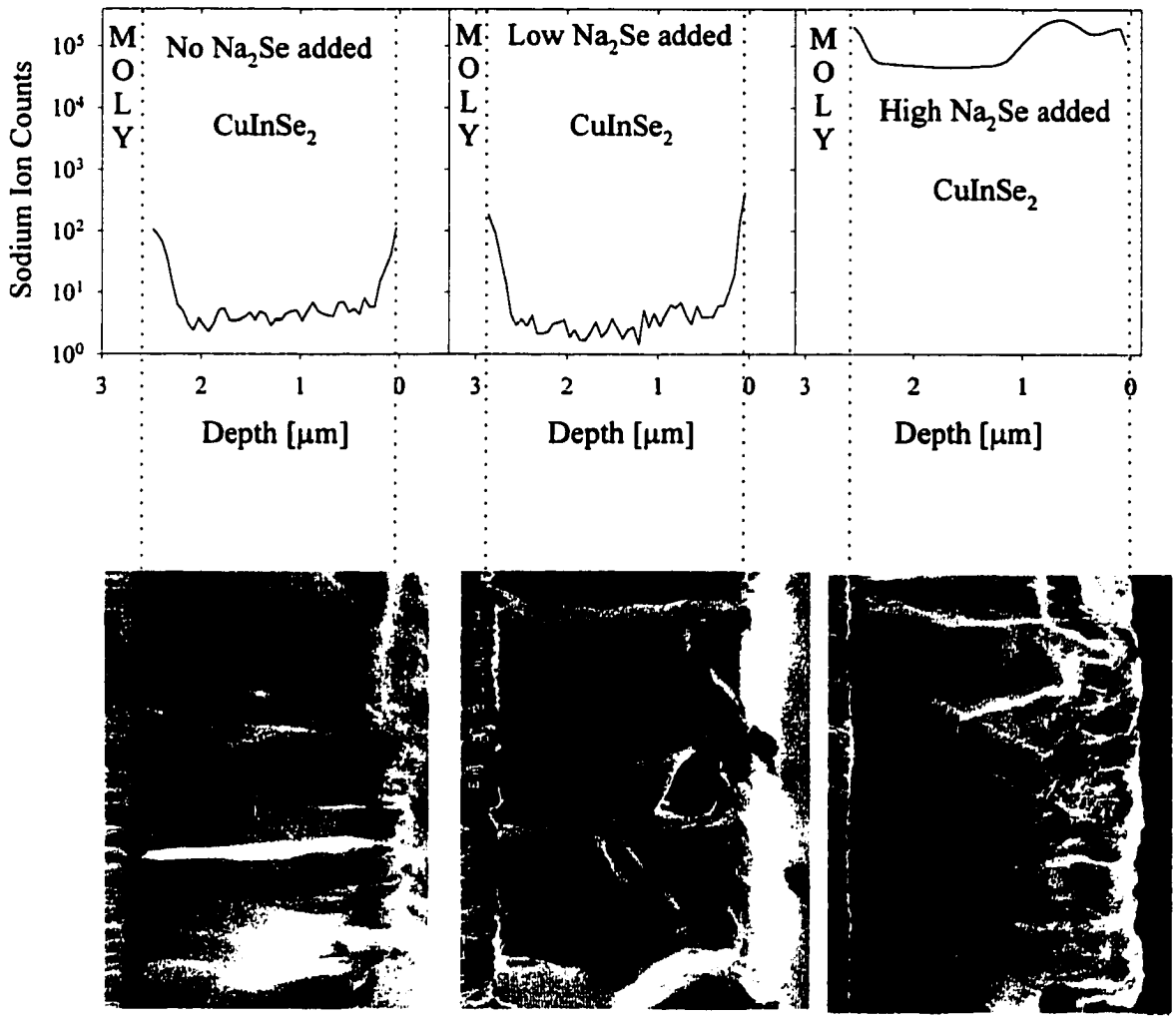

Figure 6.1. SIMS Na profiles and corresponding SEM micrographs. $CuInSe_2$ on Alumina/Mo, Set II.

calibration could be altered. This is unlikely, however, considering that nearly 100% of the sodium is ionized during SIMS analysis [47].

The work of Niles, et al., [44] demonstrated that, for a sensitivity of 0.1 at%, Auger measurements detected sodium at grain boundary surfaces, and none in the grains.

This gives further evidence that the majority of sodium affects grain boundary properties and resides there.

Although it appears clear that sodium resides at the grain boundary surfaces, it is certainly possible some sodium resides in the bulk as well. It is likely that there is a low saturation level of sodium within bulk $CuInSe_2$, as indicated by the plateau in actual sodium incorporation levels for all the low and moderate sodium addition levels (Figure 5.4). This may also indicate a low saturation level within the grain boundaries.

X-ray diffraction data can indicate changes in the structure and orientation of thin film $CuInSe_2$, as well as the presence of secondary phases. Other groups have found that the presence of sodium enhances the structure and orientation of $CuInSe_2$ crystallites [19, 20]. The same was not observed in this work. However, the growth methods used here tend to give highly 112-oriented films in all cases, and thus any sodium-induced changes may be obscured. In terms of secondary phases, one group has found that the presence of sodium appears to decrease the β-phase peak in the region between 21.5° and 22.5° 2θ [40]. This may indicate a widening of the α-phase window, as described in Chapter 2. For the samples used in this work, this peak is not present in the no-sodium and low/moderate sodium cases, indicating again that the methods used here yield highly single-phase $CuInSe_2$ independent of the sodium. However, the drop in measured Cu/In ratio versus the expected ratio at high sodium levels (Figure 5.1) may indicate a widening of the α-phase window. Sodium levels beyond 0.3 at%, however, appear to induce the β-phase peak. The highest sodium levels also showed unidentified peaks in the region between 5° and 15° 2θ. At high sodium concentrations, therefore, it appears that new phases or structures are formed. Contreras, et al., have observed similar peaks in

$Cu(In,Ga)Se_2$ with high sodium concentrations [43,48]. These results indicate that excessive sodium does induce secondary phase formation.

Along with structural changes, many groups have also reported dramatic improvements in morphology and grain growth with the addition of sodium [19, 20, and 27]. This effect was not observed here, but it also may be process-dependent. Although there was little indication that sodium affected grain growth at low sodium concentrations in these films, the changes observed at high sodium concentrations allow the possibility that low sodium concentrations do affect grain growth in films grown by other methods. Changes at grain boundaries would most likely be responsible for changes in grain growth.

A highly structured, large-grained material does not always correlate with high-performance devices. It is often the case, however, that an improvement in structure and/or grain size enhances device performance. Comparing the data given here with that in the literature, it is likely that the effects of sodium on structure and morphology are process-dependent. If this were indeed the case, adding sodium to $CuInSe_2$ during growth may allow researchers and manufacturers greater flexibility in choosing a process yielding high-quality $CuInSe_2$ to fit the application at hand.

Sodium may also affect growth by affecting the defect formation, specifically the assumed large number of $(2V_{Cu}^{-1}+In_{Cu}^{+2})$ defect-pairs [14]. Defect pairing occurs both in the bulk and at surfaces. This possibility will be explored in following sections.

Table 6.1 summarizes the possible roles for sodium at grain boundaries and in the bulk. It is clear that sodium has a strong influence on grain boundary surface properties, and very likely, the majority of the sodium in the film resides at the grain boundaries.

Table 6.1. Summary of observations pertaining to sodium's role in grain boundaries and in the bulk.

Observations noted here	Argument that Na affects grain boundaries	Argument that Na affects grains
1. Increased hole density with increasing Na	strong *passivation generally associated with surfaces*	moderate *reduced compensation*
2. Increased V_{OC} with increasing Na	strong *reduced recombination*	moderate *improved junction uniformity*
3. Increased capacitance with increasing Na	moderate *grain boundary passivation; improved junction uniformity due to surface passivation*	moderate *improved junction uniformity*
4. Changes in SIMS for small vs. large grains	strong *implies excess Na resides in grain boundaries*	weak
5. Na incorporation plateau for mid Na addition levels	moderate	moderate *implies low saturation level in bulk*
Observations noted by others:		
6. Auger detection of sodium at grain boundaries, none in grains	strong	weak
7. Removal of secondary-phase peaks at low/mid sodium; new XRD peaks with high Na	weak	moderate (strong for high sodium) *implies Na affects grain structure*
8. Improved grain growth	moderate *Na as a surfactant*	weak
9. Primary defect is $(2V_{Cu}^{-1} + In_{Cu}^{+2})$	moderate *defect pairing occurs on surfaces as well*	moderate *Na affects defect pairing in the bulk*

The results also indicate that sodium can affect bulk properties, but there is no clear indication that these changes strongly affect performance, except possibly at sodium concentrations beyond 1 at%. The results regarding grain boundary properties are encouraging. They suggest that sodium indeed improves grain boundary passivation, thereby reducing restrictions on fabrication processes.

6.3 Junction Quality

There are two main methods used to determine diode junction quality: current-voltage characterization and EBIC measurements. Changes in V_{OC}, fill factor, and diode quality factor A, as well as changes in the overall shape of the JV curve, can indicate changes in junction quality. Changes in the EBIC signal and in the y-modulated response indicate changes in junction depth and uniformity. Lesser junction uniformity often correlates with reduced quality and performance.

As shown in the previous section, V_{OC} has a general increase with increasing sodium up to 0.3 at% Na. At higher concentrations, V_{OC} drops dramatically. Fill factor behaves similarly. The diode quality factor improves (decreases) for low/moderate sodium levels in Set I samples, indicating an improved junction, but it rises again at the highest sodium levels. These results all demonstrate that the presence of sodium in moderate amounts improves junction quality.

From the analysis of the JV curves, it is apparent that some sodium improves key diode parameters. Additionally, in some cases (alumina, BSG, SiO_2), the addition of sodium removes non-diode-like behavior, indicating a more uniform junction or material in general (see Figure 5.14.b). This improved uniformity was also observed in EBIC measurements. The improvements on these substrates indicate that sodium enhances

device performance on non-sodium-containing substrates, thereby broadening the types of substrates that can be used for high-quality solar cell applications. The improvements on SLG substrates imply a lifting of restrictions on the material and structure of the back contact, as manufacturers no longer need to rely on the glass and diffusion through a back contact as the sole sodium source. The improvement in small-scale uniformity observed in EBIC data allows for the possibility that sodium can enhance large-scale uniformity as well. More research is necessary in this area.

The improvement in junction uniformity may enhance open-circuit voltage. A solar cell with a non-uniform junction can be looked at as many solar cell junctions in parallel. The lowest voltage point will dominate the measured voltage of the complete cell. Improving the uniformity of the junction increases the likelihood of each part of the cell being at the same voltage. It also decreases the likelihood of shunt paths, which funnel current away from the junction region and decrease V_{OC}.

6.4 The Mechanisms

The discussion so far has shown that adding sodium in moderate amounts improves device performance, tends to enhance material properties, improves grain boundary passivation, and improves junction uniformity and quality. The next question to be answered is what mechanisms are involved? From the summary in Table 6.1, it is clear that grain boundary passivation effects can explain the majority of the observations. Some observations suggest that sodium plays at least a minor role in the bulk as well.

6.4.1 Sodium at Grain Boundary Surfaces

Grain boundaries and grain surfaces are typically regions of high carrier recombination due to incomplete bonding of the surface atoms. Sodium likely passivates

grain boundaries, meaning it completes bonds. This passivation would serve to decrease recombination at grain boundaries in the depletion region, and hence decrease the unwanted recombination currents and increase V_{OC}. Passivation of grain boundaries can also lower grain-boundary barriers and thus decrease the impedance of the material [49]. This would be detected as decreased series resistance and/or increased capacitance. Next, passivation of the grain surfaces may act to improve the uniformity of the surface, thereby enhancing junction quality. This would enhance fill factor and collection efficiency. Finally, bond completion often means the removal of compensating states, which allows an increase in the effective acceptor concentration, which moves the Fermi level closer to the valence band and allows a larger V_{OC}.

Sodium directly passivates grain boundary surfaces most likely by occupying a copper or indium vacancy and bonding with selenium. It is highly unlikely that sodium, a column I element, would bond with a cation in place of the anion selenium. This is supported by the work of Niles, et al., [44], which showed no evidence of metallic sodium bonds at grain boundary surfaces; i.e., no Na-Cu, Na-In, or Na-Na bonds were detected. If sodium replaces a copper vacancy at a grain boundary, it would complete the valence structure, thereby removing a trap state or a recombination site and lowering the energy of the system, increasing stability. If sodium replaces an indium vacancy, it would likely act as a double acceptor, directly increasing the effective hole concentration. It is likely that sodium would remain bonded at grain boundary surfaces due to energy considerations. This is again evidenced by the detection of Na-Se bonds by Niles, et al. [44].

In high-efficiency solar cells, $CuInSe_2$ surfaces tend to have an In-rich layer. This often results in secondary phases in the top layer most likely due to repeated ($2V_{Cu}^{-}$ $+In_{Cu}^{2+}$) defect pairs. If sodium replaces a copper vacancy at the surface, the number of these defect pairs may be reduced, thereby reducing secondary phase formation. However, a reduction in copper vacancies would leave the same number of indium antisites at least initially uncompensated, directly decreasing the hole density in this layer. The top layer would therefore be less p-type than the rest of the bulk. This may actually be beneficial to the workings of the $CuInSe_2$ device in that it would push the electronic junction away from the metallurgical interface. EBIC work has shown that junction formation in good cells does not take place at the $CdS/CuInSe_2$ interface, but further into the $CuInSe_2$. It is also likely that the Cd from the CdS solution replaces Cu in the first 0.1 - 0.5 microns of the film, causing a type inversion of the surface layer [18]. The electrical junction forms up to 0.5 micron into the $CuInSe_2$. This is evidenced by the peak position in EBIC measurements. Therefore, an increased surface donor density due to uncompensated indium on copper antisites may benefit the junction formation by enhancing the inverted n-type $CuInSe_2$ layer. An increased number of unpaired copper vacancies may also enhance the efficiency of Cd doping.

Sodium may also enhance grain boundary and grain surface passivation indirectly by acting as a catalyst to oxygen. Kronik, et al., have recently proposed such a model [45]. They propose that sodium has a catalytic effect of increasing the formation of O_2^{-} on the surface, enhancing the formation of In-O, thereby occupying Se vacancies which would otherwise act as donors and recombination sites. They assert that the presence of sodium would therefore increase effective hole density and V_{OC} by this method. This is a

viable model, as oxygen is always present during $CuInSe_2$ deposition. Kronik, however, does not explain the changes in secondary-phase formation or the improved junction uniformity. It is proposed here that, in light of the recent work on junction formation, this type of passivation of the surface would enhance uniformity and allow more uniform coverage of the CdS, and hence, more uniform penetration of the Cd into the $CuInSe_2$. Grain boundary and surface passivation directly due to sodium would have the same effect on uniformity and Cd penetration.

For low/moderate sodium concentrations, grain boundary and surface passivation can explain the majority of the observations noted both here and in the literature due to sodium diffusion from the substrate or from a precursor. At high sodium concentrations, excess sodium in the grain boundaries almost certainly forms new compounds at these surfaces. These will likely be highly p-type, and will likely introduce large numbers of new recombination centers. This would act to reduce V_{OC}, and overall device performance.

There are still observations that are not explained by grain boundary and surface passivation. One such observation is the difference in performance between devices made on soda-lime glass with and without sodium co-evaporated with $CuInSe_2$. Take, for example, the Solarex Mo/SLG substrates in Set I. SIMS data showed that nearly 0.15 at% Na diffuses into the $CuInSe_2$ from the glass. Devices on this substrate have high performance without any added sodium. There appears to be enough sodium diffusing into the $CuInSe_2$ during growth to passivate grain boundaries and optimize performance. Yet, when sodium is co-evaporated with $CuInSe_2$, performance improves. For low sodium doses, only as much as $3x10^{-3}$ at% Na is added. Intuitively, this added amount of

sodium in the grain boundaries, as much as two orders of magnitude less than from diffusion, should not enhance passivation enough to improve device performance. Another mechanism must be involved. Another observation that cannot be explained by grain-boundary passivation is the results on the alumina and BSG substrates in Set II. For the low sodium levels, it is difficult to determine if any sodium is actually incorporated into the film. That is, SIMS levels are in the background region. Yet there are improvements in device performance. This must be due to changes that occur during $CuInSe_2$ growth in the presence of sodium. These two observations suggest that sodium can affect bulk properties as well as grain boundary properties when sodium is added during the growth process.

6.4.2 Sodium Impact on Growth

Due to bonding restrictions in the bulk, it is unlikely that sodium would take the place of either a cation or an anion and remain bonded within the bulk for low sodium concentrations, again evidenced by Niles, et al. However, sodium may still affect the bulk without remaining there. Sodium likely acts as a surfactant, and so tends to rise to surfaces during $CuInSe_2$ growth [50,51]. In this way, sodium interacts with each layer of growth, affecting both grain growth and structure. Sodium may then affect structure in two ways:

(1) Some evidence suggests sodium inhibits secondary-phase formation and widens the α-phase window. One way this can occur is by a reduction in the number of indium on copper antisite defects. The In_{Cu} defect formation energy ΔH_f depends on the Fermi energy and the chemical potentials of Cu and In (μ_{Cu} and μ_{In}). Specifically, in the region of interest (Cu-poor, In-rich $CuInSe_2$), ΔH_f of In_{Cu} depends on the quantity μ_{Cu} -

μ_{In}. As this quantity becomes more positive, ΔH_f of In_{Cu} increases for a given Fermi energy (see Figure 2.3).

Consider the case of sodium replacing copper in a Cu-poor sample. In this scenario, sodium would behave at least somewhat like copper. If this were the case, then the chemical potential difference would be influenced by the presence of sodium. If $\mu_{Na} > \mu_{Cu}$ (less negative), ΔH_f of In_{Cu} increases. If $\mu_{Na} < \mu_{Cu}$ (more negative), ΔH_f of In_{Cu} decreases. Since the sodium concentrations due to co-evaporation are fairly low and since it appears that the sodium saturation level in $CuInSe_2$ is low, it is likely that the chemical potential of sodium in $CuInSe_2$ will be close to zero. That is, a change in the number of sodium atoms at the surface would not greatly change the free energy of the system. In this case, the formation energy of the native defect In_{Cu} would increase in the presence of sodium for a given Cu/In ratio and a given Fermi energy. Sodium may therefore inhibit the formation of In_{Cu}, thereby decreasing the number of defect pairs, in turn decreasing the likelihood of secondary phase formation. Normally, In_{Cu} compensates two V_{Cu} defects. Since Na_{Cu} would replace one V_{Cu}, there would be one V_{Cu} remaining, which creates a single acceptor state. Effective hole density would therefore increase. By suppressing defect pair formation and secondary phase formation, the quality of the structure might improve. This would improve crystallinity, thereby improving V_{OC} and possibly fill factor. If sodium takes the place of a copper atom in a Cu-poor film, the window of Cu/In ratios for good-quality material may be enlarged. It is unlikely (energetically unfavorable) that sodium would remain bonded within the bulk at low concentrations, as stated previously. It is more likely that sodium would move out of the copper site as the $CuInSe_2$ continues to grow, thereby creating another copper vacancy,

further adding to the hole density. The enhanced structure and suppression of secondary phases would likely enhance junction uniformity and quality.

(2) If a portion of the sodium is initially in metallic form, the following reaction is favorable [51]:

$$Na_m + CuInSe_2 \dashrightarrow NaInSe_2 + Cu_m \quad (1).$$

This would also inhibit the formation of In_{Cu} defects by essentially removing copper sites in bulk $CuInSe_2$. This may or may not directly affect the hole concentration, but it would tend to reduce secondary $CuInSe_2$ phases such as $CuIn_3Se_5$. it is not known how $NaInSe_2$ would react with $CuInSe_2$, and if it itself would have secondary phases. This may be the cause of the degradation with high sodium content, since this reaction would only be significant if it removed a large number of copper sites. It may also require a large sodium concentration to relax the bonding restrictions within the bulk to allow sodium to remain bonded. XPS and Auger data on high-sodium samples are unavailable, but would be helpful in determining if sodium remains bonded in the bulk at high concentrations.

These scenarios describe how sodium may affect the bulk by altering growth. It is likely that in either case, sodium also moves along grain boundaries, and likely resides at grain boundary surfaces, enhancing grain boundary passivation.

Table 6.2 summarizes the mechanisms discussed above as they relate to low and moderate sodium concentrations. One mechanism has a high likelihood of being responsible for the effects observed for low to moderate sodium concentrations in $CuInSe_2$: sodium passivates grain boundary surfaces. This likely occurs in two ways: (a) directly through sodium replacing copper and indium vacancies, and (b) indirectly through a catalytic effect on oxygen. It is also suggested that sodium may affect the bulk

when sodium is added deliberately by (c) acting as a surfactant during growth and affecting the bulk layer by layer.

Table 6.2. Summary of possible mechanisms for low to moderate sodium concentrations in $CuInSe_2$.

Possible Mechanism	Brief Description	Expected Effects	Observed Effects	Likelihood
(a) Direct grain boundary passivation	Na bonds with Se in place of In or Cu	Increased V_{OC}; reduced impedance; improved junction quality/uniformity	All observed	Very likely for Na diffusion and addition
(b) Na as a catalyst to oxygen	Na enhances In-O formation	Increased V_{OC}, hole density	All observed	Very likely for Na diffusion and addition
(c) Na as a surfactant	Na inhibits In_{Cu} formation layer by layer	Increased hole density, V_{OC}; improved structure; enhanced Cu/In window; improved junction quality	All observed	Likely for Na addition

The effects of sodium were initially found due to sodium diffusion into the film from the soda-lime glass substrate. Diffusion of most elements in polycrystalline films occurs mainly along grain boundaries. Therefore, the effects of sodium at grain boundary surfaces, (a), are prevalent even when no sodium is deliberately added to films grown on SLG substrates, or when a sodium precursor is used. The catalytic effect on oxygen, (b), to further passivate surfaces is also likely prevalent in this case since sodium tends to collect on surfaces, even after deposition is complete. Hence, (a) and (b) can explain most of the effects of sodium as stated in the literature when a sodium precursor is used or when films grown on SLG are compared to films grown on non-sodium-containing substrates. However, the effect of sodium on the bulk, (c), is necessary to explain other phenomena such as changes due to ion implantation, changes on non-sodium-containing

substrates in a sodium ambient even when no sodium is detected in the film, and the added benefits of growing $CuInSe_2$ in the presence of sodium, even when sodium diffusion occurs.

It is clear that the presence of sodium (or a substance that behaves similarly) is essential for $CuInSe_2$ solar cells to reach optimal performance. Sodium passivation at grain boundary surfaces is certainly necessary to improve open-circuit voltage and junction quality. The enhanced ability of oxygen in the presence of sodium to further passivate surfaces most likely improves junction quality by aiding in the type-inversion of the surface layer, as well as improving V_{OC} and directly increasing hole concentration. The improvements that occur during growth are secondary, and are most likely only prevalent when sodium is deliberately added during growth.

How would this scenario of grain boundary passivation and growth affects alter the $CuInSe_2$ material and the device characteristics for both low/moderate and high sodium concentrations?

(1) Open-circuit voltage

A decrease in recombination at the grain boundaries would work to increase V_{OC} by reducing the forward recombination current. An improvement in the junction uniformity would possibly also increase V_{OC}. V_{OC} will generally increase due to an increase in hole concentration, because the Fermi level is closer to the band edge and less compensation usually correlates with fewer recombination sites. Such an increase in hole concentration would likely occur in the presence of sodium, as explained in the following paragraph. As the sodium concentration increases, excess sodium at the grain boundaries may now act as recombination centers. But the continued increase in hole concentration

with sodium compensates for this, and V_{OC} remains high. As the sodium concentration becomes excessive, recombination and morphological changes would dominate and V_{OC} would drop.

(2) Hole concentration

The net result would be an increase in effective hole concentration. The largest increase would be due to increased oxygen bonding at the surfaces, filling in selenium vacancies that would otherwise act as donors. A reduction in recombination due to sodium grain-boundary passivation would increase the measured hole concentration, as an increased number of holes would be collected. For growth-related effects, a possible increase in the number of copper vacancies that act as acceptors would directly increase hole concentration. As the sodium concentration increases, the number of acceptors grows. At extremely high sodium concentrations, a new compound would be formed, which may be highly p-type, but produces other device problems.

(3) Short-circuit current

At low sodium levels, the increase in hole concentration and possible resistance improvements should not affect the current since the morphology has already been optimized for high currents. However, at high sodium levels, the ultra-high hole concentration would shrink the depletion width such that fewer carriers would experience an electric field and the deeper ones would be less likely to be collected, thereby decreasing the current.

(4) Junction formation

The effects of sodium on junction formation depend on where the junction is formed. As mentioned above, for CBD CdS, the p-n junction most likely forms within

the $CuInSe_2$. The improved grain boundary passivation would likely reduce band bending at these surfaces, thereby improving junction uniformity. In this case, junction formation and quality would likely be positively affected by sodium due to a reduction in secondary phase formation at the surface and possibly throughout the bulk. For other methods of CdS deposition, the junction formation mechanisms are still unclear. However, the improvements in the surface and lower layers would likely improve junction formation for sputtered or evaporated CdS as well.

At high sodium levels, there are two possibilities. The first assumes no changes in $CuInSe_2$ structure. In this case, as the hole concentration increases, the abrupt junction approximation no longer holds as the acceptor concentration in the p-side approaches the donor concentration in the n-side. The p-type $CuInSe_2$ is no longer the main active region, and expected diode behavior is lost. It is also possible that a new phase is formed, as suggested by the new peaks observed in XRD data. This new phase or compound may interfere with normal junction formation, or may act as the p-type material, and may not be a good photovoltaic material.

(5) Structure

The structure of $CuInSe_2$ is very much dependent on the growth technique used. The proposed scenario would hinder the formation of secondary phases at the surface, and possibly in the bulk, thereby improving the structure of the $CuInSe_2$. It could also allow an improved structure at low Cu/In ratios, thereby allowing a wider growth window to be used. This increased window would be observed for many growth techniques. However, the direct observation of changes in secondary phases and/or orientation of the planes would most likely depend on the growth technique used. At high sodium concentrations,

a new phase may be formed which would negate the improvements at the lower sodium levels. It is possible that this phase can be detected by X-ray diffraction.

(6) Resistance

A decrease in recombination sites and an improvement in structure and uniformity would tend to decrease series resistance. Passivation of the grain boundaries reduces intragranular barriers, improving series resistance. The change in series resistance would account for some improvements in fill factor, along with changes in V_{OC}. In a material in which series resistance is low to begin with, this effect would be small. At high levels, a new compound or structure could increase recombination sites and shunt paths, thereby increasing series resistance and decreasing shunt resistance.

(7) Morphology

This scenario does not directly predict effects on morphology. However, it is possible that, if sodium does act as a surfactant, it may have the same type of fluxing properties observed with Cu_2Se [21]. When sodium reaches a critical concentration, it may react with the selenium atoms in place of copper, liberate copper from the film, and form a new phase. The sodium concentration nearing critical level may explain the bilayer observed in the Set II samples at 0.3 at% Na. Going beyond critical level may be responsible for the complete morphological change at 5.6 at% Na.

(8) Other High Sodium Effects

It is apparent that the effects of low or moderate sodium levels and the effects of high sodium concentrations are quite different. It is possible that a new phase is formed when the sodium concentration is greater than 1 at%. It is possible that a new vacancy compound is formed, which is itself highly p-type, accounting for the large increase in

hole density for high sodium concentrations. For high sodium fluxes, sodium may be able to compete for copper in the lattice, or compete for a new structure, using all the copper available or forcing copper rejection. This would decrease or even remove the Cu_2Se flux, thereby creating smaller-grained material. The excess sodium in the grain boundaries may be at too high a level to completely bond, thereby adding to the recombination centers, and destroying device performance.

As demonstrated in this section, the proposed model can explain the majority of the effects observed due to sodium incorporation as described in this thesis and in the literature.

CHAPTER 7

CONCLUSIONS

7.1 Summary

A range of sodium concentrations that yield optimal device performance has been found. This is the first time such a range has been shown definitively. $CuInSe_2$-based solar cell device performance is optimal with sodium concentrations in the range of 0.001 to 0.15 at% Na. Efficiencies can increase by as much as 4% when sodium is added. It is assumed that this range supplies sufficient sodium for well-passivated grain boundaries, but not so much as to produce secondary phases, which may diminish device performance. The main improvements are in open-circuit voltage and hole concentration. Open-circuit voltage can improve by as much as 80 mV and hole concentrations may increase by as much as a factor of 10 when sodium is added. Diode junction quality also improves as shown by improvements in fill factor and diode quality factor. Beyond this range, both device parameters and material properties show significant degradation, likely due to the formation of a new secondary phase or a new compound.

Sodium is found to have the greatest effect on grain boundary properties, and there is evidence that suggests sodium moderately affects bulk properties as well, especially when sodium is added during $CuInSe_2$ deposition. From data given here and in the literature, a significant amount, if not all, the sodium resides at grain boundary

surfaces. The material probing techniques used thus far have not been sensitive enough to detect sodium in the bulk. However, the possibility of some sodium residing in the bulk should not be ruled out.

A model including three mechanisms is proposed: (a) sodium passivates grain boundary surfaces directly through sodium replacing copper and indium vacancies, and (b) indirectly through a catalytic effect on oxygen. It is also suggested that sodium may affect the bulk when sodium is added deliberately by (c) acting as a surfactant during growth and affecting the bulk layer by layer by inhibiting indium on copper antisite formation. These mechanisms can explain the effects of low to moderate sodium concentrations due to diffusion from a substrate or precursor, and due to the deliberate addition of sodium during deposition. They also give plausible arguments to explain the effects at high sodium concentrations. This is the most complete model proposed to date.

The improvements in device quality noted here and in the literature appear to be independent of fabrication method, although the magnitude of the changes observed and changes in material properties are clearly process-dependent. Sodium incorporation is dependent upon substrate temperature, relative deposition rates, grain size, sticking coefficient, and the composition of the material at the time of incorporation.

From a technological perspective, it appears that deliberately adding sodium can enhance device performance and reduce constraints on key areas of $CuInSe_2$ solar-cell fabrication. The addition of sodium during deposition or from a precursor may allow researchers and manufacturers greater flexibility in choosing substrates and back contact materials as well.

7.2 Future Work

Areas for future study can be placed in two categories: model verification, and production issues.

The proposed model asserts the majority of the phenomena related to sodium in $CuInSe_2$ can be explained by grain-boundary passivation effects and suggests that effects on the growth may be responsible for secondary observations. As with many polycrystalline films, more work is necessary to separate the grain boundary effects from the bulk-related effects. Time-of-flight SIMS measurements and small-spot laser measurements may aid in this endeavor. More work on single-crystal $CuInSe_2$ may also be of use to determine bulk-related effects.

Within the realm of grain boundary passivation, the effects due to sodium need to be separated from those due to oxygen. Deliberately changing the oxygen content in $CuInSe_2$ materials while maintaining a constant sodium content could shed light on this issue. A more in-depth study of oxygen bonding in $CuInSe_2$ with and without sodium present would also be useful.

To test the effect of sodium on the growth, controllably adding sodium during different growth stages and at different temperatures would be ideal. Examination of the sodium bonding at points along the growth (ideally by quenching the film at different growth stages) could help verify the processes involved. Examination of the bonding at the grain boundaries and in the bulk at high sodium concentrations may also give insight into the low/moderate sodium concentration mechanisms.

Production issues for $CuInSe_2$ cells include gallium incorporation, large-scale uniformity, long-term stability, and when to add sodium for best results. Many groups

have studied the $Cu(In,Ga)Se_2$ system with sodium, and the general results are the same. However, details of the model may change when gallium is present.

EBIC data suggest sodium enhances junction uniformity on a small scale. If the same effect holds on a large scale, this would open up opportunities for large cell and module production. The simplest approach would be to study the effects of adding sodium on cells varying in size from 0.4 cm^2 to 100 cm^2, which can be done without much modification of other systems at many laboratories.

Although sodium improves performance, no studies have been conducted to test the effects of sodium on long-term stability. These tests are fairly straightforward, albeit time-consuming. A logical next step would be elevated-temperature tests of the stability of $CuInSe_2$ solar cells with and without sodium, and with varying oxygen levels.

Finally, adding sodium during the deposition of $CuInSe_2$ may not be the ideal way to incorporate it. It is possible that adding sodium during other fabrication steps may have similar effects on the performance and be easier to control.

$CuInSe_2$-based solar cells are a part of a technology that is quickly becoming a viable energy source. Photovoltaics are at present the only energy source in many regions of third-world countries, and are fast becoming the mainstay for remote areas of all countries. Solar cell technology has the potential to become one of the world's primary energy producers. Fundamental research in all areas of photovoltaics is vital, not only to build the core of knowledge, but to help bring about clean, non-depletable solutions to the challenge of providing energy to more than six billion people for ages to come.

REFERENCES

1. J. R. Tuttle, J. S. Ward, A. Duda, T. A. Berens, M. A. Contreras, K. R. Ramanathan, A. L. Tennant, J. Keane, E. D. Cole, K. Emery and R. Noufi, " The Performance of Cu(In,Ga)Se_2-Based Solar Cells in Conventional and Concentrator Applications," *MRS Symposium Proceedings Volume 426*, 8-11 April, 1996, San Francisco, CA (MRS, Pittsburgh, 1996) p. 143.

2. C. Ferekides, J. Britt, and Y. Ma, "High Efficiency CdTe Solar Cells by Close Spaced Sublimation," *Proceedings of the 23rd IEEE Photovoltaics Specialists Conference*, Louisville, KY, 1993, p. 389.

3. H. Ohyama, T. Aramoto, S. Kumazawa, H. Higuchi, T. Arita, S. Shibutani, T. Nishio, J. Nakajima, M. Tsuji, A. Hanafusa, T. Hibino, K. Omura, and M. Murozono, "16.0% Efficient Thin-Film CdS/CdTe Solar Cells," *Proceedings of the 26th IEEE Photovoltaics Specialists Conference*, Anaheim, CA, 1997, p. 343.

4. L. Stolt, K. Granath, E. Niemi, M. Bodegård, S. Bocking, M. Carter, M. Burgelman, B. Dimmler, R. Menner, M. Powalla, U. Rühle, and H. W. Schock, "Thin Film Solar Cell Modules Based On Cu(In,Ga)Se_2 Prepared by the Coevaporation Method," *13th European Photovoltaic Solar Energy Conference*, 23-27 October, 1995, Nice, France p. 1451.

5. L. Margulis, G. Hodes, A. Jakubowicz, and D. Cahen, "Aggregate structure in $CuBSe_2$/Mo films (B=In,Ga): Its relation to their electrical activity," *J. Appl. Phys.* **66**, p. 3554 (1989).

6. A. L. Fahrenbruch and R. H. Bube, Fundamentals of Solar Cells, Academic Press, Inc., New York, New York, 1983.

7. S. M. Sze, Physics of Semiconductor Devices, John Wiley & Sons, Inc., 1969.

8. J. R. Tuttle, "An Optical and Microstructural Characterization Study and Microstructural Model of Co-evaporated Polycrystalline Thin Film $CuInSe_2$ for Photovoltaic Applications," PhD Thesis, University of Colorado, 1990, published.

9. A. M. Gabor, "The Conversion of $(In,Ga)_2Se_3$ Thin Films to $Cu(In,Ga)Se_2$ for Application to Photovoltaic Solar Cells," PhD Thesis, University of Colorado, 1995, unpublished.

10. J. L. Shay and J. H. Wernick, Ternary Chalcopyrite Semiconductors: Growth, Electronic Properties, and Applications, Pergamon Press, 1975.

11. M. L. Fearheiley, "The Phase Relations in the Cu, In, Se System and the Growth of $CuInSe_2$ Single Crystals," *Solar Cells*, **16**, p. 91, 1986.

12. U. C. Boehnke and G. Kühn, "Phase Relations in the Ternary System Cu-In-Se," *Journal of Materials Science*, **22**, p. 1635, 1987.

13. C. Rincon and C. Bellabarba, *Phys. Rev. B* **33**, p. 7160 (1986); S. M. Wasim, *Solar Cells* **16**, p. 289 (1986).

14. S. B. Zhang, S. H. Wei, and A. Zunger, "Stabilization of Ternary Compounds via Ordered Arrays of Defect Pairs," *Phys. Rev. Let.* **78**, p. 4059 (May 1997); A. Zunger, S. B. Zhang, and S. H. Wei, "Revisiting the Defect Physics in $CuInSe_2$ and $CuGaSe_2$," *Proceedings of the 26th IEEE Photovoltaics Specialists Conference*, Anaheim, CA, 1997, p. 313; S. B. Zhang, S. H. Wei, and A. Zunger, "Defect Physics of the $CuInSe_2$ Chalcopyrite Semiconductor," submitted to *Phys. Rev. B.*

15. J. R. Sites and P. H. Mauk, "Diode Quality Factor Determination for Thin-Film Solar Cells," *Solar Cells* **27** (1989), p. 411 - 417.

16. G. Stollwerck, "Quantitative Separation of Photon and Back-Contact Losses in CdTe Solar Cells," Master's Thesis, Colorado State University, 1995, unpublished.

17. P. H. Mauk, H. Tavakolian and J. R. Sites, "Interpretation of Thin-Film Polycrystalline Solar Cell Capacitance," *IEEE Transactions on Electron Devices* **37**, No. 2 (Feb. 1990), p. 422 - 427.

18. K. Ramanathan, H. Wiesner, S. Asher, D. Niles, R.N. Bhattacharya, J. Keane, M. A. Contreras, and R. Noufi, "High Efficiency $Cu(In,Ga)Se_2$ Thin Film Solar Cells Without Intermediate Buffer Layers," *Presented at the 2nd World Conference and Exhibition on Photovoltaic Solar Energy Conversion,* Vienna, Austria, 1998, to be published.

19. J. Hedström, H. Ohlsén, M. Bodegård, A. Kylner, L. Stolt, D. Hariskos, M. Ruckh and H. W. Schock, "ZnO/CdS/$Cu(In,Ga)Se_2$ Thin Film Solar Cells with Improved Performance," *Proceedings 23rd IEEE PVSC*, Louisville, 1993 p. 364.

20. M. Bodegård, L. Stolt and J. Hedström, "The Influence of Sodium on the Grain Structure of $CuInSe_2$ Films for Photovoltaic Applications," *12th European*

Photovoltaic Solar Energy Conference, 11-15- April, 1994, Amsterdam, The Netherlands p. 1743.

21. R. Klenk, T. Walter, H. W. Schock, and D. Cahen, "A Model for the Successful Growth of Polycrystalline Films of $CuInSe_2$ by Multisource Physical Vacuum Evaporation," *Adv. Mater.* **5**, p. 114 (1993).

22. J. Holz, F. Karg and H. von Philipsborn, "The Effect of Substrate Impurities on the Electronic Conductivity in CIS Thin Films," *12th European Photovoltaic Solar Energy Conference*, 11-15- April, 1994, Amsterdam, The Netherlands p. 1592.

23. B. M. Basol, V. K. Kapur, C. R. Leidholm, A. Minnick and A. Halani, "Studies on Substrates and Contacts for CIS Films and Devices," *First World Conference on Photovoltaic Energy Conversion*, Dec. 5-9, 1994, Hawaii p. 148.

24. D. F. Dawson-Elli, C. B. Moore, R. R. Gay and C. L. Jensen, "Substrate Influences on CIS Device Performance," *First World Conference on Photovoltaic Energy Conversion*, Dec. 5-9, 1994, Hawaii p. 152.

25. M. Ruckh, D. Schmid, M. Kaiser, R. Schäffler, T. Walter and H. W. Schock, "Influence of Substrates on the Electrical Properties of $Cu(In,Ga)Se_2$ Thin Films," *First World Conference on Photovoltaic Energy Conversion*, Dec. 5-9, 1994, Hawaii p. 156.

26. J. H. Scofield, S. Asher, D. Albin, J. Tuttle, M. Contreras, D. Niles, R. Reedy, A. Tennant and R. Noufi, "Sodium Diffusion, Selenization, and Microstructural Effects Associated with Various Molybdenum Back Contact Layers for CIS-Based Solar Cells," *First World Conference on Photovoltaic Energy Conversion*, Dec. 5-9, 1994, Hawaii p. 164.

27. V. Probst, J. Rimmasch, W. Riedl, W. Stetter, J. Holz, H. Harms, F. Karg and H. W. Schock, "The Impact of Controlled Sodium Incorporation on Rapid Thermal Processed $Cu(InGa)Se_2$-Thin Films and Devices," *First World Conference on Photovoltaic Energy Conversion*, Dec. 5-9, 1994, Hawaii p. 144.

28. S. Zweigart, G. Bilger and H. W. Schock, "Comparison of Different Sequential Processes for the Formation of $Cu(In,Ga)Se_2$: Growth Mechanism and Incorporation of Sodium," *13th European Photovoltaic Solar Energy Conference*, 23-27 October, 1995, Nice, France p. 1991.

29. R. Menner, E. Gross, A. Eicke, H. Dittrich, J. Springer, B. Dimmler, U. Rühle, M. Kaiser, T. Friedlmeier and H. W. Schock, "Investigations on Sputter-Deposited Molybdenum Back Contacts for $Cu(In,Ga)Se_2$ Solar Cells, *13th European Photovoltaic Solar Energy Conference*, 23-27 October, 1995, Nice, France p. 2067.

30. C. Heske, R. Fink, D. Jacob and E. Umbach, "Electronic Structure, Composition, and Local Surface Photovoltage Effects of Polycrystalline Cu(InGa)Se_2 Thin Films After Na Deposition," *13th European Photovoltaic Solar Energy Conference*, 23-27 October, 1995, Nice, France p. 2003.

31. M. Bodegård, J. Hedström, K. Granath, A. Rockett and L. Stolt, "Na Precursors for Coevaporated Cu(In,Ga)Se_2 Photovoltaic Films," *13th European Photovoltaic Solar Energy Conference*, 23-27 October, 1995, Nice, France p. 2080.

32. V. Probst, J. Rimmasch, W. stetter, H. Harms, W. Riedl, J. Holz and F. Karg, "Improved CIS Thin Film Solar Cells Through Novel Impurity Control Techniques," *13th European Photovoltaic Solar Energy Conference*, 23-27 October, 1995, Nice, France p. 2123.

33. T. Tanaka, N. Tanahashi, Y. Yamamoto, T. Yamaguchi and A. Yoshida, "Characterization of Cu(In,Ga)$_2Se_{3.5}$ Thin Films Prepared by RF Sputtering from Cu(In,Ga)Se_2 with Na_2Se," *Technical Digest of the International PVSEC-9*, Miyazaki, Japan, 1996 p. 383.

34. C. Heske, G. Richter, Z. Chen, R. Fink, E. Umbach, W. Riedl and F. Karg, "Influence of Humidity on Polycrystalline Cu(In,Ga)Se_2 Thin Films for Solar Cells: A Study of Na and H_2O Coadsorption," *Proceedings of the 25th IEEE Photovoltaic Specialists Conference*, 13-17 May, 1996, Washington, D. C. p. 861.

35. B. J. Stanbery, A. Davydov, C. H. Chang and T. J. Anderson, "Reaction Engineering and Precursor Film Deposition for CIS Synthesis," *Proceedings of the 14th NREL/SNL Photovoltaics Program Review Meeting*, 18-22 November, 1996, Lakewood, CO p. 579.

36. T. Nakada, H. Ohbo, M. Fukuda and A. Kunioka, "Improved Compositional Flexibility of Cu(In,Ga)Se_2-Based Thin Film Solar Cells by Sodium Control Technique," *Technical Digest of the International PVSEC-9*, Miyazaki, Japan, 1996 p. 139.

37. U. Rau, M. Schmitt, D. Hilburger, F. Engelhardt, O. Seifert and J. Parisi, "Influence of Na and S Incorporation on the Electronic Transport Properties of Cu(In,Ga)Se_2 Solar Cells," *Proceedings of the 25th IEEE Photovoltaic Specialists Conference*, 13-17 May, 1996, Washington, D. C. p. 1005.

38. A. Rockett, M. Bodegård, K. Granath and L. Stolt, "Na Incorporation and Diffusion in $CuIn_{1-x}Ga_xSe_2$," *Proceedings of the 25th IEEE Photovoltaic Specialists Conference*, 13-17 May, 1996, Washington, D. C. p. 985.

39. J. R. Tuttle, T. A. Berens, J. Keane, K. R. Ramanathan, J. Granata, R. N. Bhattacharya, H. Wiesner, M. A. Contreras and R. Noufi, "Investigations Into

Alternative Substrate, Absorber, and Buffer Layer Processing for Cu(In,Ga)Se_2-Based Solar Cells," *Proceedings of the 25th IEEE Photovoltaic Specialists Conference*, 13-17 May, 1996, Washington, D. C., p. 797.

40. R. Herberholz, H. W. Schock, U. Rau, J. H. Werner, T. Haalboom, T. Gödecke, F. Ernst, C. Beilharz, K. W. Benz and D. Cahen, "New Aspects of Phase Segregation and Junction Formation in $CuInSe_2$," *Proceedings of the 26th IEEE Photovoltaics Specialists Conference*, Anaheim, CA, 1997, p. 323.

41. B. J. Stanbery, E. S. Lambers and T. J. Anderson, "XPS Studies of Sodium Compound Formation and Surface Segregation in CIGS Thin Films," *Proceedings of the 26th IEEE Photovoltaics Specialists Conference*, Anaheim, CA, 1997, p. 499.

42. B. M. Keyes, F. Hasoon, P. Dippo, A. Balcioglu and F. Abulfotuh, "Influence of Na on the Electro-Optical Properties of Cu(In,Ga)Se_2," *Proceedings of the 26th IEEE Photovoltaics Specialists Conference*, Anaheim, CA, 1997, p. 479.

43. M. A. Contreras, B. Egaas, P. Dippo, J. Webb, J. Granata, K. Ramanathan, S. Asher, A. Swartzlander and R. Noufi, "On the Role of Na and Modifications to Cu(In,Ga)Se_2 Absorber Materials Using Thin-MF (M=Na, K, Cs) Precursor Layers," *Proceedings of the 26th IEEE Photovoltaics Specialists Conference*, Anaheim, CA, 1997, p. 359.

44. D. W. Niles, K. Ramanathan, F. Hasoon, R. Noufi, B. J. Tielsch, and J. E. Fulghum, "Na Impurity Chemistry in Photovoltaic CIGS Thin fFlms: Investigation With X-ray Photoelectron Spectroscopy," *Journal of Vacuum Science and Technology A*, **15(6)**, p. 3044, 1997; D. W. Niles, M. Al-Jassim, and K. Ramanathan, "Direct Observation of Na and O Impurities at Grain Surfaces of $CuInSe_2$ Thin-films," accepted for publication in *Journal of Vacuum Science and Technology A*, October 1998.

45. L. Kronik, D. Cahen, and H. W. Schock, "Effects of Sodium on Polycrystalline Cu(In,Ga)Se_2 and Its Solar Cell Performance," *Adv. Mater.* **10**, p. 31, 1998.

46. J. Kessler, K. O. Velthaus, M. Ruckh, R. Laichinger, H. W. Schock, D. Lincot, R. Ortega, and J. Vedel, "Chemical Bath Deposition of CdS on $CuInSe_2$, Etching Effects and Growth Kinetics," *Proceedings of the 6th International Photovoltaic Science and Engineering Conference,* New Delhi, India, 1992, p. 1005.

47. Sally Asher, private communication, July 1998.

48. M. Contreras, private communication, September 1997.

49. X. Liu, "Current Transport With and Without Grain-Boundary Recombination for Polycrystalline $CuInSe_2$ Solar Cells," Ph.D. Thesis, Colorado State University, 1994, unpublished.

50. B. J. Stanbery, C.-H. Chang, and T. J. Anderson, "Engineered Phase Inhomogeneity for CIS Device Optimization," *Proceedings of the 11th International Conference on Ternary and Multinary Compounds,* Salford, 1997, p. 915.

51. Alex Zunger, private communication, June 1998.